Western Graduate&PostdoctoralStudies

Western University
Scholarship@Western

Electronic Thesis and Dissertation Repository

12-12-2012 12:00 AM

Detection and Mapping of Phragmites australis using High Resolution Multispectral and Hyperspectral Satellite Imagery

Nicholas J. Lantz, *The University of Western Ontario*

Supervisor: Dr Jinfei Wang, *The University of Western Ontario*

A thesis submitted in partial fulfillment of the requirements for the Master of Science degree in Geography

© Nicholas J. Lantz 2012

Follow this and additional works at: https://ir.lib.uwo.ca/etd

Part of the Remote Sensing Commons

Recommended Citation

Lantz, Nicholas J., "Detection and Mapping of Phragmites australis using High Resolution Multispectral and Hyperspectral Satellite Imagery" (2012). *Electronic Thesis and Dissertation Repository*. 1012.
https://ir.lib.uwo.ca/etd/1012

This Dissertation/Thesis is brought to you for free and open access by Scholarship@Western. It has been accepted for inclusion in Electronic Thesis and Dissertation Repository by an authorized administrator of Scholarship@Western. For more information, please contact wlswadmin@uwo.ca.

DETECTION AND MAPPING OF *PHRAGMITES AUSTRALIS* USING HIGH RESOLUTION MULTISPECTRAL AND HYPERSPECTRAL SATELLITE IMAGERY

(Spine title: Mapping of *Phragmites australis* using satellite imagery)

(Thesis format: Integrated Article)

by

Nicholas Lantz

Graduate Program in Geography

A thesis submitted in partial fulfillment
of the requirements for the degree of
Master of Science

The School of Graduate and Postdoctoral Studies
The University of Western Ontario
London, Ontario, Canada
December 2012

© Nicholas Lantz 2012

THE UNIVERSITY OF WESTERN ONTARIO
School of Graduate and Postdoctoral Studies

CERTIFICATE OF EXAMINATION

Supervisor

_____
Dr. Jinfei Wang

Examiners

_____
Dr. Micha Pazner

_____
Dr. Jane Bowles

_____
Dr. Ben Rubin

The thesis by

Nicholas John Lantz

entitled:

Detection and Mapping of *Phragmites australis* Using High Resolution Multispectral and Hyperspectral Satellite Imagery

is accepted in partial fulfillment of the
requirements for the degree of
Master of Science

_____
Date

_____
Chair of the Thesis Examination Board

Abstract

Mapping invasive plant species is important to establish an invasion baseline, monitor plant propagation, and to implement an effective plan to deal with the invasion. In this thesis, methods are proposed to map invasive *Phragmites australis* in a Great Lakes coastal wetland. Chapter 2 presents an object-based *Phragmites* extraction method using Worldview-2 high-spatial-resolution satellite imagery. For the 4024 ha study area at Walpole Island, Ontario, 94% overall accuracy was achieved.

Chapter 3 uses CHRIS PROBA hyperspectral satellite imagery for mapping the pixel abundance of *Phragmites* using a spectral mixture analysis method. An evaluation method was developed to assess the accuracy of the spectral mixture analysis fractions using the classification from Chapter 2. A *Phragmites* invasion classification identifying pixels where *Phragmites* was non-dominant, potentially dominant, and dominant was 85.2% accurate. The overall accuracy for a *Phragmites*, native vegetation and water classification based on the dominant fraction in each pixel was 82.8%.

Keywords

Phragmites australis, Invasive Species, Non-Native Species, Great Lakes Coastal Wetland, Worldview-2, CHRIS PROBA, Object-Based Classification, Spectral Mixture Analysis, Walpole Island First Nation

Acknowledgments

First, I would like to thank my supervisor, Dr. Jinfei Wang. She has taught me what I know about remote sensing, starting back in 2008 in her undergraduate introduction to remote sensing course. Her ideas, advice, and criticism were invaluable to the production of this thesis and she has motivated me to become a better researcher.

The Worldview-2 image used in Chapter 2 was purchased with funds from an NSERC research grant awarded to Dr. Wang. I would like to thank my GITA lab members for their support, ideas and comments on my research. Much gratitude is owed to Francisco Flores de Santiago, Monserrat Santiago, Chuiqing Zeng, Autumn Gambles, and Dr. Wang for enduring long hours helping me with field work at Walpole Island First Nation, often on short notice. I would like to thank Ting Zhao and Qin Ma for their help with the accuracy assessment in Chapter 2.

The CHRIS PROBA image used in Chapter 3 was provided by the European Space Agency. I would like to thank Chuiqing Zeng for his help with ENVI and IDL, and Cheng Qiao for her helpful comments on spectral mixture analysis for Chapter 3. I would like to thank Kathy Tang for her knowledge of GIS procedures used for the accuracy assessment in Chapter 3. Much thanks to Karen Van Kerkoerle for producing the study area maps in Chapters 1, 2 and 3.

I would like to thank the people of Walpole Island First Nation for allowing me conduct research on their island. Thank you to Clint Jacobs and the Walpole Island Heritage Centre for their hospitality and for organizing guides for fieldwork. I would like to thank Mike Blackbird and Carl Smith for sharing with me their knowledge of the Walpole Island marshes and for providing invaluable guide services in the marsh.

Lastly, I would like to thank my wife Leigh, and my family for their endless patience, help, and encouragement throughout my study. I am very thankful to have such wonderful people in my life. I could not have accomplished what I have without your love and support.

Table of Contents

CERTIFICATE OF EXAMINATION ii

Abstract iii

Acknowledgments iv

Table of Contents v

List of Tables ix

List of Figures xi

List of Appendices xiii

List of Abbreviations xiv

Chapter 1 1

1 Introduction 1

1.1 Research Context 1

1.2 Research Objectives 5

1.3 Study Area 6

1.4 Background 10

1.4.1 Object-Based Classification 10

1.4.2 Spectral Mixture Analysis 11

1.5 Thesis Format 12

1.6 References 12

Chapter 2 16

2 Object-Based Classification of Worldview-2 Imagery for Mapping Invasive *Phragmites australis* 16

2.1 Introduction 16

2.2 Study Area 19

2.3 Imagery 20

2.4 Methods 21
2.4.1 Pre-processing 22
2.4.2 Indices Calculation 22
2.4.3 Worldview-2 Classification 23
2.4.3.1 Classification of Agricultural Fields 25
2.4.3.2 Classification of Water 28
2.4.3.3 Classification of Built-Up 30
2.4.3.4 Separation of Vegetation and Shadowed Objects 31
2.4.3.5 Nearest-Neighbor Classification of *Phragmites* and Other Vegetation 32
2.4.3.6 Post-Processing 33
2.4.4 Accuracy Assessment 33
2.5 Results and Discussion 34
2.5.1 Land Cover Estimates and Distribution 34
2.5.2 Classification Methods 36
2.5.2.1 Four Band Object-Based Versus Per-Pixel Classification 36
2.5.2.2 Eight Band Object-Based Versus Per-Pixel Classification 37
2.5.2.3 Pixel-Based Classification – Four Versus Eight Band 38
2.5.2.4 Object-Based Classification – Four Versus Eight Band 39
2.5.2.5 *Phragmites* and Non-*Phragmites* Classification 43
2.6 Conclusions 44
2.7 References 45
Chapter 3 48
3 Mapping and Evaluating *Phragmites australis* Abundance Derived from Spectral Mixture Analysis of Hyperspectral Data 48
3.1 Introduction 48

3.2 Methods 52
3.2.1 Study Site 52
3.2.2 Data 54
3.2.2.1 Remotely Sensed Imagery 54
3.2.2.1.1 CHRIS PROBA 54
3.2.2.1.2 Worldview-2 57
3.2.2.2 Reflectance Spectra Field Data 58
3.2.3 Spectral Mixture Analysis Method Overview 60
3.2.3.1 Hyperspectral Data Dimensionality Reduction 61
3.2.3.2 Endmember Selection 63
3.2.3.3 Pixel Purity Index Endmember Selection 64
3.2.3.4 N-Dimensional Visualization Endmember Selection 66
3.2.3.5 ASD Field Measurement Endmember Selection 66
3.2.4 Spectral Mixture Analysis 67
3.2.5 Spectral Mixture Analysis Accuracy Assessments 69
3.2.6 *Phragmites* Invasion Mapping 72
3.2.7 Dominant Fraction Classification 72
3.3 Results and Discussion 73
3.3.1 ASD Measurements and Image Derived Spectral Signatures 73
3.3.2 Spectral Mixture Analysis Results 76
3.3.2.1 Model Performance 76
3.3.2.2 Ground Truth Versus Spectral Mixture Analysis Plots 77
3.3.2.3 *Phragmites* Fraction Difference Histogram 80
3.3.2.4 Land Cover Abundance Layers 84
3.3.2.4.1 Grayscale Distribution and Abundance 84

3.3.2.4.2 Colour Composite Distribution and Abundance 86

3.3.2.4.3 Classified Worldview-2 as a Ground Truth Source 87

3.3.2.5 *Phragmites* Invasion Mapping 91

3.3.2.6 Dominant Fraction Classification 93

3.4 Conclusions 95

3.5 References 99

Chapter 4 103

4 Conclusion 103

4.1 Summary 103

4.2 Conclusions 105

4.3 Contributions of this Research 106

4.4 Possible Future Research 107

4.4.1 High Resolution Imagery 107

4.4.2 Multiple Endmember Spectral Mixture Analysis 107

4.5 References 108

Appendices 109

A.1 Smoothing Filter-based Intensity Modulation 109

A.1 References 109

A.2 Land Cover Types of Walpole Island 110

Curriculum Vitae 123

List of Tables

Table 2.1 Comparison of the spectral bands captured by high-resolution multispectral satellites IKONOS-2 and Worldview-2 21

Table 2.2 Spectral indices used for additional information for image classification..... 22

Table 2.3 Land cover class areas mapped using method 2: eight band imagery and object-based method. 35

Table 2.4 Area covered by wetland vegetation for the WIFN study area mapped using the eight band imagery and object-based method..... 36

Table 2.5 Accuracy statistics for the four classification methods. 41

Table 2.6 Accuracy statistics for the four classification methods and binary Phragmites versus Non-Phragmites classification. 43

Table 3.1 Details of the CHRIS PROBA spectral bands acquired for this study. 56

Table 3.2 Overview of CHRIS PROBA operating modes..... 57

Table 3.3 Endmembers chosen using Pixel Purity Index values. 65

Table 3.4 Spectral Mixture Analysis model performance. 77

Table 3.5 Accuracy of the SMA fractions when Phragmites ground truth fraction is broken down into categories of 0, mixed and 1 fraction cover..... 84

Table 3.6 Colour composite interpretation key..... 87

Table 3.7 Accuracy of the Phragmites invasion map from thresholding spectral mixture analysis (SMA) Phragmites fractions. 92

Table 3.8 Results of the spectral angle mapper (SAM) classification compared against the dominant fraction based on ground truth fractions from Worldview-2. 93

Table 3.9 Classification results based on the dominant fraction in each pixel. 94

List of Figures

Figure 1.1 The Walpole Island First Nation study area 7

Figure 1.2 Worldview-2 imagery acquired for *Phragmite*s mapping..... 8

Figure 1.3 CHRIS PROBA imagery acquired for Phragmites mapping 9

Figure 2.1 The study site of Walpole Island First Nation..... 20

Figure 2.2 An overview of the object-based classification method..... 24

Figure 2.3 Image segmentation of Agricultural Fields 26

Figure 2.4 Image segmentation of Water..... 29

Figure 2.5 Image segmentation of Roads. 31

Figure 2.6 Worldview-2 object-based and per-pixel classification results. 42

Figure 3.1 Walpole Island First Nation study site 54

Figure 3.2 Worldview-2 and CHRIS PROBA imagery of the study area. 55

Figure 3.3 Worldview-2 classification result for SMA fraction accuracy assessment. 58

Figure 3.4 Flowchart outlining the method used in this study. 61

Figure 3.5 Eigenvalue plot for the 37 Minimum Noise Fraction (MNF) bands 63

Figure 3.6 The method used to extract land cover ground truth fractions from the classified Worldview-2 image. 71

Figure 3.7 The method used to assign the dominant class to each pixel 73

Figure 3.8 Reflectance spectra of the three land covers from field ASD spectroradiometer measurements and pure CHRIS PROBA image pixels. 75

Figure 3.9 Regression plots of the six SMA models for the *Phragmites* class..... 79

Figure 3.10 Fraction error histograms of the six SMA models for the *Phragmites* class. 81

Figure 3.11 Fraction error histograms for Test1 (PPI-1) for the *Phragmites* class, broken down by Phragmites ground truth cover of 0%, mixed and 100%. 83

Figure 3.12 The ground truth and SMA predicted fraction maps for Test1 (PPI-1) for the three land cover types 85

Figure 3.13 Colour composite maps for the ground truth and Test1 SMA fraction layers 87

Figure 3.14 Canopy structure differences between *Typha* and *Phragmites* 90

Figure 3.15 *Phragmites* three class invasion map based on spectral mixture analysis (SMA) fractions and thresholds. 92

Figure 3.16 Spectral angle mapper (SAM) classification of *Phragmites* and Other land cover class map. 93

Figure 3.17 Classification maps based on the dominant land cover fraction in each pixel for a) ground truth from Worldview-2, b) spectral mixture analysis and c) spectral angle mapper from CHRIS PROBA. 95

List of Appendices

Appendices 109

A.1 Smoothing Filter-based Intensity Modulation 109

A.1 References 109

A.2 Land Cover Types of Walpole Island First Nation 110

List of Abbreviations

AISA – Airborne Imaging Spectrometer for Applications

ASD – Analytical Spectral Device

ASD-A – ASD measurements for August

ASD-O – ASD measurements for October

B – Blue

CB – Coastal Blue

CHRIS PROBA – Compact High Resolution Imaging Spectrometer on Project for On-Board Autonomy – 1

G – Green

GIS – Geographic Information System

ha – hectares

LiDAR – Light Detection and Ranging

MESMA – Multiple Endmember Spectral Mixture Analysis

MLC – Maximum Likelihood Classifier

MNF – Minimum Noise Fraction

NAD83 – North American Datum 1983

N-DV – N-Dimensional Visualizer

NDVI – Normalized Difference Vegetation Index

NDWI – Normalized Difference Water Index

NIR1 – Near Infrared 1

NIR2 – Near Infrared 2

NMV – Native Marsh Vegetation

OB – Object-Based

P – Panchromatic

PA – Producer's Accuracy

PCA – Principal Components Analysis

PPI – Pixel Purity Index

R – Red

R-E – Red-Edge

RMSE – Root Mean Square Error

SAM – Spectral Angle Mapper

SFIM – Smoothing Filter-based Intensity Modulation

SMA – Spectral Mixture Analysis

SR – Simple Ratio

UA – User's Accuracy

UTM – Universal Transverse Mercator

WIFN – Walpole Island First Nation

WV-2 – Worldview-2

Y – Yellow

Chapter 1

1 Introduction

1.1 Research Context

Healthy wetlands provide many environmentally valuable functions. Wetlands are capable of recharging groundwater resources and providing storage of flood waters. Wetland vegetation provides pollution control by trapping and reducing sediments in the water column and by acting as sinks for nutrients and toxic substances. Vegetation also acts as a buffer for coastal protection from erosion by waves. Wetland vegetation also provides habitat and resources for fish, birds, mammals, reptiles and amphibians. Wetlands have high economic value providing many natural products and recreational opportunities (Jaworski, 1978, cited by Herdendorf, 1992).

Despite these beneficial functions, wetlands continue to be drained, filled, and converted to other uses such as agricultural land and urban areas. Prior to European settlement, southern Ontario contained an estimated 2.4 million hectares of wetlands, of which less than 39% remained by 1982 (Snell, 1987). Projected future population increases in Ontario (Ontario Ministry of Finance, 2012), will put even more pressure on these remaining wetland areas.

Additional pressure is put on wetland vegetation by non-native plant species. Non-native species are recognized as a serious threat to vegetation communities in Canada. This has led to the recent development of an invasive species strategy for Ontario (Ontario Ministry of Natural Resources, 2012), and Canada (Canadian Food Inspection Agency, 2004). Identified in 2005 by Agriculture and Agri-Food Canada as the nation's worst invasive plant species (Ontario Ministry of Natural Resources, 2011), *Phragmites australis* (Cavenilles) Trinius ex. Steudel subsp. *australis* (common reed) presents an immediate threat to native wetland vegetation. The invasive *Phragmites* is a superior competitor compared with native North American species of *Phragmites*, *Phragmites australis* subsp. *americanus* Saltonstall, P.M. Peterson & Soreng (Saltonstall et al., 2004) having a higher root and stem density, higher aboveground biomass, longer growing

season, and is tolerant of a wider range of salinities (Chambers et al., 1999; League et al., 2006). These traits also give invasive *Phragmites* an advantage over native wetland plants that cannot compete for nutrients, light and space resources, allowing *Phragmites* monocultures to develop quickly (Meyerson et al., 2009). These traits have allowed invasive *Phragmites* to spread throughout fresh, brackish, and salt water marsh systems in the United States and Canada (Mal & Narine, 2004). *Phragmites* is now well established along the Atlantic coast (Chambers et al., 1999), and in the Great Lakes region, where expansion has been noted in Lake Erie (Wilcox et al., 2003; Ghioca-Robrecht et al., 2008), Lake St. Clair (Arzandeh & Wang 2003), and Lake Michigan (Pengra et al., 2007; Tulbure et al., 2007). It is hypothesized that recent climatic changes, have allowed for rapid growth of this species in Lake Erie coastal wetlands (Wilcox et al., 2003). With the forecasted rise in atmospheric CO_2 levels in the future, *Phragmites* growth is expected to increase (Farnsworth & Meyerson, 2003).

To deal with this invasion effectively, it is crucial that methods are developed to monitor the distribution and abundance of invasive and native vegetation species over time (Adam et al., 2010). These methods should be capable of establishing an invasion baseline, and allow for monitoring the invasive plant propagation with the goal of providing information needed to implement an effective plan to deal with the invasion. Collection of this type of information has traditionally been acquired by labour intensive, costly, and time-consuming field work (Lee & Lunetta, 1996). The characteristics of the wetland environment make the amount of field work needed to monitor a rapidly propagating species like *Phragmites* impractical.

Remote sensing provides an alternative method for the production of this important information which reduces costs, labour, and saves time relative to field work. The design of remote sensing systems allows for repeat coverage of large areas providing up-to-date information and an archive of images that can be used for detecting change. Assessment of the remote sensing results still requires field work, but at a greatly reduced effort. The information collected and extracted from imagery is already in digital format which allows for integration and further analysis in a Geographic Information System (GIS) (Ozesmi & Bauer, 2002).

Two types of remote sensing sensors have typically been used for *Phragmites* mapping. High-spatial-resolution satellite imagery provides the ability to detect very small patches of vegetation, which is important for early detection and removal of the invader. One disadvantage of these sensors is their poor spectral resolution which can lead to confusion between *Phragmites* and other vegetation species if their spectral properties are similar (e.g. Laba et al., 2008). A method commonly used to overcome this shortfall, is to incorporate additional information into the mapping process to increase separation of vegetation at the species level. Additional information has included obtaining multiple images over the growing season (e.g. Ghioca-Robrecht et al., 2008) to take advantage of the changes in spectral signature of the *Phragmites* and native vegetation throughout the year. Gilmore et al. (2008) used several QuickBird-2 images collected over multiple years and height information from Light Detection and Ranging (LiDAR) data to classify *Phragmites* in an Eastern North American coastal estuary and obtained high accuracy for the *Phragmites* class. Adding this additional information to the classification increases cost and may not be available for large areas, making accurate monitoring of *Phragmites* at regular time intervals and over large areas less likely to be successful.

The other commonly employed sensor for mapping *Phragmites* has been airborne hyperspectral imagery. This sensing platform has the ability to collect many narrow and contiguous spectral bands at high spatial resolution, allowing for detailed *Phragmites* mapping. Artigas and Yang (2005) used an Airborne Imaging Spectrometer for Applications (AISA) image with 2.5m spectral resolution and 34 spectral bands to map *Phragmites* vigour gradients in an Eastern North American coastal estuary with high accuracy. Artigas and Pechmann (2010) used AISA imagery for *Phragmites* mapping and were able to map the fractional abundance of *Phragmites* in mixed land cover type pixels with 75% or more coverage with 96% accuracy. However, classification accuracy dropped substantially when *Phragmites* coverage was 50% or less. Airborne hyperspectral sensors are capable of monitoring *Phragmites* spread, however, the data is more expensive than satellite imagery, and the revisit time depends on aircraft availability and tasking (Adam et al., 2010).

A recently launched high-resolution satellite sensor, Worldview-2, has expanded spectral capabilities compared to traditional high-resolution sensors such as QuickBird-2 or IKONOS-2, and may provide the spectral information needed to discriminate accurately between invasive *Phragmites* and native marsh vegetation. Additional spectral bands include a second blue band, a yellow band, a red-edge band, and a second near-infrared band. Worldview-2 has not been used previously to map *Phragmites* in Great Lakes coastal wetlands. The combination of high-spatial and spectral-resolution data may allow for more accurate mapping of *Phragmites* in this environment.

The Compact High Resolution Imaging Spectrometer on the Project for On-Board Autonomy – 1 (CHRIS PROBA) platform, a hyperspectral satellite, capable of acquiring 37 spectral bands at 17m resolution, may provide another source of data for monitoring *Phragmites*. Pengra et al. (2007) used 30m Hyperion hyperspectral satellite imagery and the Spectral Correlation Mapper algorithm to map *Phragmites* on Green Bay, Lake Michigan, and it is the only other known study to use satellite hyperspectral imagery for *Phragmites* mapping in the Great Lakes. CHRIS PROBA imagery has not been used previously to map *Phragmites* and will be evaluated for this purpose in a Great Lakes coastal wetland.

1.2 Research Objectives

The objective of this research is to evaluate two imagery sources, Worldview-2 high-spatial resolution multispectral imagery and CHRIS PROBA hyperspectral satellite imagery, for mapping *Phragmites* cover in a Great Lakes coastal wetland. Imagery from neither satellite has been used for this purpose before. The expanded spectral capability of Worldview-2 may allow for more accurate mapping of *Phragmites* from a single image. CHRIS PROBA has high spectral resolution and the highest spatial resolution available from any hyperspectral satellite sensor. A single date of imagery may provide highly accurate sub-pixel abundance estimates of *Phragmites* cover that can be used to monitor the spread of this species in Great Lakes coastal wetlands.

The research in this thesis will seek to provide the answers to these questions:

1. How accurately can *Phragmites* cover be classified from Worldview-2 high-resolution satellite imagery?

2. How do the four additional bands acquired by the Worldview-2 sensor, not captured by traditional high-resolution satellites (e.g. QuickBird-2, IKONOS-2), affect the accuracy of the *Phragmites* classification?

3. How accurate are the fraction estimates for the three land cover classes derived from CHRIS PROBA hyperspectral satellite imagery using spectral mixture analysis?

4. Can the classified Worldview-2 image from be used as ground truth to evaluate the fraction estimates derived by spectral mixture analysis methods from CHRIS PROBA?

5. Can the *Phragmites* fraction layer provide accurate information about the state of *Phragmites* invasion in a marsh?

6. Can the individual fraction layers be combined to provide accurate information about the distribution of dominant land covers in a marsh?

The studies presented in Chapter 2 and Chapter 3 answer these research questions by addressing these research objectives:

1. a) To develop an object-based method for *Phragmites* cover extraction from a single date high-spatial-resolution Worldview-2 image. b) To evaluate the differences in classification accuracy when four and eight spectral band datasets are used for object-based classification of *Phragmites*.

2. a) To assess the capability of CHRIS PROBA hyperspectral satellite imagery to produce highly accurate sub-pixel abundance estimates of *Phragmites* cover using a linear spectral mixture analysis method. b) To assess the ability of the classified Worldview-2 image from to be used as ground truth to determine the accuracy of the abundance estimates from spectral mixture analysis. c) To evaluate the capability of the abundance layers to provide information about the state of *Phragmites* invasion and the distribution of dominant land covers in the marsh.

1.3 Study Area

Walpole Island First Nation (WIFN) (82° 30’ W and 42° 33’ N) is the study area for this research (Figure 1.1). It is located at the north end of Lake St. Clair in Lambton County, Ontario, Canada. Walpole Island is a delta, formed as the sediments carried by the St. Clair River are deposited as the river slows to meet Lake St. Clair (Environment Canada, 2003). The six islands of WIFN cover 24,000 ha (Woodliffe, 1989) and of this area, the coastal wetlands cover approximately 10,360 ha. They represent one of the largest remaining coastal wetlands in the Great Lakes (Environment Canada, 2003). About half of the wetlands in the St. Clair delta have been diked and pumps manipulate water levels for marsh management related to the production of waterfowl (Bookhout et al., 1989). The delta coastal marshes provide habitat for many plants and animals, some of which are provincially, nationally, and even globally rare (Environment Canada, 2003). *Typha* spp. (Cattail spp.) are the dominant native vegetation while *Zizania palustris* (Wild Rice), *Scirpus* spp. (Bulrush spp.), *Pontederia cordata* (Pickerelweed), *Nuphar variegatum* (Yellow Pond Lily), and *Nymphaea odorata* (Fragrant White Water Lily) are sparsely

distributed. *Phragmites australis* subsp. *australis*, is of concern at Walpole as it is expanding at the expense of native species (Arzandeh & Wang, 2003). Based on herbarium samples, the first occurrence of non-native *Phragmites* in southwestern Ontario was at Walpole Island in 1948 (Catling & Mitrow, 2012).

Figure 1.1 shows the study area for this research. Chapter 2 will utilize a 40km^2 high-resolution Worldview-2 image covering portions of Bassett, Squirrel, and Walpole Islands (Figure 1.2), to extract *Phragmites* cover using an object-based method. Chapter 3 will focus on a small area on Squirrel Island to allow a detailed accuracy assessment of the fraction layers extracted from CHRIS PROBA imagery (Figure 1.3) using a linear spectral unmixing method. Detailed descriptions of the respective study areas are given in each chapter.

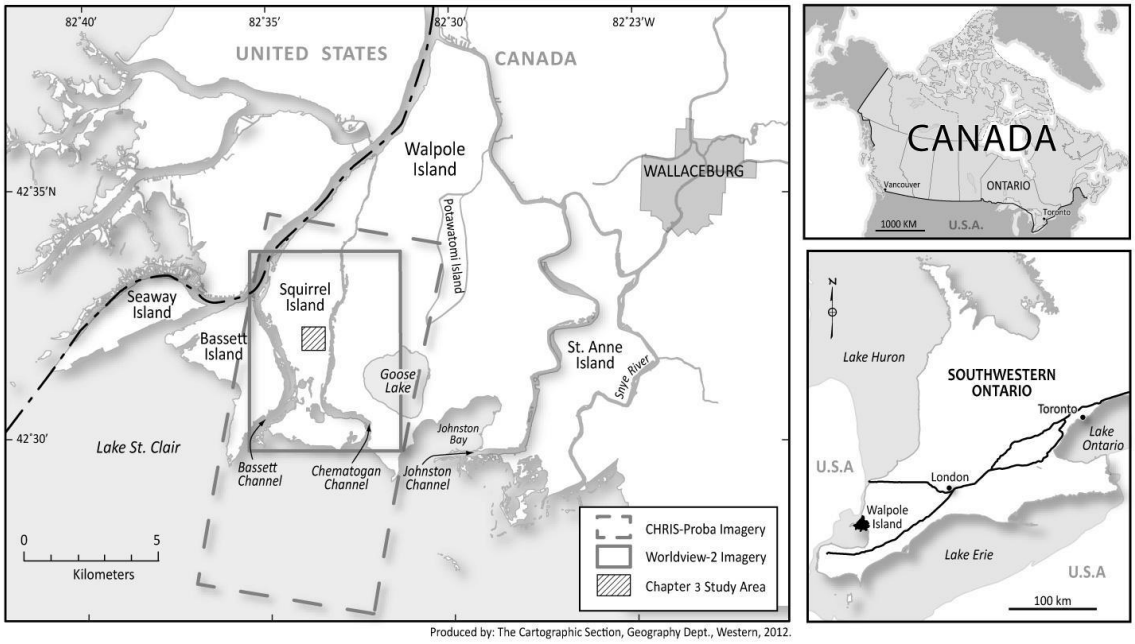

Figure 1.1 The Walpole Island study area. Chapter 2 uses the entire Worldview-2 image for wetland classification while Chapter 3 focuses on a small area on Squirrel Island.

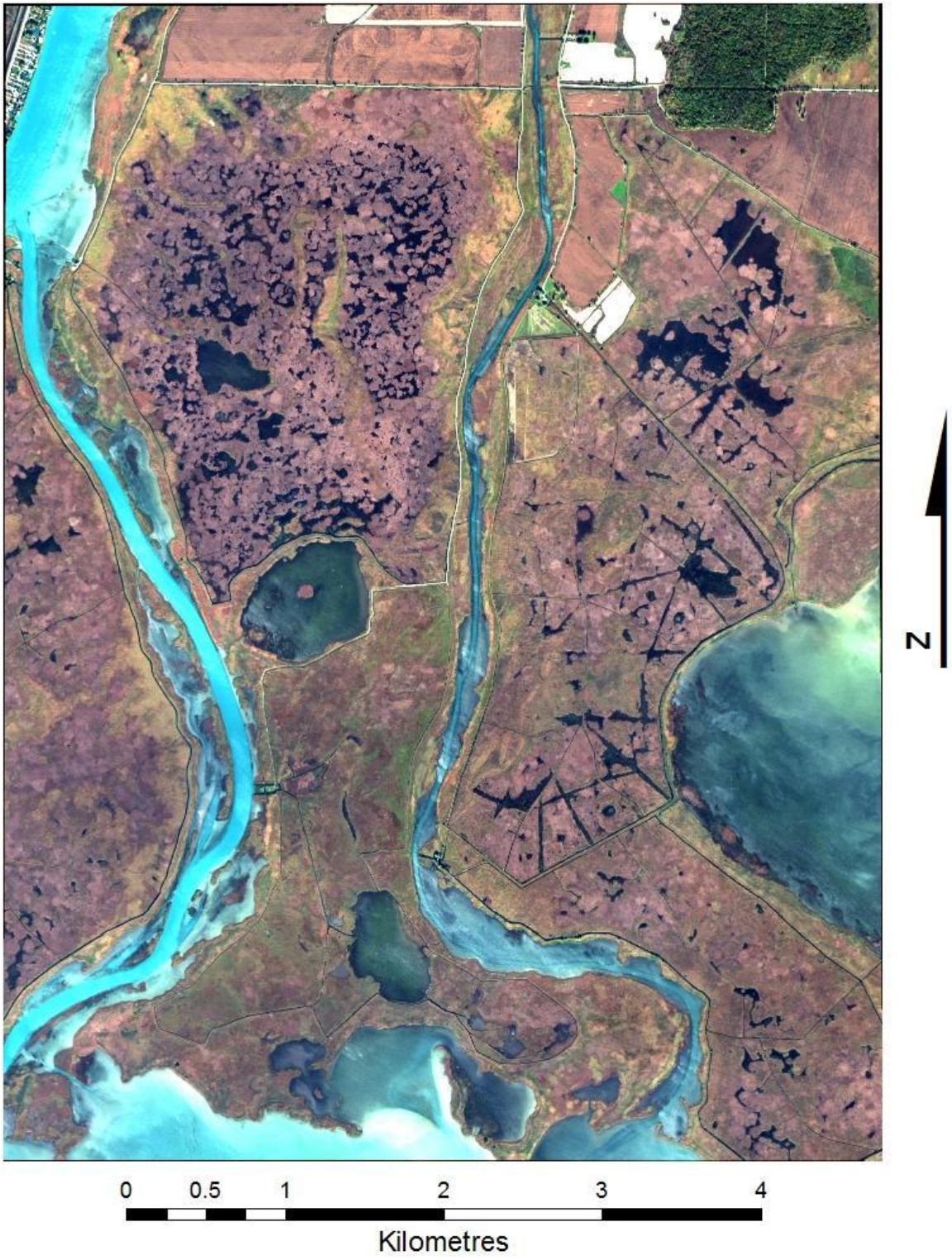

Figure 1.2 Worldview-2 imagery acquired October 17, 2010, shown in true colour (Red: Band 5, Green: Band 3, Blue: Band 2).

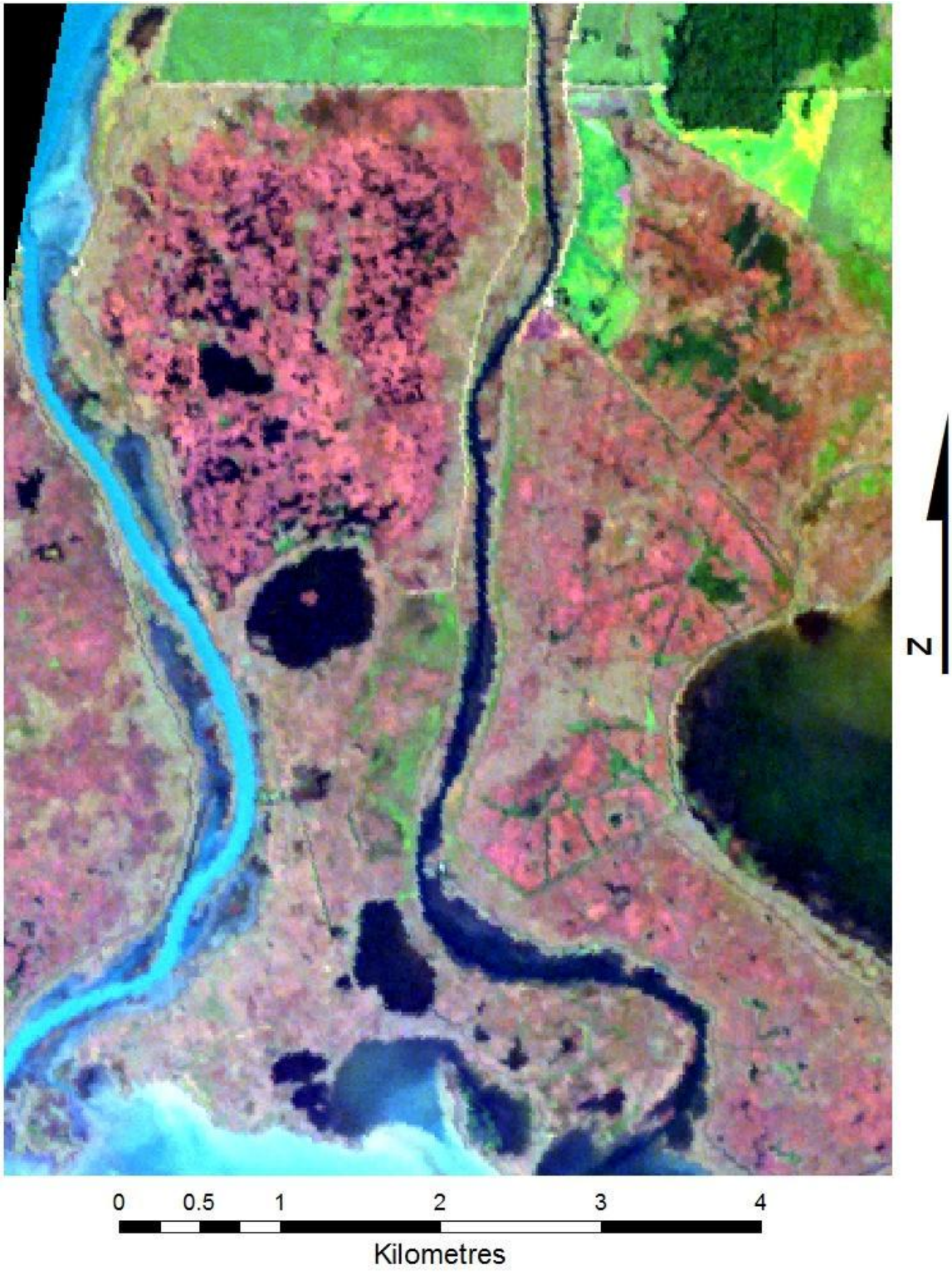

Figure 1.3 CHRIS PROBA image acquired September 14, 2011, shown in true colour (Red: Band 7, Green: Band 4, Blue: Band 1).

1.4 Background

The two main methods used in the analysis of the imagery in this research are discussed below. Chapter 2 uses an object-based classification method to extract the wetland land cover classes. Chapter 3 uses a spectral mixture analysis method to extract sub-pixel abundances of *Phragmites*, native marsh vegetation, and water.

1.4.1 Object-Based Classification

In object-based classification, image objects form the basic unit which is used to classify the image. This is much different from traditional image classification methods where the pixel forms the basic unit. These image objects are created in a process called image segmentation. The multiresolution segmentation algorithm is a commonly used method for grouping pixels into image objects and is used in Chapter 2. With this algorithm, image objects start out as individual pixels, and are merged with neighbouring pixels or other image objects until a threshold describing the image objects homogeneity is exceeded (Definiens, 2010). The homogeneity criterion is controlled by adjusting the weight assigned to spectral homogeneity and shape homogeneity. More weight given to the spectral criterion results in grouping of pixels into objects that are more spectrally similar. More weight given to the shape criterion optimizes objects according to object compactness or border smoothness. A scale parameter is also specified which controls the size of the resulting objects. Higher scale values result in larger objects, while lower scale values result in smaller objects (Definiens, 2010). Segmentation can be applied to original image layers, or existing object layers can be segmented again. This creates multiple levels of objects and allows for image objects to be classified in a hierarchical structure (Definiens, 2010). For example, objects at the first object level, can be separated into vegetation and water objects, and a second level of objects could be separated into wetland and non-wetland vegetation.

Once the user is satisfied with the resulting image object layer, the image objects can be classified by their attributes. Object attributes include their colour, shape, texture, or context within the image. One option is to classify objects using rules. For example, a rule can specify that all image objects with a value less than 20 in the red band are

assigned to the class “Water”. A second option is to use a semi-automated supervised classification to classify objects. The user selects training sample objects for each class and specifies object features which the classifier will use to assign objects to each class. Example objects features could include mean value of blue band, standard deviation of NDVI, length-to-width ratio, etc. In Chapter 2, both rules and a supervised classification are used to map land cover types in the Worldview-2 image.

1.4.2 Spectral Mixture Analysis

The spectral mixture analysis model used in this research is described in detail in Chapter 3, however, a brief overview will be given here. The spatial resolution of the CHRIS PROBA imagery is relatively large at 17m and this creates a problem when assigning each pixel to a land cover class. If the average size of marsh vegetation patches is larger than the image pixel resolution, the number of pixels containing multiple classes is reduced. However, smaller patches increase the likelihood that multiple land covers will be represented by a single pixel (Artigas & Yang, 2005). A traditional classifier such as maximum likelihood, would misrepresent or oversimplify mixed pixels (Rosso et al., 2005) by assigning them to the class with the highest probability based on training data (Jensen, 2005). To overcome the mixed pixel problem, the spectral mixture analysis method decomposes the pixel spectrum to extract the land cover type contained within it. If there is minimal scattering of the energy between different surface components before the signal is measured by the sensor, the mixing within a single pixel is assumed to be linear (Adams et al., 1993). This means that the pixel spectrum is a linear sum of the reflectance received from each land cover contained within it (Roberts et al., 1998). The land cover types present in the image are referred to as endmembers. When the spectral signatures of all pure endmember pixels are known, the signal of a mixed pixel is equal to the area or abundance of each endmember within that pixel. By using the linear spectral mixture analysis model, every pixel in the image can be broken down into its fraction abundance for each endmember. The fractional abundance for each endmember is output to a separate fraction layer so that the distribution and relative abundance of each endmember in the image can be known (Jensen, 2005).

1.5 Thesis Format

This research is presented in an integrated-article format. Chapter 1 provides background on the research problem, the objectives of the research, the study area, and the methods used to address the research problem.

A version of Chapter 2 was presented at the 33rd Canadian Symposium on Remote Sensing (CSRS), in Ottawa, Ontario in June, 2012. A version of Chapter 2 was submitted for publication in the Special Issue of the Canadian Journal of Remote Sensing for the 33rd CSRS.

The focus of both studies is to extract *Phragmites* cover as accurately as possible. The chapters work toward this goal using different imagery sources and image processing methods. The focus of Chapter 2 is on extracting *Phragmites* cover from a single date high-resolution multispectral Worldview-2 image using an object-based method. Chapter 3 uses hyperspectral satellite imagery and a linear spectral mixture analysis method to extract the sub-pixel abundance of *Phragmites* in each pixel. The classification results from Chapter 2 are used as ground truth in Chapter 3 to assess the accuracy of the spectral mixture analysis derived fraction layers. The fraction layers are classified to produce important information about the state of *Phragmites* invasion and distribution of dominant land covers within the marsh.

1.6 References

Adam, E., Mutanga, O., & Rugege, D. (2010). Multispectral and hyperspectral remote sensing for identification and mapping of wetland vegetation: a review. *Wetlands Ecology and Management, 18*(3), 281-296. DOI: 10.1007/s11273-009-9169-z.

Adams, J.B., Smith, M.O. & Gillepsie, A.R. (1993). Imaging spectroscopy: Interpretation based on spectral mixture analysis. In C. M. Pieters & P. Englert (Eds.), *Remote geochemical analysis: Elemental and Mineralogical Composition.* New York, NY: Cambridge University Press. pp. 145-166.

Artigas, F., & Pechmann, I.C. (2010). Balloon imagery verification of remotely sensed *Phragmites australis* expansion in an urban estuary of New Jersey, USA. *Landscape and Urban Planning*, *95*(3), 105-112.

Artigas, F. J., & Yang, J. S. (2005). Hyperspectral remote sensing of marsh species and plant vigour gradient in the New Jersey Meadowlands. *International Journal of Remote Sensing*, *26*(23), 5209-5220.

Arzandeh, S., & Wang, J. (2003). Monitoring the change of *Phragmites* distribution using satellite data. *Canadian Journal of Remote Sensing, 29*(1), 24-35.

Bookhout, T. A., Bednarik, K. E., & Kroll, R. W. (1989). The Great Lakes marshes. *Smith, LM, Pederson, RL, Kaminski, RM, Habitat Management for Migrating and Wintering Waterfowl in North America*, 131-156.

Canadian Food Inspection Agency. (2004). An Invasive Alien Species Strategy for Canada. Ottawa. 46 pp.

Catling, P. M., & Mitrow, G. (2012). The Recent Spread and Potential Distribution of *Phragmites australis* subsp. *australis* in Canada. *The Canadian Field-Naturalist, 125*(2), 95-104.

Chambers, R. M., Meyerson, L. A., & Saltonstall, K. (1999). Expansion of *Phragmites australis* into tidal wetlands of North America. *Aquatic Botany, 64*(3), 261-273.

Definiens. (2010). *Definiens eCognition 8.0.1 Reference Book*. Definiens AG, Munchen, Germany.

Environment Canada. (2003). *The Ontario great lakes coastal wetland atlas: A summary of information (1983-1997)* (Catalogue Number CW66-221/1997E). Peterborough, ON: Ontario Ministry of Education.

Farnsworth, E. J., & Meyerson, L. A. (1999). Species composition and inter-annual dynamics of a freshwater tidal plant community following removal of the invasive grass, *Phragmites australis*. *Biological Invasions, 1*(2), 115-127.

Ghioca-Robrecht, D. M., Johnston, C. A., & Tulbure, M. G. (2008). Assessing the use of multiseason Quickbird imagery for mapping invasive species in a Lake Erie coastal marsh. *Wetlands, 28*(4), 1028-1039. DOI: http://dx.doi.org/10.1672/08-34.1.

Gilmore, M. S., Wilson, E. H., Barrett, N., Civco, D. L., Prisloe, S., Hurd, J. D., & Chadwick, C. (2008). Integrating multi-temporal spectral and structural information to map wetland vegetation in a lower Connecticut River tidal marsh. *Remote Sensing of Environment, 112*(11), 4048-4060. doi:10.1016/j.rse.2008.05.020.

Herdendorf, C. E. (1992). Lake Erie coastal wetlands: an overview. *Journal of Great Lakes Research, 18*(4), 533-551.

Jaworski, E., & Raphael, C. N. (1978). *Fish, wildlife and recreational values of Michigan's coastal wetlands*. U.S. Fish and Wildlife Services, Twin Cities, Minnesota.

Jensen, J. R. (2005) *Introductory digital image processing: A remote sensing perspective* (3rd ed.) (p. 456). Upper Saddle River, N.J.: Pearson Prentice Hall.

Laba, M., Downs, R., Smith, S., Welsh, S., Neider, C., White, S., Richmond, M., Philpot, W. & Baveye, P. (2008). Mapping invasive wetland plants in the Hudson River National Estuarine Research Reserve using quickbird satellite imagery. *Remote Sensing of Environment, 112*(1), 286-300. doi:10.1016/j.rse.2007.05.003.

League, M. T., Colbert, E. P., Seliskar, D. M., & Gallagher, J. L. (2006). Rhizome growth dynamics of native and exotic haplotypes of *Phragmites australis* (common reed). *Estuaries and Coasts*, *29*(2), 269-276.

Lee, K. H., & Lunetta, R. S. (1996). Wetland detection methods. In: Wetland and Environmental Application of GIS. Lyon, J.G., McCarthy, J. (eds). Lewis Publishers, New York, pp. 249–284.

Mal, T. K., & Narine, L. (2004). The biology of Canadian weeds. 129. Phragmites australis (Cav.) Trin. ex Steud. *Canadian Journal of Plant Science*, *84*(1), 365-396.

Meyerson, L. A., Saltonstall, K., and Chambers, R. M. (2009). *Phragmites australis* in Eastern North America: A Historical and Ecological Perspective. In Human impacts on salt marshes: a global perspective. Silliman, B.R., Grosholz, E.D., and Bertness, M.D. (eds). University of California Press, Berkeley, pp. 57-82.

Ontario Ministry of Finance. (2012). Ontario Population Projections Update. Available from <http://www.fin.gov.on.ca/en/economy/demographics/projections/> [cited (July 6, 2012)].

Ontario Ministry of Natural Resources. (2011). Invasive Phragmites – Best Management Practices, Ontario Ministry of Natural Resources, Peterborough, Ontario. 15 pp.

Ontario Ministry of Natural Resources. (2012). Ontario Invasive Species Strategic Plan. Toronto: Queen's Printer for Ontario. 58 pp.

Ozesmi, S. L., & Bauer, M. E. (2002). Satellite remote sensing of wetlands. *Wetlands Ecology and Management*, *10*(5), 381-402.

Pengra, B. W., Johnston, C. A., & Loveland, T. R. (2007). Mapping an invasive plant, *Phragmites australis*, in coastal wetlands using the EO-1 Hyperion hyperspectral sensor. *Remote Sensing of Environment*, *108*(1), 74-81.

Roberts, D. A., Gardner, M., Church, R., Ustin, S., Scheer, G., & Green, R. O. (1998). Mapping chaparral in the Santa Monica Mountains using multiple endmember spectral mixture models. *Remote Sensing of Environment*, *65*(3), 267-279.

Saltonstall, K. (2002). Cryptic invasion by a non-native genotype of the common reed, *Phragmites australis*, into North America. Proceedings of the National Academy of Sciences, 99(4), 2445-2449.

Saltonstall, K., Peterson, P. M., & Soreng, R. J. (2004). Recognition of *Phragmites australis* Subsp. *americanus* (Poaceae: Arunidnoideae) in North America: Evidence from Morphological and Genetic Analyses.

Snell, E. A. (1987). Wetland Distribution and Conservation in Sothern Ontario. Working Paper No. 48. Ottawa: Environment Canada, Inland Waters and Lands Directorate.

Rosso, P. H., Ustin, S. L., & Hastings, A. (2005). Mapping marshland vegetation of San Francisco Bay, California, using hyperspectral data. *International Journal of Remote Sensing*, *26*(23), 5169-5191.

Tulbure, M. G., Johnston, C. A., & Auger, D. L. (2007). Rapid Invasion of a Great Lakes Coastal Wetland by Non-Native *Phragmites australis* and *Typha*. *Journal of Great Lakes Research, 33,* 269-279.

Wilcox, K. L., Petrie, S. A., Maynard, L. A., & Meyer, S. W. (2003). Historical distribution and abundance of *Phragmites aust*ralis at Long Point, Lake Erie, Ontario. *Journal of Great Lakes Research, 29*(4), 664-680.

Woodliffe, P. A. (1989). Inventory, Assessment, and Ranking of Natural Areas of Walpole Island.

Chapter 2

2 Object-Based Classification of Worldview-2 Imagery for Mapping Invasive *Phragmites australis*

2.1 Introduction

Wetlands provide important habitat for plants and animals such as nesting sites for waterfowl and spawning grounds for fish. Wetland vegetation protects shorelines from erosion and traps sediment before it enters water bodies. The quality of water passing through wetlands can be improved because wetlands filter contaminants and nutrients. Wetlands also renew groundwater supplies, and help to control flooding which in turn reduces damage caused by flooding. Finally, wetlands are an important economic resource as they provide natural products and provide recreational opportunities such as hunting, fishing, and bird watching (Jaworski, 1978, as cited by Herdendorf, 1992).

Unfortunately, wetlands are being lost at a fast rate due to drainage, conversion, pollution, and over-exploitation of their resources. In southern Ontario prior to European settlement, it is estimated that there were 2.4 million ha of wetlands. Roughly 933,000 ha or 61% of this wetland area had been lost to development by 1982 (Snell, 1987). As of 2011, southern Ontario was home to 13.4 million people and the population is expected to increase to 17.7 million by 2036 (Ontario Ministry of Finance, 2012), which will increase the level of pressure on the existing wetland areas. Another problem facing wetlands is the detrimental effects of the introduction of invasive species. Invasive plant species can decrease plant diversity, threaten rare and endangered native species, and decrease habitat quality for birds and animals (Laba et al., 2008). Of particular concern in North American wetlands is the introduction of *Phragmites australis* (Cavenilles) Trinius ex. Steudel subsp. *australis* (common reed) (Saltonstall, 2002, Mal and Narine, 2004), hereafter referred to as *Phragmites*. This invasive subspecies has been displacing native *Phragmites* (Saltonstall, 2002) as well as other wetland vegetation species (Lavoie, 2008). The effects of the invasion by *Phragmites* on fish, birds, and mammals is mixed and not well studied in freshwater wetlands (Lavoie, 2008).

An important tool for the management of invasive wetland vegetation is accurate and up-to-date vegetation maps (Parker Williams and Hunt, 2002). If the location and abundance of the species of interest is known, then an effective plan for controlling the spread can be implemented. Traditionally on-ground field surveys have provided information about wetland vegetation species distribution and abundance. However, this method is time consuming and labour intensive (Laba et al., 2008), especially when conducted over large areas. Also, field surveys may not be feasible due to restrictions on accessibility posed by the wetland environment. Remote sensing provides an alternative to on-ground field surveys. Imagery from aerial or satellite platforms can be captured over large areas, and can make repeat observations of the same area (Ozesmi and Bauer, 2002). This makes remote sensing imagery an ideal source for mapping wetlands for widespread management of invasive plant species such as *Phragmites* (Adam et al., 2010).

Mapping of *Phragmites* using satellite remote sensing in North American freshwater coastal wetlands and estuarine marshes has been limited. Laba et al. (2008) used a single-date QuickBird-2 image from August and the maximum likelihood classifier to map *Phragmites* in an estuarine marsh. User's and producer's accuracy of *Phragmites* was 76% and 100% respectively. Ghioca-Robrecht et al. (2008) conducted an unsupervised classification using multi-date QuickBird-2 multispectral imagery (April and September) of Erie Marsh, one of the largest marshes in Lake Erie. *Phragmites* was mapped with a user's and producer's accuracy of 76% and 53% respectively. Separation of *Phragmites* and other wetland plant species from multi-date imagery alone was not good. Individual plant species can be mapped from multi-date high resolution multispectral imagery with high accuracy if additional data are included. Gilmore et al. (2008) used LiDAR along with multi-temporal QuickBird-2 high spatial resolution imagery to map three wetland vegetation species *Phragmites*, *Typha* spp., and *Spartina patens* in a brackish tidal marsh. Based on a fuzzy accuracy assessment, *Phragmites* was mapped with 97% accuracy. However, LiDAR data is expensive for use in widespread wetland vegetation mapping on an annual basis. Also, multiple images increase the cost and may not be available due to weather conditions or satellite tasking restrictions.

Therefore, there is some room for improvement for mapping *Phragmites* using single-date satellite imagery. Individual land managers are limited in resources and expertise, therefore obtaining data gathered from multiple satellites, from multiple seasons, or non-optical data such as LiDAR may not be possible. An accurate method of mapping *Phragmites* from single-date imagery is a more attractive mapping solution.

Worldview-2 (WV-2) is a recently launched, high resolution satellite with eight 2 metre spatial resolution multispectral bands and a 0.5 metre Panchromatic band. WV-2 contains a Coastal Blue, Yellow, Red-Edge, and a second Near Infrared band (NIR2) in addition to the Blue, Green, Red, and Near Infrared (NIR1) bands of other high resolution multispectral satellites such as IKONOS-2 and QuickBird-2. Despite the increased spatial and spectral resolution, the WV-2 satellite has similar imaging capabilities as QuickBird-2 and IKONOS-2 including image acquisition size, large area and long strip collection, as well as stereo imaging abilities (refer to eoPortal Directory, 2012). With the launch of Worldview-3 in 2014, the Worldview constellation will be able to image a location on the earth's surface every two days (eoPortal Directory 2012).

WV-2 imagery has not been previously used for mapping individual wetland species. The goal of this research was to evaluate the use of WV-2 for mapping the invasive emergent species *Phragmites* in a Great Lakes coastal wetland. It was hypothesized that the eight multispectral bands possessed by Worldview-2 would increase classification results compared with other multispectral sensors (such as IKONOS-2, QuickBird-2) containing only four bands. Object-based methods were developed for both four and eight band imagery and the results compared. This comparison showed the advantage of using the full eight bands provided by the Worldview-2 sensor.

2.2 Study Area

Walpole Island First Nation (WIFN) was chosen as the study area for this investigation (Figure 2.1). It is located at the delta of the St. Clair River (82° 30’ W and 42° 33’ N) in Lambton County, Ontario, Canada. Two dominant wetland vegetation cover types are present in these extensive (greater than 10,000 ha) coastal freshwater marshes. *Typha* spp. are the dominant vegetation found in the marshes. Other native vegetation that are sparsely distributed included Wild Rice (*Zizania palustris*), Bulrush (*Scirpus* spp.), Pickerelweed (*Pontederia cordata*), Yellow Pond Lily (*Nuphar variegatum*), and Fragrant White Water Lily (*Nymphaea odorata*). An invasive wetland plant, *Phragmites*, is also present and it forms dense monotypic stands and displaces native vegetation. *Phragmites* is found within the diked marsh, in roadside ditches, directly beside road edges, and on the banks of rivers and streams (personal observation). WIFN marshes are the second most important staging area for waterfowl in southern Ontario (McCullough, 1985). *Phragmites* invasion of native vegetation species represents a loss of habitat for waterfowl and other wildlife.

Phragmites colonization has been a problem in North America and the Great Lakes region. Wilcox et al. (2003) noted an expansion of *Phragmites* at Long Point, Canada on Lake Erie. Digital mapping of aerial photographs revealed an exponential increase in non-native *Phragmites* from 1995 to 1999, with 33% of this change coming at the expense of *Typha* spp. (Wilcox et al. 2003). The marshes of WIFN have also been colonized by *Phragmites*. A previous study by Arzandeh and Wang (2003) detected a change of 1000 ha from *Typha* spp. to *Phragmites* between 1992 and 1998.

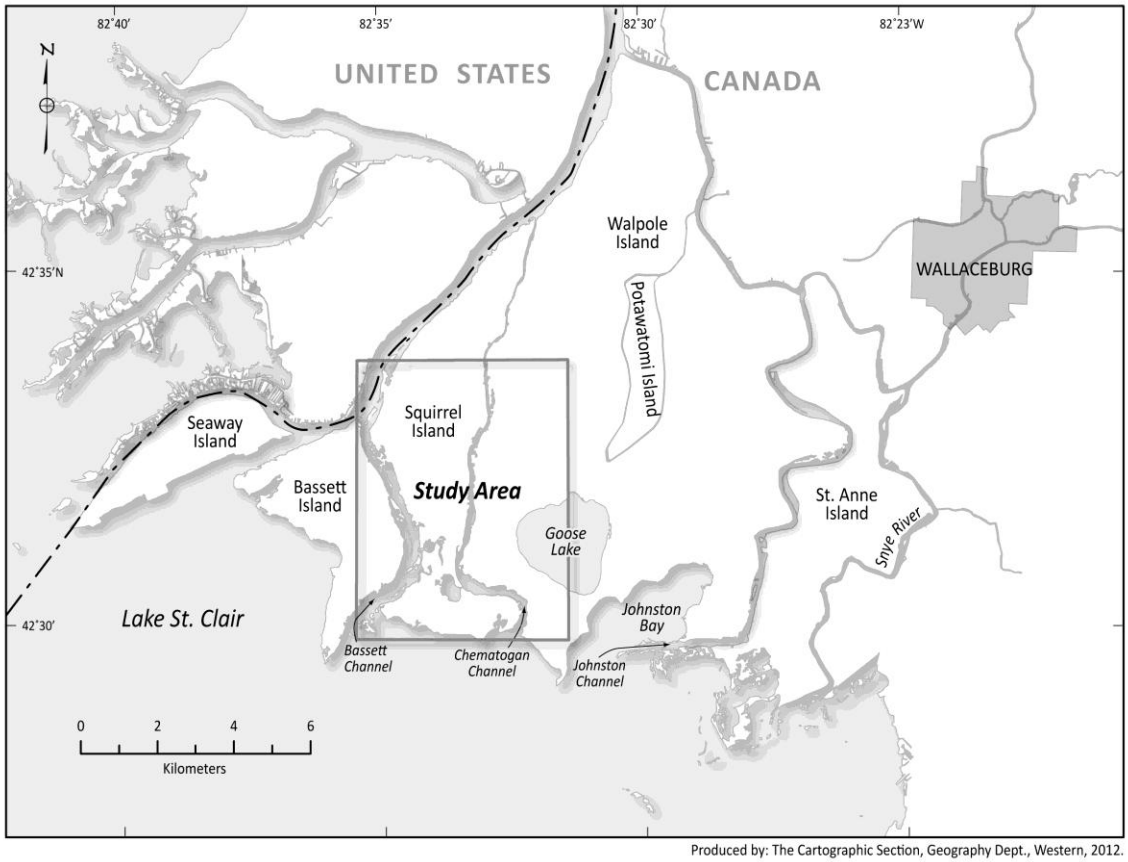

Figure 2.1 The study site of Walpole Island. The St. Clair River empties into Lake St. Clair here and is the site of one of the largest remaining coastal marshes in the southern Great Lakes region.

2.3 Imagery

The WV-2 satellite is a promising new source of imagery to test for this application due to its expanded spectral capabilities in the near infrared region. The WV-2 satellite collects three bands in the near infrared: Red-Edge, NIR1, and NIR2. Gilmore et al. (2008) found that *Phragmites* has a high NIR response late in the autumn and suggest that a single date of imagery captured during this time could be used to map this species. A Worldview-2 image collected on October 17, 2010 with 0% cloud cover was used for this study. The data were 11-bit radiometric resolution and were geo-referenced to the Universal Transverse Mercator (UTM) coordinate system, Zone 17 North, North American Datum 1983 (NAD83) by the image provider MacDonald, Dettwiler, and Associates Ltd., Richmond, British Columbia. Details of the individual spectral bands are

found in Table 2.1. The image is centered on Squirrel Island and includes the east side of Bassett Island and the west portion of the main Walpole Island (Figure 2.1).

Table 2.1 Comparison of the spectral bands captured by high-resolution multispectral satellites IKONOS-2 and Worldview-2

		Band Wavelength Coverage (nm)	
Spectral Band	Band Code	IKONOS-2*	Worldview-2†
Coastal Blue	CB	-	400-450
Blue	B	445-516	450-510
Green	G	506-595	510-580
Yellow	Y	-	585-625
Red	R	632-698	630-690
Red-Edge	R-E	-	705-745
Near Infrared 1	NIR1	757-853	770-895
Near Infrared 2	NIR2	-	860-1040
Panchromatic	P	526-928	450-800

*Satellite Imaging Corporation (2012), †eoPortal (2012)

2.4 Methods

An overview of the method is presented here. Pre-processing of the imagery included pansharpening, which is an image fusion technique using the panchromatic band to increase the spatial information in the coarser multispectral bands. Band indices such as NDVI and NDWI were calculated to add additional information for classification. An object-based classification method was developed to separate the objects into six classes. Three classes not associated with marsh vegetation; Agricultural Fields, Built-Up, and Water, were extracted first using rules. The remaining unclassified vegetation was separated using the nearest-neighbor classifier into three classes, Native Marsh Vegetation, *Phragmites*, and Tree/Grass. Finally, rules were created to classify shadow

objects correctly, and to reassign obviously misclassified objects. The detailed method is explained below in the following sections.

2.4.1 Pre-processing

Image fusion is a commonly used method to increase the information in an image. The coarser multispectral bands can be enhanced with the greater spatial information provided by the finer resolution panchromatic band. In this study, the Smoothing Filter-based Intensity Modulation (SFIM) image fusion technique described by Liu (2000) was used to create a new dataset of 0.5 metre spatial resolution. These pansharpened bands and the original panchromatic band were used as input layers for classification.

2.4.2 Indices Calculation

Vegetation indices calculated from specific image bands are commonly used in vegetation classification. The simple ratio (SR) and the normalized vegetation difference index (NDVI) are two vegetation indices that are widely used in vegetation classification (Jensen, 2005). The vegetation indices used in classification of the Worldview-2 image are presented in Table 2.2.

Table 2.2 Spectral indices used for additional information for image classification.

	Index		
Method	Simple Ratio (SR)	Normalized Difference Vegetation Index (NDVI)	Normalized Difference Water Index (NDWI)
	SR = R/NIR	NDVI = (NIR-R)/(NIR+R)	NDWI = (B-NIR)/(B+NIR)
Four Band	SR = R/NIR1	NDVI = (NIR1-R)/(NIR1+R)	NDWI = (B-NIR1)/(B+NIR1)
Eight Band	SR= R/NIR2	NDVI = (NIR2-R/(NIR2+R)	NDWI = (CB-NIR2)/(CB+NIR2)

2.4.3 Worldview-2 Classification

The overall purpose of the object-based classification of Worldview-2 imagery was to extract *Phragmites* cover. However, the method developed used detailed steps for the classification of six main land cover types: Agricultural Fields, Built-Up, Native Marsh Vegetation, *Phragmites,* Tree/Grass, and Water. The extraction of six classes was done for two reasons. First, more accurate classification of *Phragmites* may be possible when neighbouring objects are classified accurately, since context, such as class of neighbouring objects, within the scene can be used as additional classification information. Second, it is important to understand how the invasion of *Phragmites* changes with time. By developing a method which provides more classes than a simple binary *Phragmites* and Non-*Phragmites* map, specific changes regarding what land cover types are replaced by *Phragmites* over time will allow for more detailed change detection.

An overview of the object-based method is shown in Figure 2.2. Changes to default shape or compactness values (0.1 and 0.5 respectively) did not improve object segmentation of any class so these values were left as default for all segmentations. The overall classification schemes for the object-based methods were very similar. The order in which the classes were extracted from the imagery was important and differed slightly between four and eight band methods.

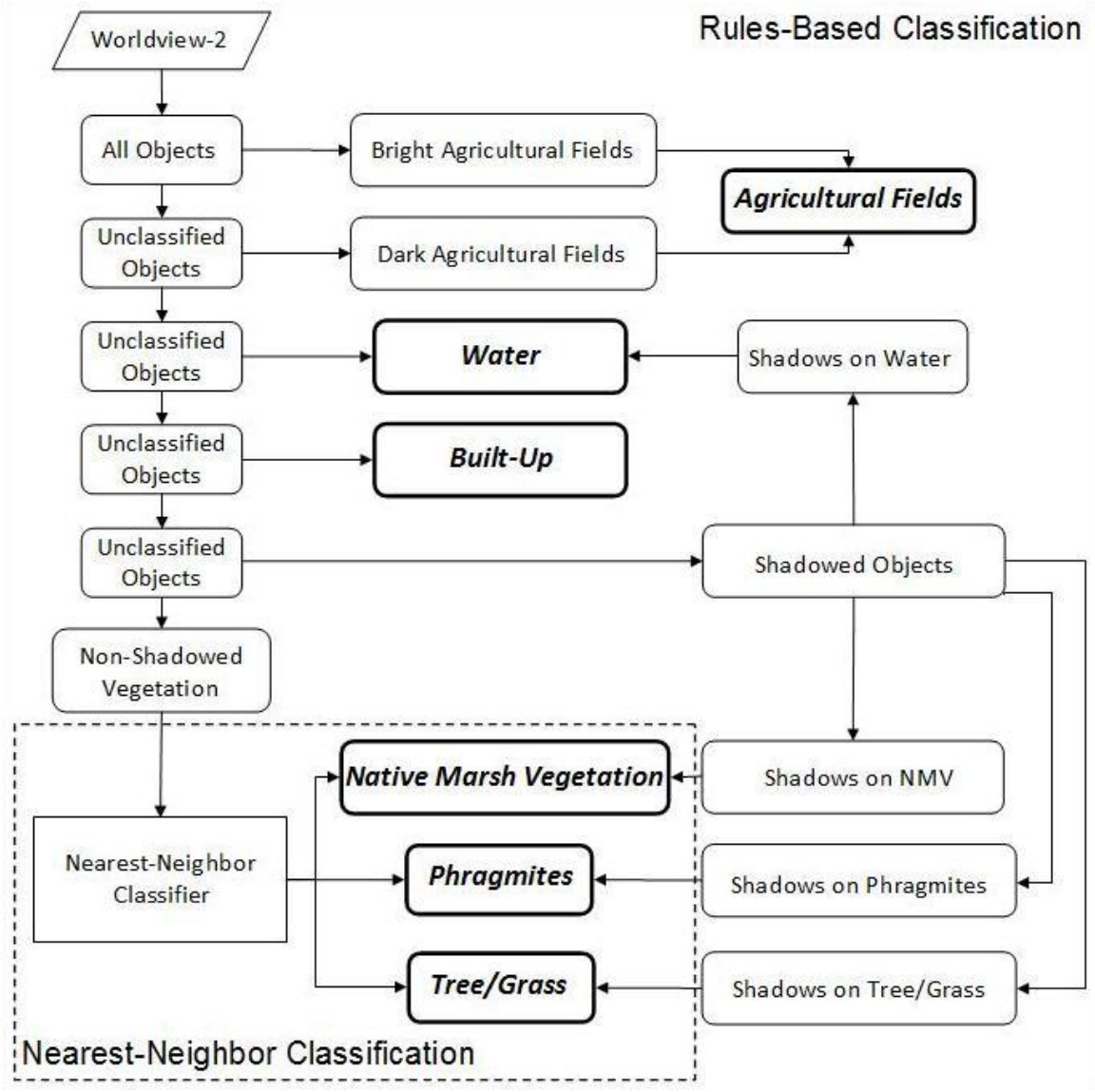

Figure 2.2 An overview of the object-based classification method. Using a rules-based classification, all objects were assigned to five classes: Agricultural Fields, Water, Built-Up, Shadowed Objects, and Non-Shadowed Vegetation. The nearest-neighbor classifier further separated Non-Shadowed Vegetation into three classes: Native Marsh Vegetation, *Phragmites*, and Tree/Grass. Rules were developed to assign Shadowed Objects to their correct class.

2.4.3.1 Classification of Agricultural Fields

Agricultural Fields had two different appearances in the imagery and required two separate sets of rules to extract them. Bright appearing Agricultural Fields represented bare soils or harvested fields. Dark appearing Agricultural Fields had the mature crop still present as the fields had not yet been harvested. Because of the spectral differences, the fields were extracted using different rules. The first step was to segment the image into image objects. To get accurate bright field image objects, the simple ratio (SR) layer was utilized for the segmentation. This band was ideal for creating an accurate boundary between Agricultural Fields and vegetation surrounding the fields.

Of concern along the edges of these Agricultural Fields were shadows cast by trees. The SR layer reduced the effects of shadows and allowed better delineation of field objects at field edges due to strong contrast between fields and surrounding vegetation (Figure 2.3). The multiresolution segmentation algorithm was used for creating bright field objects. The optimal scale value was determined by gradually decreasing the scale value until the edges of fields were outlined accurately. A large scale value results in field objects which cross field boundaries. Reducing the scale value further makes objects smaller and more difficult to separate from other classes. For example, shadows within bright Agricultural Fields become confused with water (Figure 2.3(b)), and small bright field objects become confused with roads (Figure 2.3(e)). To classify bright Agricultural Field objects, a custom “brightness” criterion was used as well as NDWI values. Brightness was calculated as the mean of CB, B, G, Y, and R layer values. Bright Agricultural Fields were extracted by thresholding high brightness values. Some areas of water were misclassified as bright Agricultural Fields so objects with high NDWI values were removed.

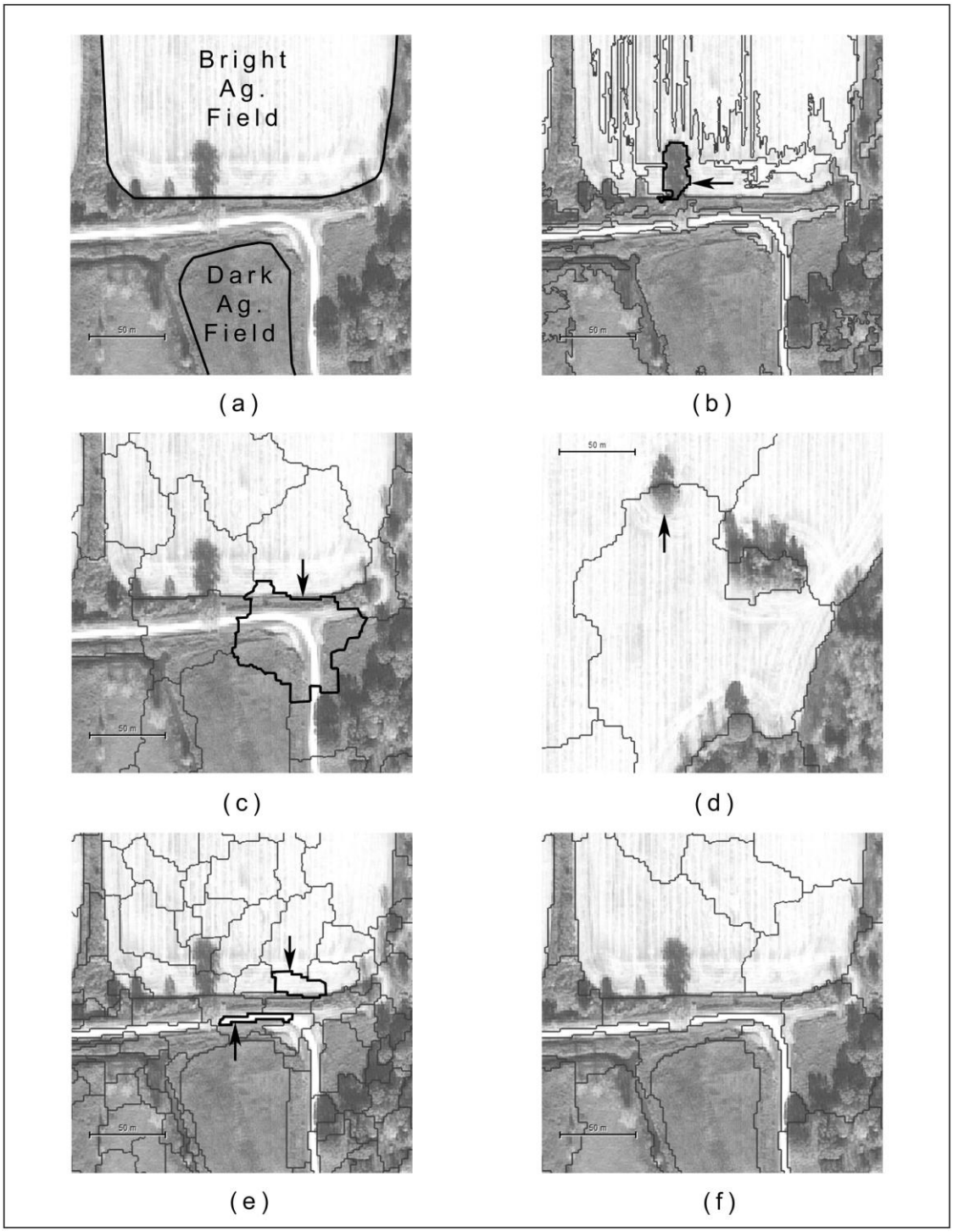

Figure 2.3 Image segmentation of Agricultural Fields. (a) A subset of the Worldview-2 image focused on bright and dark appearing Agricultural Fields outlined in black. (b) When spectral bands in the visible range are used for segmentation, a shadow object (black) interferes with the field boundary. (c) Using NDVI results in objects that contain both field classes within the same object (black). (d) Using a large scale value misses individual trees within Agricultural Fields. Using too small a scale value leads to confusion between bright Agricultural Fields and roads during classification (two objects with black outline) (e). By using the correct scale value and the simple ratio layer for segmentation, both bright and dark Agricultural Field boundaries are accurately represented by the image objects (f).

Although the boundaries of the current objects separate fields from other classes, these objects were not suitable for distinguishing dark Agricultural Fields from Native Marsh Vegetation objects. Both size and spectral properties of these objects were very similar. To separate these two classes, the objects were modified by the spectral difference segmentation algorithm. This algorithm creates a new image object layer by merging neighbouring objects based on a maximum spectral difference threshold. If the spectral difference is below this threshold, the two image objects are merged, otherwise they remain separate objects. Image layers and weights that influence the spectral threshold are specified. The spectral difference segmentation was applied to all unclassified objects in the existing image object level. The SR layer was given a weight of 1 and the maximum spectral difference threshold was set to 0.35. This threshold value allowed neighbouring dark field objects to merge without merging with non-field objects. Dark Agricultural Field objects were still spectrally similar to Native Vegetation objects. Specific rules regarding spectral properties and size were employed to discriminate between these classes. Dark Agricultural Field objects were found to have NDVI values within a specified range, between 0.16 and 0.25. A size threshold was applied to eliminate any remaining Native Vegetation objects. Agricultural Fields were found to have characteristic sizes whereas other land cover types were quite large after the spectral difference segmentation. Both bright and dark fields were assigned to the Agricultural Fields class. Some Agricultural Fields contained areas of higher NDVI values such as weed areas (personal observation). A rule was defined that assigned objects with very high relative border to Agricultural Fields and high NDVI values to the Agricultural Field class. All unclassified objects were then merged for further processing.

2.4.3.2 Classification of Water

Water objects were created using the multiresolution segmentation algorithm and the NIR1, NIR2, R-E, SR, NDVI, and NDWI layers. All layers were given an equal weight and a scale value of 50 was used (Figure 2.4). The optimal scale value was found by gradually decreasing the scale value until all small patches of water in the marsh were separated from vegetation. Smaller scale values increased processing time without any visibly noticeable increase in water classification. Confusion occurred between objects of the shadow and water classes. The image was captured in October when the sun angle is low in the Northern hemisphere which resulted in tall features such as trees, buildings, and *Phragmites* casting shadows. Shadows were confused with water because they have low NDVI values. Also, water objects displayed increased NDVI values and lower NDWI values if they contain floating plants or aquatic plants that reach the surface. To avoid confusing shadow and water, the value for NDWI was increased slowly until shadow objects were unselected and only water objects remained. Not all water objects were selected using the NDWI threshold rule. However, objects surrounding classified water can be tested to see if they belong to the water class: objects with a high mean NDWI value that border existing water objects are water objects and are assigned to the water class. This second step was repeated until no changes occurred to ensure all connected water was identified. Unclassified objects were merged in preparation for further processing.

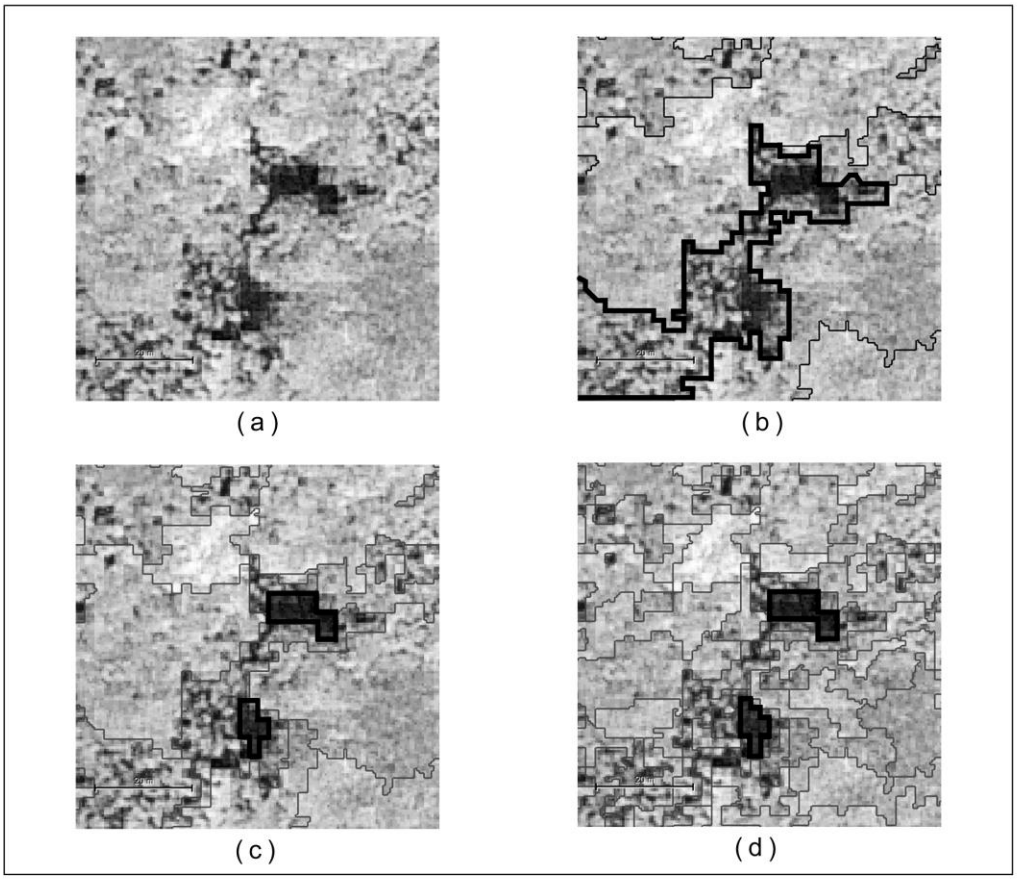

Figure 2.4 Image segmentation of Water. The most suitable scale value for water was determined by examining small water features within the marsh (a). Using a large segmentation scale value results in an object (black outline) that cannot accurately represent small water areas (b). A scale value of 50 was selected for the segmentation of water (c). Using a smaller scale value results in an increased number of objects without any visible improvement in water object outlines (d).

2.4.3.3 Classification of Built-Up

The Built-Up class refers mainly to roads and other manmade features such as buildings. These features do not cover a large area of the image but detailed steps are needed to extract them. The panchromatic layer was chosen as the segmentation layer for Built-Up for two reasons. First, roads appear very bright in the panchromatic layer, which makes them easily separable from surrounding vegetation on either side which appears darker. Secondly, the panchromatic layer was acquired at 0.5 metre resolution which allows for very precise road objects to be made at the road/vegetation boundary (Figure 2.5a) and b)). Whereas had the multispectral layers been used, they are only simulated 0.5 metre resolution and the road/vegetation boundary becomes less defined (Figure 2.5c) and d)). The scale value was determined by slowly decreasing the scale value until road objects were precisely defined. Built-Up objects were created by using the multiresolution segmentation algorithm, and a scale value of 100. A few thresholds and contextual rules were applied to extract road objects. The majority of road objects were extracted with a threshold of high mean yellow values. Iterating two contextual/threshold rules, objects bordering roads with high mean yellow values, and objects bordering roads with high mean blue values, identified the remaining road objects.

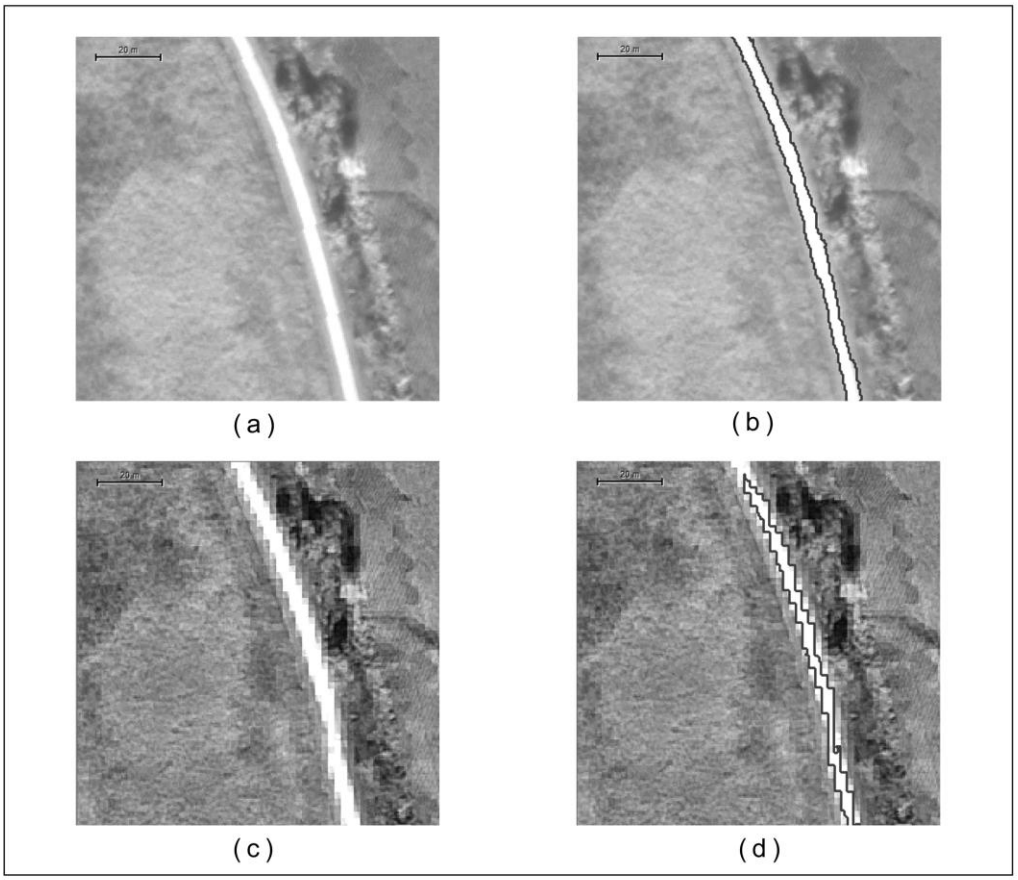

Figure 2.5 Image segmentation of Roads. The panchromatic layer is a true 0.5 metre spatial resolution and the road has a smooth edge (a). Therefore, road objects created from the panchromatic layer are more representative of the road's boundary (b). Although the road is highly visible in the pansharpened layers (c), the edge appears jagged. This leads to less accurate road object boundaries (d).

2.4.3.4 Separation of Vegetation and Shadowed Objects

At this stage, the unclassified areas belonged to the vegetation class. However, shadows cast onto vegetation present a problem for classification since the shadowed vegetation does not reflect in the same manner as illuminated vegetation. Therefore, shadows on vegetation were separated from brightly illuminated vegetation before classifying vegetation. Unclassified objects were segmented using the multiresolution segmentation algorithm with scale value of 40, and R-E, NIR1, NIR2, NDVI , SR image layers with equal weights. These layers were best for creating shadow image objects as the shadow outline was well defined. The brightness threshold (average mean of CB, B, G, R) was used to separate shadowed and illuminated vegetation. The brightness value was slowly

decreased until only illuminated vegetation remained. Extracted shadow objects were later assigned to the correct vegetation class using post-processing steps.

2.4.3.5 Nearest-Neighbor Classification of *Phragmites* and Other Vegetation

Following the classification of Agricultural Fields, Water, Built-Up, and Shadow on Vegetation, only illuminated vegetation remained. Vegetation classes included *Phragmites*, Native Marsh Vegetation, and Tree/Grass. *Phragmites* occurs along the shoreline of lakes and rivers, within the marsh, within drainage ditches and growing right up to the edge of roads. Native Marsh Vegetation is restricted to drainage ditches, within the marsh, and to the shoreline of lakes and rivers. Trees occur along dikes, roads, on residential properties and in a forest in the northeast corner of the image. Grass is restricted to residential properties where it is manicured and maintained at a short height. To segment vegetation into objects, the eight multispectral layers, and NDVI layer were used as image layers. This allowed the multiresolution segmentation algorithm to be guided by all the spectral information available from the Worldview-2 imagery. The scale value was determined by slowly decreasing the value until objects contained one vegetation type only. Next a nearest neighbor classification was performed on the vegetation objects. The nearest neighbor classifier works in three steps. First, samples were chosen for each class by visually interpreting the imagery. Since *Phragmites* had high spectral variation, multiple training classes were needed to map its cover accurately. Alternatively, Trees, Grass, and Native Marsh Vegetation remained spectrally consistent throughout the image and only one training class was needed for each of these respective classes. Second, image layers used by the classifier to separate these classes are specified. The mean value of all image layers was considered for the eight band imagery classification. The optimal combination of input layers to maximize class separability was determined by the Feature Space Optimization feature in eCognition (Trimble GeoSpatial, Munich, Germany). Feature space optimization uses the class training samples to determine the optimal layer combination which maximizes class separability. Training samples were adjusted and the nearest neighbor classification repeated until the classification results agreed best with the visual interpretation of the imagery.

2.4.3.6 Post-Processing

After classification of the six classes, obvious errors could be corrected. For example, Native Marsh Vegetation objects that bordered an Agricultural Field were reassigned to Agricultural Field. Tree objects with a high length-to-width ratio were *Phragmites* objects that occurred along linear features such as roads, drainage channels, etc. and were reassigned to the *Phragmites* class. Trees with a high relative border to *Phragmites* were assigned to *Phragmites*. This correctly reassigned tree objects that were misclassified within the marsh area. Now that all six classes were separated, shadows could be assigned to their appropriate classes. For example, shadows with a high relative border to trees most likely represented shadows in the forest area and were assigned to the tree class. The remaining shadow on vegetation was assigned to the *Phragmites* class.

2.4.4 Accuracy Assessment

Ideally, a large number of points would be visited in the field and the land cover surveyed prior to image classification. However, Great Lakes coastal freshwater wetlands provide a unique challenge for conducting field work since water levels do not fluctuate in the short term. This is a major difference between Great Lakes coastal wetlands and coastal estuarine environments where field work is possible during low tide (e.g. Gilmore et al., 2008). It was not possible to visit a large number of points in the field due to time and equipment (e.g. shallow bottom boats) constraints.

Instead, an accuracy assessment was completed by visually interpreting randomly selected points from imagery sources. The number of random sample points was determined by an equation based on the multinomial distribution (Jensen, 2005). The required number of sample points was calculated as follows:

$$N = B\Pi_i(1-\Pi_i)/b_i^2 \quad (1)$$

Where Π_i is the proportion of a population in the ith class out of k classes that has the proportion closest to 50%, b_i is the desired precision ($\alpha = 0.05$, in this study) for this class, B is the upper $(\alpha/k) \times 100^{th}$ percentile of the chi square (χ^2) distribution with 1 degree of freedom, and k is the number of classes (Jensen, 2005). *Phragmites* covers the

proportion of the image closest to 50% (roughly 40%) therefore this area percentage was used. A minimum of 677 points were required, so 707 random sample points were chosen to fulfill this criteria. Individual sample points were interpreted by visual inspection as belonging to one of the six land cover classes. Sample points were assigned their class from experience gained from fieldwork completed in mid-August and early October 2011, and Southwestern Ontario Orthophotography Project (SWOOP) 20cm aerial true colour imagery from April 2010. To increase the objectivity of the accuracy assessment, a majority vote of the sample points was conducted (Lehrbass and Wang, 2010). Each sample point was interpreted separately by three people. The sample point was assigned to the class for which the majority of the interpreters had assigned it. The sample point was assigned to a class if at least two out of three interpreters had agreed in their interpretation. Sample points that were assigned to a different class by all three interpreters were discarded. In the end, 700 sample points remained for the accuracy assessment. A confusion matrix and accuracy statistics were used to compare the accuracy of the classifications. Statistics produced included the Kappa statistic, overall, user's and producer's accuracy for the six classes.

2.5 Results and Discussion

2.5.1 Land Cover Estimates and Distribution

The overall area covered by the six classes mapped by the proposed eight band object-based method is shown in Table 2.3. The invasive wetland plant species *Phragmites* was the dominant vegetation present, covering approximately 43% of the total study area. Native Marsh Vegetation only accounted for approximately 22.2% of the area. Of the area occupied by wetland vegetation (not Agricultural Fields, Built-Up, Tree/Grass, or Water), *Phragmites* and Native Marsh Vegetation occupy 64%, and 36% respectively. This translates to approximately 1.8 times more *Phragmites* than Native Marsh Vegetation. In a study of expansion of *Phragmites* at Long Point, Lake Erie, Wilcox et al. (2003) found *Phragmites* expansion occurred at an exponential rate between 1995 and 1999. One of the most frequent plant communities replaced by *Phragmites* was *Typha* spp. A previous study of Walpole Island by Arzandeh and Wang (2003) also found that *Phragmites* increased at the expense of *Typha* spp. In 1992, *Typha* spp. were the more

abundant wetland vegetation type covering approximately 89% of the total area compared with 11% for *Phragmites*. By 1998, *Phragmites* had more than doubled its area, and *Typha* spp. covered only 73% of the wetland area. In this study that focused on a subset area of WIFN coastal marshes, the proportion of *Phragmites* to *Typha* was found to be 64 to 36. This may show that *Phragmites* has continued to expand over the past 14 years.

Table 2.3 Land cover class areas mapped using method 2: eight band imagery and object-based method.

Class	Area (ha)	Percent of study area
Agricultural Fields	252.2	6.3
Built-Up	1.3	0.0
Native Marsh Vegetation	894.1	22.2
Phragmites	1729.7	43.0
Tree/Grass	81.9	2.0
Water	1065.7	26.5

By visually comparing the map from Arzandeh and Wang (2003) with the map generated by the eight band object-based method, the areas of expansion are very noticeable. Native Marsh Vegetation has almost completely been replaced by *Phragmites* along the shorelines of the Bassett and Chematogan channels, and the shoreline of Goose Lake. The abundance of *Phragmites* and Native Marsh Vegetation cover for the three islands is presented in Table 2.4. On Bassett Island, a large area of Native Marsh Vegetation still remains within the diked marsh. However, *Phragmites* is present the full length of the edge of the dike, along the Bassett Channel. Smaller patches of *Phragmites* are also spread throughout large areas of Native Marsh Vegetation. Overall, Native Marsh Vegetation covers 49.5% of the marsh area on Bassett Island while the rest is *Phragmites*. On Squirrel Island, *Phragmites* cover is 68% and inhabits almost the entire southern half of the marsh. Some small areas of Native Marsh Vegetation remain scattered throughout. In the northern half, the diked marsh still contains large areas of Native Marsh Vegetation

while the majority of *Phragmites* is restricted to the perimeter of the diked area. On Walpole Island, *Phragmites* is well established in all areas of the marsh. The proportion of Native Marsh Vegetation to *Phragmites* is 29 to 71% respectively. Most of the Native Marsh Vegetation is found in the center of the marsh.

Table 2.4 Area covered by wetland vegetation for the WIFN study area mapped using the eight band imagery and object-based method.

	Bassett Island		Squirrel Island		Walpole Island	
Class	Area (ha)	%	Area (ha)	%	Area (ha)	%
Native Marsh Vegetation	168.6	49.5	441.7	32.0	303.0	29.0
Phragmites	172.3	50.5	744.9	68.0	743.5	71.0

2.5.2 Classification Methods

To evaluate the effectiveness of the eight band object based method, three other methods were also tested. Methods 1 and 2 used object-based methods for classification, while Methods 3 and 4 used the maximum likelihood classifier (MLC), a pixel-based method. Method 1 and 3 used a subset of Worldview-2 layers simulating the four multispectral band set (B, G, R, and NIR) acquired by traditional high resolution multispectral satellites. Method 2 and 4 used the full eight band capabilities of the Worldview-2 satellite. The maximum likelihood classifications used the same band set that were utilized for the object-based classifications. Training samples for MLC were chosen for the six different land classes from knowledge gained from fieldwork. The same training samples were used for both four and eight band per-pixel based classifications.

2.5.2.1 Four Band Object-Based Versus Per-Pixel Classification

The four band object-based classification had an overall accuracy of 92.7% and a 19.7% higher overall accuracy than the four band per-pixel of 73.0% (Table 2.5). Although six classes were trained for the four band per-pixel, the majority of pixels were mapped as one of four classes: Built-Up, Native Marsh Vegetation, *Phragmites*, and Water (Figure 2.6(c)). The majority of errors occurred between classes with similar spectral signatures. Bright Agricultural Fields which represented bare soil or harvested fields were confused

with Built-Up which mostly represented roads. Dark Agricultural Fields were highly confused with Native Marsh Vegetation. This is expected as both classes had similar spectral values and overall appearance. Tree/Grass was highly confused with *Phragmites* most likely due to both classes maintaining high green, NIR and NDVI values at the time of image acquisition. Alternatively, the four band object-based classification showed much better separation of all six classes (Figure 2.6(a)). The biggest improvement occurred in the Agricultural Field classes. Bright Agricultural Fields were correctly separated from Built-Up. Dark Agricultural Fields were more accurately separated from Native Marsh Vegetation which resulted in higher producer's and user's accuracies for Agricultural Fields and higher user's accuracies for Native Marsh Vegetation. The four band object-based method was also more accurate in separating *Phragmites* from Tree/Grass. Although object-based methods were successful in reducing the Tree/Grass commission error, Tree/Grass omission error was still high due to large areas of trees being mapped as *Phragmites* in the forested area in the northeast corner. Overall, object-based methods improved classification accuracy of four band imagery. Object-based methods are important for classifying imagery when the spectral content available is low. The addition of image objects, image object hierarchy, and rules-based classification greatly improved image classification. Despite these improvements, object-based methods still struggle with classification when two classes, such as *Phragmites* and Tree/Grass in this case, are spectrally similar and rules to separate them are complex. Overall, the four band object-based classification was better at separating all six classes due to the ability to define very detailed rules to separate spectrally similar classes. Increased accuracy is also likely due to classification of larger image objects compared to individual pixels which reduced the salt and pepper effect that is a common trait of the per-pixel classifier.

2.5.2.2 Eight Band Object-Based Versus Per-Pixel Classification

Similar to the four band results, the eight band object-based classification outperformed the eight band per-pixel classification. The eight band object-based classification had an overall accuracy of 94.0% and a 10.6% higher overall accuracy than the eight band per-pixel of 83.4% (Table 2.5). Agricultural fields were mapped with high producer's and

user's accuracies of 78.0% and 86.7%, respectively, however the weedy areas within fields were mapped inaccurately as *Phragmites* for the per-pixel classification. The eight band object-based classification handled this problem with some rules to assign objects with high NDVI within field objects to the correct Agricultural Field class. There was some confusion between Built-Up and Bright Agricultural Fields for the eight band per-pixel. Despite the increased spectral information provided by the eight bands, there was still not enough information to distinguish field soil from the spectrally similar road materials. The eight band object-based classification took care of this problem with some rules to differentiate objects of these two classes. The Tree/Grass class was well mapped in the forest area of the eight band per-pixel however in the marsh area *Phragmites* was sometimes mapped as Tree/Grass (Figure 2.6(d)). For the eight band object-based classification, rules could be defined to correct these *Phragmites* objects misclassified as Tree/Grass (Figure 2.6(b)). There was confusion between Native Marsh Vegetation and *Phragmites* in the per-pixel classification. The maximum likelihood per-pixel classifier tended to classify Native Marsh Vegetation as *Phragmites*. This could be due to mixing between these two land covers and misclassification of individual pixels at mixing boundaries. On the other hand, the object-based classification resulted in fewer Native Marsh Vegetation objects being confused with *Phragmites*. This could be due to individual image objects being more accurate where these two plant species mix compared to classifying individual pixels in these areas. Again, object-based classification was more accurate. Combining increased spectral information and object-based methods allowed for the overall highest classification accuracy as well as the highest classification accuracies for the wetland vegetation classes of interest.

2.5.2.3 Pixel-Based Classification – Four Versus Eight Band

The differences between using four and eight spectral bands for per-pixel classification were tested with Methods 3 and 4 respectively. Classification of eight bands resulted in an overall accuracy 10.4% higher than using only four bands (Table 2.5). This result is expected as additional spectral information allows for the separation of spectrally similar classes. Most importantly was the increase in separation of the Tree/Grass and *Phragmites* classes when eight bands were used for classification. The red-edge and

second near infrared (NIR2) layers likely contributed the most to this separation since more information was available in the electromagnetic region where vegetation differs spectrally. The extra bands were also important for distinguishing between Native Marsh Vegetation and Agricultural Fields where mature crops were still present. These two results highlight the importance of the additional spectral bands provided by the Worldview-2 satellite when classifying wetland vegetation in a complex environment such as a Great Lakes coastal marsh where humans have changed the natural landscape (addition of agricultural fields) and distinct vegetation communities reside in close proximity (upland deciduous forest). Traditional four band high resolution sensors may not be able to provide the spectral information needed for accurate classification in this complex environment.

2.5.2.4 Object-Based Classification – Four Versus Eight Band

The differences between using four and eight spectral bands for object-based classification were tested with Methods 1 and 2 respectively. The four band classification had an overall accuracy of 92.7%, while the eight band had a slightly higher accuracy of 94.0% (Table 2.5). There were no major differences in the accuracies of the Agricultural Fields, Built-Up, or Water classes as both object-based methods applied here resulted in high accuracies for these three classes. Similarly, both wetland classes achieved similar high overall accuracies for both methods. Four band *Phragmites* producer's accuracy was slightly higher at 95.8%, compared to 95.5% for eight band. Four band *Phragmites* user's accuracy was slightly lower at 90.8% compared to 93.2% for eight band. Four band Native Marsh Vegetation producer's accuracy was slightly higher at 88.8% compared to 87.5% for eight band. Four band Native Marsh Vegetation user's accuracy was slightly lower at 87.7% compared to 90.3% for eight band. However, the main difference was between the accuracies for the Tree/Grass class for the respective methods. Eight band had a much higher producer's accuracy (50 versus 95%). The user's accuracy however, was slightly higher for four band than eight (100 versus 90%). These differences are evident when comparing the two classifications (Figures 2.6(a) and (b)). The forest in the northeast corner of the study area is more accurately mapped by eight band as the forested area is highly confused with *Phragmites* in four band. In the case of Tree/Grass

classification, the extra spectral bands in eight band seem to be an advantage in discriminating between Tree/Grass and *Phragmites*. The eight band method was able to separate more Tree/Grass objects from *Phragmites* objects initially. This allowed for better assignment of shadows during the last stage of classification. The final rules assign shadow objects based on the surrounding objects. More accurate classification of Tree/Grass objects initially result in more shadow objects be correctly assigned to Tree/Grass in eight band. Alternatively for four band, more Tree/Grass in the forest was initially classified as *Phragmites* which resulted in more shadow objects being incorrectly assigned to the *Phragmites* class. For other classes, the extra spectral bands did not have a large impact on overall classification accuracy. Instead, the object-based rules that were developed for four band were able to separate these classes with high accuracy. Therefore, the extra spectral bands may be more useful when the goal is to separate more vegetation classes than was attempted in this study.

Table 2.5 Accuracy statistics for the four classification methods.

	Method			
	1	2	3	4
Producer's Accuracy	4 Band, OB	8 Band, OB	4 Band, MLC	8 Band, MLC
Agricultural Fields	100	98.0	0.0	78.0
Built-Up	0.0	50.0	100.0	0.0
Native Marsh Vegetation	88.8	87.5	89.4	74.4
Phragmites	95.8	95.5	73.7	89.3
Tree/Grass	50.0	95.0	35.0	100.0
Water	95.0	96.7	81.6	82.7
User's Accuracy				
Agricultural Fields	100	96.1	0.0	86.7
Built-Up	0.0	100.0	5.9	0.0
Native Marsh Vegetation	87.7	90.3	61.4	80.6
Phragmites	90.8	93.2	85.2	86.6
Tree/Grass	100.0	90.5	38.9	33.9
Water	98.3	98.3	100.0	100.0
Overall Accuracy	92.7	94.0	73.0	83.4
Kappa	0.896	0.915	0.625	0.768

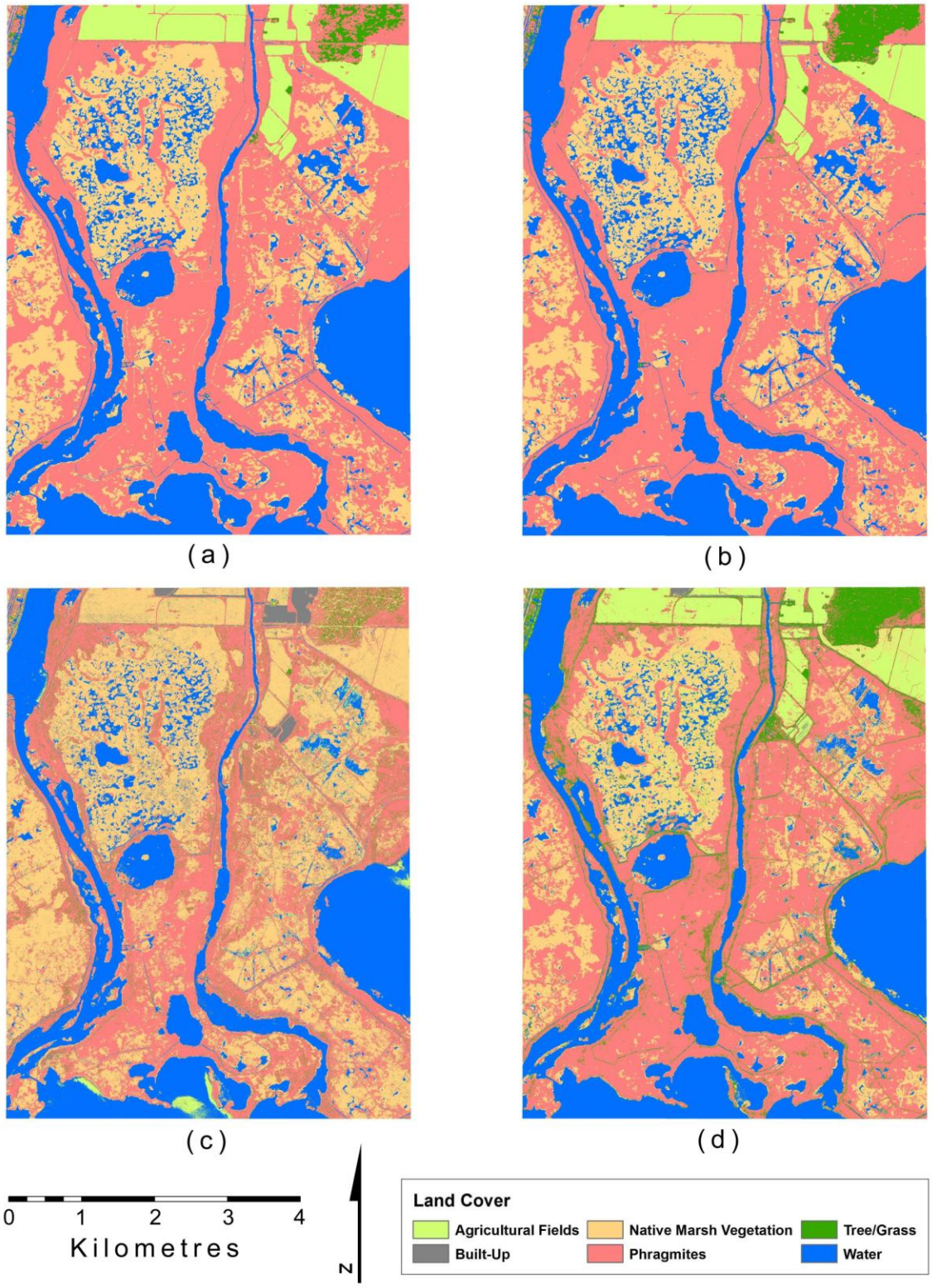

Figure 2.6 Worldview-2 object-based and per-pixel classification results. Land cover map of the study area generated by (a) Method 1 – object-based classification of four multispectral bands, (b) Method 2 – object-based classification of eight multispectral bands, (c) Method 3 – pixel-based classification of four multispectral bands, (d) Method 4 – pixel-based classification of eight multispectral bands.

2.5.2.5 *Phragmites* and Non-*Phragmites* Classification

To assess which method was most accurate in extracting *Phragmites*, the six class classification was aggregated into a binary classification containing only *Phragmites* and a single Non-*Phragmites* class made up of the other five classes. The producer's, user's, and overall accuracies as well as the Kappa statistic were calculated for this new classification (Table 2.6). Following previous results based on the six class classification, *Phragmites* was most accurately extracted using the eight band object-based method. With the exception of the four band object based producer's accuracy, *Phragmites* user's and producer's accuracies for eight band object based were higher than all of the other methods tested. Finally, the Kappa statistic for method 2 is the highest of the four methods tested meaning that reference data and derived classification agree strongly. Classification of *Phragmites* was most accurate using the object based method combined with the full eight band set of the Worldview-2 sensor.

Table 2.6 Accuracy statistics for the four classification methods and binary Phragmites versus Non-Phragmites classification.

	Method			
	1	2	3	4
Producer's Accuracy	4 Band, OB	8 Band, OB	4 Band, MLC	8 Band, MLC
Phragmites	95.8	95.5	73.7	89.3
Non-*Phragmites*	93.2	95.1	91.0	90.3
User's Accuracy				
Phragmites	90.8	93.2	85.2	86.6
Non-*Phragmites*	97.0	96.8	83.1	92.3
Overall Accuracy	94.3	95.3	83.9	89.9
Kappa	0.883	0.903	0.660	0.792

2.6 Conclusions

Four different classification methods were tested on a Worldview-2 image to classify six land cover types with an objective of accurately mapping the invasive wetland plant *Phragmites*. Four and eight band datasets were classified using the per-pixel maximum likelihood classifier and object-based methods. Three major conclusions have been determined as a result. First, object-based methods resulted in higher classification accuracy than their respective per-pixel maximum likelihood classifications. Using four band imagery, the overall classification accuracy for the object-based method was 19.7% higher than per-pixel MLC. Similarly, eight band imagery and object-based classification resulted in an increase of 10.6% in overall classification accuracy over eight band per-pixel MLC. Therefore, object-based methods were superior than per-pixel MLC for classification. Second, for both per-pixel MLC and object-based methods, eight band imagery resulted in higher classification accuracy than four band imagery. Eight band per-pixel MLC was 10.4% overall more accurate than four band, while eight band object-based was 1.3% overall more accurate. Although the eight band object-based method did not result in a large increase in accuracy over the four band object-based method, the accuracy of the vegetation classes was improved by using the eight band imagery and the associated method. Therefore, the additional spectral information provided by the Worldview-2 satellite was useful in separating the classes on Walpole Island and mapping the invasive plant. Third, the best method for mapping *Phragmites* was the eight band object-based method. This method increased overall accuracy of the six class classification by 21% over the four band per-pixel MLC, 10.6% over the eight band per-pixel, and 1.3% over the four band object-based method. The Kappa statistic for the *Phragmites* and Non-*Phragmites* classification for the eight band object-based method was also 0.422 higher than the four band per-pixel MLC, 0.211 higher than the eight band per-pixel, and 0.025 higher than the four band object-based method. Therefore, the eight band object-based method was the best for both classifying the six land covers and for distinguishing between *Phragmites* and Non-*Phragmites*.

This study showed that a single date, eight band high resolution image classified with object-based methods was effective for mapping an invasive wetland plant species in a southwestern Ontario Great Lakes coastal wetland. Although detailed steps for Method 2 presented here were significant for extracting the six classes, its extension for classifying other images collected by the Worldview-2 satellite for this purpose may not be appropriate. A similar classification scheme may be appropriate for images collected late in the growing season when vegetation conditions are similar. The Worldview-2 satellite may be an option for mapping *Phragmites* for management as a single date image can provide high accuracy for the invasive wetland plant.

2.7 References

Adam, E., Mutanga, O., & Rugege, D. (2010). Multispectral and hyperspectral remote sensing for identification and mapping of wetland vegetation: a review.*Wetlands Ecology and Management*, *18*(3), 281-296. DOI: 10.1007/s11273-009-9169-z.

Arzandeh, S., & Wang, J. (2002). Texture evaluation of RADARSAT imagery for wetland mapping. *Canadian Journal of Remote Sensing*, *28*(5), 653-666.

Arzandeh, S., & Wang, J. (2003). Monitoring the change of *Phragmites* distribution using satellite data. *Canadian journal of remote sensing*, *29*(1), 24-35.

Environment Canada. (2003). *The Ontario great lakes coastal wetland atlas: A summary of information (1983-1997)* (Catalogue Number CW66-221/1997E). Peterborough, ON: Ontario Ministry of Education.

eoPortal Directory. 2012. Worldview-2. Available from <https://directory.eoportal.org/web/eoportal/satellite-missions/v-w-x-y-z/worldview-2> [accessed (November 28, 2012)]

Ghioca-Robrecht, D. M., Johnston, C. A., & Tulbure, M. G. (2008). Assessing the use of multiseason Quickbird imagery for mapping invasive species in a Lake Erie coastal marsh. *Wetlands*, *28*(4), 1028-1039.

Gilmore, M. S., Wilson, E. H., Barrett, N., Civco, D. L., Prisloe, S., Hurd, J. D., & Chadwick, C. (2008). Integrating multi-temporal spectral and structural information to map wetland vegetation in a lower Connecticut River tidal marsh.*Remote Sensing of Environment*, *112*(11), 4048-4060. doi:10.1016/j.rse.2008.05.020.

Herdendorf, C. E. (1992). Lake Erie coastal wetlands: an overview. *Journal of Great Lakes Research*, *18*(4), 533-551.

Jaworski, E., & Raphael, C. N. (1978). *Fish, wildlife and recreational values of Michigan's coastal wetlands*. U.S. Fish and Wildlife Services, Twin Cities, Minnesota.

Jensen, J. R. (2005). *Introductory digital image processing: A remote sensing perspective* (3rd ed.) (pp 311 & 501). Upper Saddle River, NJ: Pearson Prentice Hall, Upper Saddle River, N.J.

Laba, M., Downs, R., Smith, S., Welsh, S., Neider, C., White, S., Richmond, M., Philpot, W. & Baveye, P. (2008). Mapping invasive wetland plants in the Hudson River National Estuarine Research Reserve using quickbird satellite imagery. *Remote Sensing of Environment, 112*(1), 286-300. doi:10.1016/j.rse.2007.05.003.

Laba, M., Blair, B., Downs, R., Monger, B., Philpot, W., Smith, S., Sullivan, P., and Baveye, P.C. (2010). Use of textural measurements to map invasive wetland plants in the Hudson River National Estuarine Research Reserve with IKONOS satellite imagery. *Remote Sensing of Environment, 114*(4), 876-886. doi:10.1016/j.rse2009.12.002.

Lavoie, C. (2008). The Common Reed (*Phragmites australis*): A Threat to Quebec's Wetlands? Available from <http://www.canards.ca/province/qc/nouvelle/pdf/phra_08e.pdf > [accessed (January 6, 2012)].

Lehrbass, B., & Wang, J. (2010). Techniques for object-based classification of urban tree cover from high-resolution multispectral imagery. *Canadian Journal of Remote Sensing, 36*(S2), 287-297.

Liu, J. G. (2000). Smoothing filter-based intensity modulation: a spectral preserve image fusion technique for improving spatial details. *International Journal of Remote Sensing, 21*(18), 3461-3472. DOI: 10.1080/01431160110088772.

Mal, T. K., & Narine, L. (2004). The biology of Canadian weeds. 129. *Phragmites australis* (Cav.) Trin. ex Steud. *Canadian journal of plant science, 84*(1), 365-396.

McCullough, G.B. (1985). *Coastal wetlands: Wetland threats and losses in Lake St Clair* (pp. 201-208). H.H. Prince and F.M. D'Itri. (Ed.) Michigan: Lewis Publishers Inc.

Ontario Ministry of Finance 2012. Ontario Population Projections Update. Available from <http://www.fin.gov.on.ca/en/economy/demographics/projections/> [accessed (July 6, 2012)].

Ozesmi, S. L., & Bauer, M. E. (2002). Satellite remote sensing of wetlands. *Wetlands Ecology and Management, 10*(5), 381-402.

Parker Williams, A., & Hunt, E. R. (2002). Estimation of leafy spurge cover from hyperspectral imagery using mixture tuned matched filtering. *Remote Sensing of Environment, 82*(2), 446-456.

Saltonstall, K. (2002). Cryptic invasion by a non-native genotype of the common reed, *Phragmites australis*, into North America. *Proceedings of the National Academy of Sciences, 99*(4), 2445-2449. doi: 10.1073/pnas.032477999.

Satellite Imaging Corporation (2012). IKONOS Stereo Satellite Imagery. Available from <http://www.satimagingcorp.com/svc/ikonos-stereo-satellite-images.html> [accessed (December 10, 2011)].

Snell, E.A. (1987). Wetland Distribution and Conservation in Sothern Ontario. Working Paper No. 48. Ottawa: Environment Canada, Inland Waters and Lands Directorate.

Wilcox, K. L., Petrie, S. A., Maynard, L. A., & Meyer, S. W. (2003). Historical distribution and abundance of *Phragmites australis* at Long Point, Lake Erie, Ontario. *Journal of Great Lakes Research*, *29*(4), 664-680.

Chapter 3

3 Mapping and Evaluating *Phragmites australis* Abundance Derived from Spectral Mixture Analysis of Hyperspectral Data

3.1 Introduction

Phragmites australis (Cavenilles) Trinius ex. Steudel (common reed) is found on all continents, with the exception of Antarctica, making it one of the most widely distributed plant species in the world (Mal & Narine, 2004). *Phragmites* abundance and distribution in North America was low in the nineteenth century, but increased in the twentieth century and the plant was widely distributed throughout the United States and southern Canada by the mid-1970s (Meyerson et al., 2009). Recent genetic evidence confirms that a non-native strain of *Phragmites, Phragmites australis* subspec. *australis*, is present in North America, along with the North American native, *Phragmites australis* subsp. *americanus* Saltonstall, P.M. Peterson & Soreng (Saltonstall et al., 2004). The non-native was most likely introduced from populations originating in Europe or Asia (Saltonstall, 2002). The aggressively spreading non-native *Phragmites* can grow in a range of marsh systems including fresh, brackish, and salt water (Mal & Narine, 2004). This has allowed it to spread throughout coastal marsh systems in the United States and Canada. *Phragmites* is now well established along the Atlantic coast (Chambers et al., 1999), and in the Great Lakes region, where recent rapid expansion has been noted in Lake Erie (Wilcox et al., 2003; Ghioca-Robrecht et al., 2008), Lake St. Clair (Arzandeh & Wang 2003), and Green Bay, Lake Michigan (Pengra et al., 2007; Tulbure et al., 2007). The invasive *Phragmites* is a superior competitor compared with native *Phragmites*, having a higher root and stem density, higher aboveground biomass, longer growing season, and being tolerant of a wider range of salinities (Chambers et al., 1999; League et al., 2006). These traits also give an advantage over other native wetland plants that cannot compete with invasive *Phragmites* for nutrients, light and space resources, allowing a *Phragmites* monoculture to develop quickly (Meyerson et al., 2009). In 2005, Agriculture and Agri-Food Canada identified non-native *Phragmites* as the nation's worst invasive plant

species (Ontario Ministry of Natural Resources, 2011). It is hypothesized that the decrease in Great Lakes water levels, combined with increase in ambient air temperature has allowed for increased expansion of the non-native *Phragmites* in Great Lakes coastal wetlands in the past 30 years (Wilcox et al., 2003). *Phragmites* growth is also expected to increase with the predicted future rise in CO_2 levels (Farnsworth and Meyerson 2003).

The sustainable management of wetlands relies on monitoring the distribution and quantity of the invasive species over time (Adam et al., 2010). This allows for the establishment of an invasion baseline, monitoring of the invasive plant propagation, and to implement an effective plan to deal with the invasion. Collection of this type of information has traditionally been acquired by labour intensive, costly, and time-consuming field work. Wetland environments have poor accessibility due to dense, tall emergent vegetation and varying depths of water, making field work impossible or impractical for large areas (Lee and Lunetta, 1996). These limitations are barriers to providing up-to-date information and detecting changes to the distribution and quantity of wetland vegetation species over short time intervals.

Remote sensing provides an alternative method for obtaining this important information. It reduces costs, labour, and saves time relative to field work. The design of remote sensing systems allows for repeat coverage of large areas providing up-to-date information and an archive of images that can be used for detecting change. Assessment of the remote sensing results still requires field work, but at a greatly reduced effort and with increased efficiency. The information collected and extracted from imagery is already in digital format which allows for convenient integration and further analysis in a Geographic Information System (GIS) (Ozesmi and Bauer, 2002).

It is due to these advantages that remote sensing information has been used to monitor invasive *Phragmites* and other wetland species. Multispectral imagery is capabile of discriminating *Phragmites* from native wetland vegetation, however, this often requires additional information such as multi-season imagery (e.g. Ghioca-Robrecht, 2008), or multi-season imagery combined with height information from LiDAR (e.g. Gilmore et al., 2008). Additional classification information increases cost and may not be available.

The limited number and broad spectral bands of these sensors alone are not capable of discriminating between the slight differences in vegetation signatures with high accuracy (Adam et al., 2010).

Airborne and satellite hyperspectral sensors with many narrow and contiguous bands offer the potential to detect small spectral differences and therefore detect and map the invasive species without additional information (Adam et al., 2010). Airborne hyperspectral imagery typically acquired by a sensor on a plane flown at low altitude, can provide high spatial and spectral imagery and result in high accuracy for *Phragmites* mapping (e.g. Artigas and Yang, 2005). However, data acquired with airborne sensors is expensive, and the revisit period depends on specific tasking. Hyperspectral satellites on the other hand, acquire data at regular intervals and generally lower cost (Adam et al., 2010). The images are archived and can be accessed at a later date when a time series is needed for change analysis. One problem with these satellite sensors however, is the trade off between spectral and spatial resolution. As the spectral resolution increases, the amount of energy returning to the sensor decreases, resulting in a less accurate recording of the signal, also known as a low signal to noise ratio. To increase this ratio, the sensor must observe the area on the ground for longer period of time, or sample a larger area (Jensen, 2005). As a result, hyperspectral satellite sensors such as Hyperion and CHRIS PROBA have low spatial resolutions at 30m (eoPortal, 2012a) and 17m (eoPortal, 2012b), respectively.

The spatial resolution of a sensor creates a problem if the average size of the marsh vegetation patches is smaller than the image pixel as this leads to multiple land covers within a single pixel (Artigas and Yang, 2005). A traditional classifier such as maximum likelihood, would misrepresent or oversimplify mixed pixels (Rosso et al. 2005) by assigning them to the class with the highest probability based on training data (Jensen, 2005). The result is a loss of information as other land classes are assumed not to be present in the pixel. Alternatively, the spectral mixture analysis (SMA) method assumes that a pixel's spectrum is a combination of one or more pure land cover types, known as endmembers (Adams et al., 1993). When the spectral signature of each endmember in the image is known, the pixel's spectrum can be broken down into its component land cover

fractions. Linear spectral unmixing models assume that a pixel's spectrum is a linear combination of the endmembers present. SMA provides information about the abundance and distribution of each endmember instead of thematic classes, which provides valuable information for monitoring the invasion of *Phragmites*.

To assess the results of SMA, the percent canopy cover of each endmember would be ideally measured in the field and these fraction estimates compared to SMA derived fractions. As mentioned previously, wetlands present a difficult environment in which to conduct field work. Dense, tall stands of *Phragmites* and other emergent vegetation combined with the water of varying depths make it a challenge to collect percent canopy cover estimates. As a result, it was not possible to collect fraction estimates of *Phragmites*, Native Marsh Vegetation, and Water in the field. The percent cover of each endmember can also be manually interpreted from aerial photographs (e.g. Rosso et al. 2005). However, this method relies heavily on accurate and consistent estimation of percent canopy cover by the interpreter and is labour intensive if many areas are to be evaluated. A third option is to use classified results from high resolution imagery. He et al. (2010) used classified QuickBird-2 imagery to evaluate the results of SMA derived fractions from 30m Landsat TM imagery. If the accuracy of the classification is high for all endmember classes, it can be used as a reference image to assess the accuracy of SMA modelling (He et al. 2010). Using a classified image will allow for a more automated and thorough evaluation of more pixels than either field work or image interpretation. A similar method will be used in this study, using the classification results from Worldview-2 high resolution imagery from Chapter 2.

CHRIS PROBA hyperspectral imagery using the SMA method has not previously been used to estimate the fraction abundance of *Phragmites* in Great Lakes coastal wetlands. The objective of this chapter is to determine if the sub-pixel abundance of the three main land covers, *Phragmites*, Native Marsh Vegetation, and Water can be accurately estimated using the outlined method. A classification was performed to produce a *Phragmites* invasion map where the progress of the *Phragmites* invasion was displayed for each pixel. A classification of the three land cover abundance layers was performed to create a dominant land cover map where the pixel class reflects the dominant land cover

in it. The appropriateness of using a classified Worldview-2 image as a reference image to approximate the real surface cover for SMA fraction accuracy assessment was also evaluated.

3.2 Methods

3.2.1 Study Site

Walpole Island First Nation (82° 30’ W and 42° 33’ N) is located at the north end of Lake St. Clair in Lambton County, Ontario, Canada (Figure 3.1). Walpole Island is a delta, formed as the sediments carried by the St. Clair River are deposited as the river slows to meet Lake St. Clair (Environment Canada, 2003). This site is unique as it is a bird-foot delta which is an uncommon feature in the Great Lakes system (Herdendorf, 1992). The six islands of Walpole cover 24,000 ha (Woodliffe, 1989) and of this area, the coastal wetlands cover approximately 10,360 ha or roughly 80% of all coastal wetlands on the Canadian side of Lake St. Clair (Environment Canada, 2003). About half of the wetlands the in St. Clair delta have been diked and pumps manipulate water levels for marsh management related to the production of waterfowl (Bookhout et al., 1989). The coastal marshes provide spawning, nursery, and feeding grounds for fish, provide breeding, migratory and wintering grounds for birds, and provide habitat for plant, reptile, amphibian and mammal species, some of which are provincially, nationally, and even globally rare (Environment Canada, 2003). *Typha* spp. (Cattails) form the dominant native vegetation while Z*izania palustris* (Wild Rice), *Scirpus* spp. (Bulrushes), *Pontederia cordata* (Pickerelweed), *Nuphar variegatum* (Yellow Pond Lily), and *Nymphaea odorata* (Fragrant White Water Lily) are sparsely distributed. An invasive species, *Phragmites australis* (Cavenilles) Trinius ex. Steudel subspec. *australis* (Saltonstall, 2002), is of concern at Walpole as it is expanding at the expense of native species (Arzandeh & Wang, 2003). Based on herbarium samples, the first occurrence of non-native *Phragmites* in southwestern Ontario was at Walpole Island in 1948 (Catling & Mitrow 2012). The Lake St. Clair wetlands may be especially susceptible to future *Phragmites* invasion because of climate change and the shallow depth of Lake St. Clair. The lake is naturally 6.5m at its deepest point and 8.5m in the dredged shipping channel (Environment Canada, 2003). The extent and position of the undiked wetlands are greatly

affected by lake water level fluctuations since the topography of the delta and land surrounding the lake is almost flat. The St. Clair River only drops 20 cm over 17km through the delta (Edsall et al., 1988). If Great Lakes water levels drop due to a warming climate, newly exposed lake bottom is likely to be invaded by *Phragmites* as *Phragmites* colonization was found to be related to decreases in water depth and increase in bare soil area (Tulbure & Johnston, 2010).

An 850m by 850m area within the coastal wetland was selected for this study (Figure 3.1). By choosing a small area as the focus, a more detailed assessment of the abundance estimates from the spectral mixture analysis method could be made. The specific site was selected to be representative of pure areas of three land cover types and the different mixing scenarios that could occur between the land cover types. The study site under investigation is shown in true colour for both satellite images in Figure 3.2. In this small area, large patches of the three land cover types are present. A large unmixed water feature (dark blue) is present in the southwest corner. Pure *Phragmites* stands (green) surround this large water feature and also dominates the east portion of the image. Native marsh vegetation (light brown) inhabits large areas of the north and central study area. Also represented, are different ways in which the three land cover types can mix. A long, thin patch of *Phragmites* is surrounded by monodominant Native Marsh Vegetation in the north central portion of the study area. Alternatively, small patches of Native Marsh Vegetation are surrounded by monodominant *Phragmites* in the southeast. Both native and invasive vegetation border water in some part of the study area.

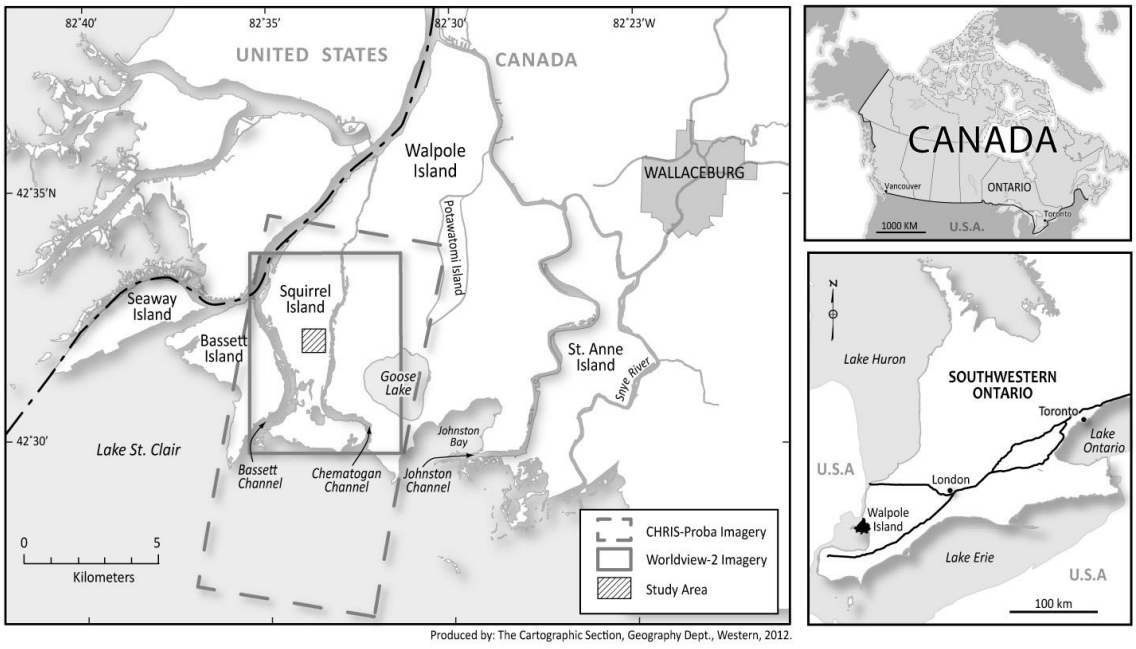

Figure 3.1 Walpole Island study site. Walpole Island is located in the southern Great Lakes region of Ontario, Canada. The five islands of Walpole have formed where the St. Clair River flows into Lake St. Clair. CHRIS PROBA and Worldview-2 imagery were acquired over parts of the coastal marshes of Bassett, Squirrel, and Walpole Island. The area of study is focused on a small portion of marsh on Squirrel Island.

3.2.2 Data

3.2.2.1 Remotely Sensed Imagery

3.2.2.1.1 CHRIS PROBA

Two sets of remotely sensed data were used in this study (Figure 3.2). First, a hyperspectral image from the Compact High Resolution Imaging Spectrometer on the Project for On-Board Autonomy satellite (hereafter referred to as CHRIS PROBA) was acquired on September 14, 2011. The CHRIS sensor has five different imaging modes which allow for imagery to be acquired with various sets of spectral bands, spatial resolutions, and scene sizes. CHRIS PROBA is also able to capture imagery in the in-orbit path at five viewing angles: -55°, -36°, 0° (nadir), +36°, +55°. The multiple imagery acquisition angles allow for bidirectional reflectance properties to be evaluated (for more information see Surrey Satellite Technology Ltd., 2008). The imagery for this study was acquired in Mode 5 with a spatial resolution of 17m, a set of 37 spectral bands covering the wavelength range of approximately 437-1040nm, a scene size of 14km x 7km, and individual bandwidths ranging from 6.1 to 33.1nm (Table 3.1). For this study, the

additional spectral bands at 17m spatial resolution of Mode 5 provided more important information compared with a larger image acquisition area (Table 3.2) available with other modes. Only the nadir image was used for this study as bidirectional reflectance properties were not the focus. The raw CHRIS imagery was corrected for two kinds of noise. First, CHRIS band 2 suffers from inconsistent pixel values in some image rows which are referred to as drop-outs. These pixels were identified and fixed as they will affect later processing stages. The second type of noise is vertical striping which is typical of push-broom sensors. The CHRIS sensor suffers from irregularities of the entrance slit due to changes in in-orbit instrument temperature. The change in the slit shape results in a complex vertical pattern related to the sensor's temperature which can was modelled and adjusted. Drop-out and vertical striping correction was completed using VISAT V4.10.3 (Brockmann Consult, 2012). Radiance values were then converted into reflectance values with a processing module in the VISAT software package developed specifically for CHRIS PROBA imagery based on Guanter et al. (2006). The CHRIS hyperspectral imagery was used as the input data for spectral mixture analysis (SMA) to determine the pixel fractions of the marsh land cover types.

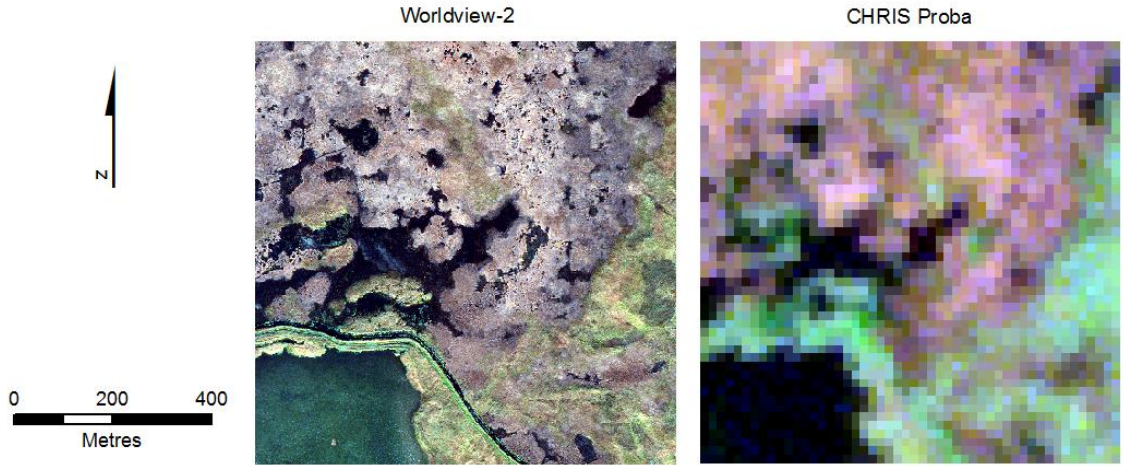

Figure 3.2 Worldview-2 and CHRIS PROBA imagery of the study area. Imagery for the study area displayed in true colour, Worldview-2 (Red: Band 5, Green: Band 3, Blue: Band 2) and CHRIS PROBA (Red: Band 7, Green: Band 4, Blue: Band 1).

Table 3.1 Details of the CHRIS PROBA spectral bands acquired for this study.

Band Number	Band Center (nm)	Bandwidth (nm)	Band Number	Band Center (nm)	Bandwidth (nm)
1	442.2	10.5	20	765.3	7.2
2	489.9	11.6	21	772.6	7.3
3	529.6	11.4	22	783.8	15.2
4	550.9	12.9	23	795.2	7.7
5	569.5	10.6	24	803.1	7.9
6	630.8	14.0	25	866.6	18.1
7	660.5	15.7	26	884.9	18.7
8	673.9	11.0	27	899.1	9.5
9	685.0	11.4	28	908.7	9.8
10	696.7	11.8	29	918.4	9.7
11	705.7	6.1	30	928.4	10.1
12	711.8	6.2	31	943.5	20.3
13	718.1	6.3	32	958.9	10.5
14	724.4	6.4	33	969.4	10.4
15	730.9	6.6	34	979.9	10.6
16	737.5	6.7	35	990.6	10.8
17	744.3	6.8	36	1001.4	10.7
18	751.2	6.9	37	1023.2	33.1
19	758.2	7.1			

Table 3.2 Overview of CHRIS PROBA operating modes.

Operating Mode	Number of Bands	GSD (m)	Swath Width	Application
1	62	34	Full (14km x 14km)	Aerosols
2	18	17	Full	Water
3	18	17	Full	Land
4	18	17	Full	Chlorophyll
5	37	17	Half (14km x 7km)	Land

Source: eoPortal 2012b

3.2.2.1.2 Worldview-2

A Worldview-2 image was acquired on October 17, 2010 with 0% cloud cover. The data are 11-bit radiometric resolution and were geo-referenced to the Universal Transverse Mercator (UTM) coordinate system, Zone 17 North, North American Datum 1983 (NAD83) by the image provider (MacDonald, Dettwiler, and Associates Ltd., Richmond, British Columbia).

Both images in this study were acquired late in the growing season to capitalize on the spectral differences between native and non-native vegetation at this time of year. Gilmore et al. (2008) found that *Phragmites* has a high NIR response late in the growing season relative to other vegetation and suggests that a single date of imagery captured during this time could be used to map this invasive species adequately. Chapter 2 described how the high spatial resolution Worldview-2 satellite was used for mapping of native and non-native marsh vegetation in Chapter 2. The classified Worldview-2 image for the study area is shown in Figure 3.3.

Since high classification accuracies were achieved from the 0.5m Worldview-2 imagery, it can be assumed to approximate the real surface cover (He et al., 2010), and be used to compare the fraction results of the SMA method. The WV-2 image was taken one year prior to the hyperspectral image, and as a result there could be changes in the amount of *Phragmites* and Native Marsh Vegetation cover. It is assumed the difference in cover

between years is small and changes that do occur will be at the edge of *Phragmites* stands as the invasive species spreads. The CHRIS PROBA imagery was carefully geo-referenced to the Worldview-2 imagery with root mean square error (RMSE) of less than 0.5 of CHRIS PROBA pixel dimension.

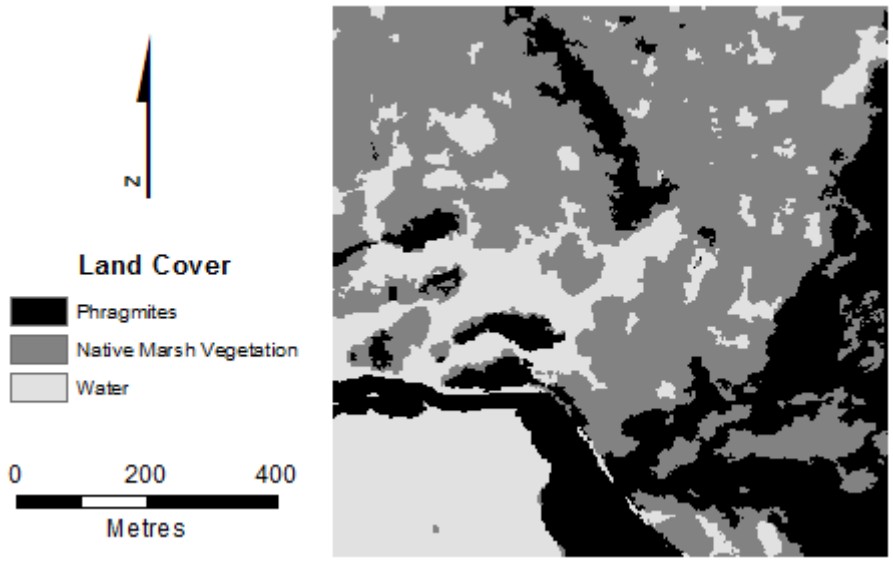

Figure 3.3 Worldview-2 classification result for SMA fraction accuracy assessment. This area is composed of three land covers: *Phragmites*, Native Marsh Vegetation, and Water.

3.2.2.2 Reflectance Spectra Field Data

An Analytical Spectral Devices (ASD) Fieldspec HH UV/VIR handheld spectroradiometer (ASD, Inc., Boulder, CO) was used to measure the reflectance spectra of land cover types in the field. The device has a wavelength range of 325-1075nm, a sampling interval of 1.6nm, and a spectral resolution of 3nm (ASD Technical Guide, 1999). Individual spectral measurements were an average of 10-25 scans to obtain an accurate spectral signature of the sampled vegetation canopy. The land cover was sampled between 3-5 times and the average of these measurements was used to provide a single spectrum for each target. A white Spectralon panel (Labsphere, Inc., North Sutton, NH) was used to normalize the reflectance spectra. Reflectance spectra were taken using the bare head of the spectroradiometer with a field of view (FOV) of 25°. Spectra were measured by hand-positioning the ASD approximately at nadir within 1 meter of the

species canopy. Spectra were measured two hours before and after solar noon to minimize the effects of shade.

Reflectance spectra were collected for the dominant native wetland vegetation species, *Typha* spp., the invasive plant *Phragmites*, and for water. The selected vegetation stands were dense monocultures in order to determine each cover's endmember characteristics. For *Typha* spp. and *Phragmites*, spectral measurements were not taken where understory species were observed. Measurements were taken of water when there was no aquatic vegetation near the surface. Spectral measurements were taken August 16 and 17, 2011 to coincide with a CHRIS PROBA satellite overpass, however thin cloud cover during image acquisition rendered the image unusable for SMA analysis. Instead, a cloud-free CHRIS image acquired September 14, 2011 was used for SMA modeling. It was not possible to conduct fieldwork close to the September CHRIS image acquisition as a local guide was not available, and the waterfowl hunting season prevented safe conditions in the marsh. Additional fieldwork was conducted October 7, 2011, under clear skies. Access to the marsh was gained by land via roads on top of dykes, and by boat. For the ASD to be held a sufficient height above the *Phragmites* canopy to collect spectral measurements late in the growing season when *Phragmites* reaches its maximum height, the ASD was held above the canopy while standing on the cargo bed of a pick up truck. The height of *Phragmites* did pose a challenge for ASD measurements obtained in the boat so shorter stands were targeted to allow adequate space between the spectrometer and canopy.

3.2.3 Spectral Mixture Analysis Method Overview

The flow chart in Figure 3.4 illustrates the steps conducted in the deriving the SMA fractions and assessing the accuracy of these fractions with the ground truth fractions calculated from Worldview-2 imagery. The spectrally calibrated and georectified CHRIS PROBA imagery was the input data for the SMA method. The minimum noise fraction transformation was used to separate the useful data from the noise, eliminating the redundant spectral information from further processing. The image derived endmembers were selected by two methods based on their values from the PPI index. Endmembers were also selected based on ASD measurements of pure endmember areas in the field. The different sets of endmembers were used as input for the spectral mixture analysis model to derive the endmember fraction estimations. The *Phragmites* fraction was used to develop a *Phragmites* invasion map showing the degree of *Phragmites* dominance in each pixel. A dominant classification map showing the dominant land cover for each pixel was produced from the endmember fraction values. The accuracy of the endmember fractions, *Phragmites* invasion map and dominant land cover map were evaluated by comparison with ground truth derived from the object-based classification from Chapter 2. The individual steps taken are described in more detail in the following sections.

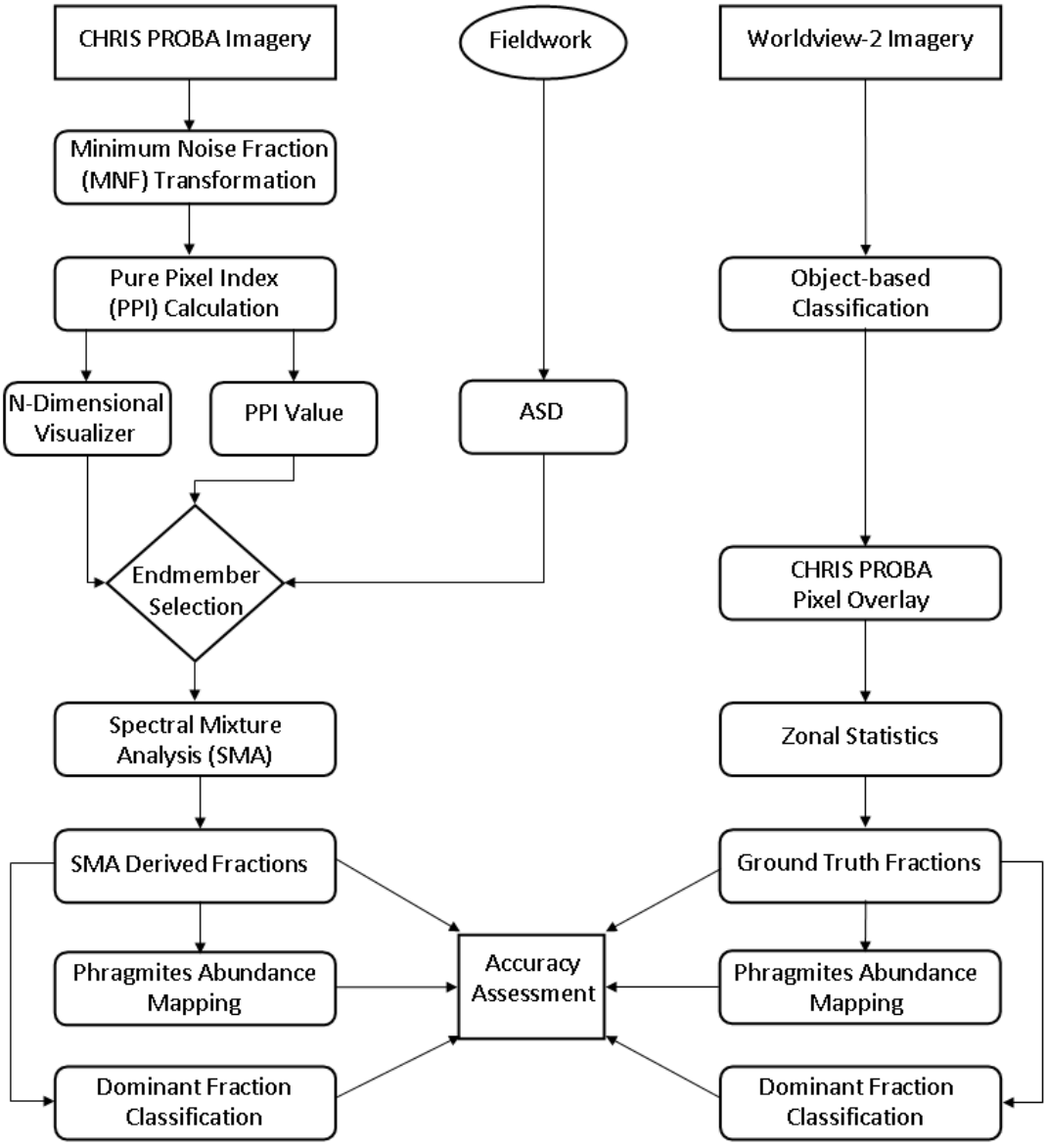

Figure 3.4 Flowchart outlining the method used in this study.

3.2.3.1 Hyperspectral Data Dimensionality Reduction

Hyperspectral imagery contains highly correlated bands due to the narrow and continuous placement of the spectral bands (see Table 3.1 for CHRIS PROBA bandwidths and band placement). Reducing the spectral dimensionality of the imagery removes redundant information from the analysis, which decreases the amount of data carried forward and reduces computing requirements (Jensen, 2005). To reduce the spectral dimensionality of the data, a forward Minimum Noise Fraction (MNF) transformation (Green et al. 1988)

was applied to the hyperspectral image bands to separate the useful information from the noise. The MNF transformation is the product of two principal components analyses (PCA). The first PCA transformation decorrelates and rescales the noise in the bands resulting in data with no correlation between bands and for which the noise has unit variance. The second PCA produces MNF eigenimages ranging from coherent MNF eigenimages that contain useful information to completely noise-dominated MNF eigenimages (Jensen, 2005). By inspecting the resulting eigenvalues and MNF eigenimages, the true spectral dimensionality can be determined. MNF bands with high eigenvalues or that are visually coherent, contain useful information and are kept for later processing (Exelis Visual Information Solutions, 2012). MNF bands with low eigenvalues (value of 1) or that are visually incoherent, are dominated by noise and are discarded. MNF bands with eigenvalues greater than 1, and typically of an order of magnitude greater than MNF bands dominated by noise, contain useful information (Jensen, 2005).

MNF bands were evaluated by investigating eigenvalues (Figure 3.5) and the spatial coherency of the MNF bands (not shown). Analysis of the eigenvalues showed that the first eight MNF bands had high eigenvalues ranging from 42.16 for the first MNF band to 2.15 for the eighth. After the eighth band, the relative difference between MNF band eigenvalues was small and MNF band eigenvalues approached 1, indicating that they were dominated by noise. Inspection of the MNF eigenimages supported this conclusion as the spatial coherency of the eigenimages diminished after MNF band 8. The first two MNF bands have much higher eigenvalues compared to bands 3 through 8. This indicates that the majority of the information (~75%) is contained in the first two MNF bands. Although the hyperspectral data cube should be reduced to a small number of significant bands, caution should be taken not to throw out bands supplying important information (Bedini et al. 2009). Also, a requirement of the SMA model to solve the pixel mixture is that the number of input bands is one more than number of endmembers (Exelis Visual Information Solutions, 2012). Therefore, the first eight MNF bands were kept for SMA to retain the majority of information, and to allow up to seven endmembers to be included in the mixture model.

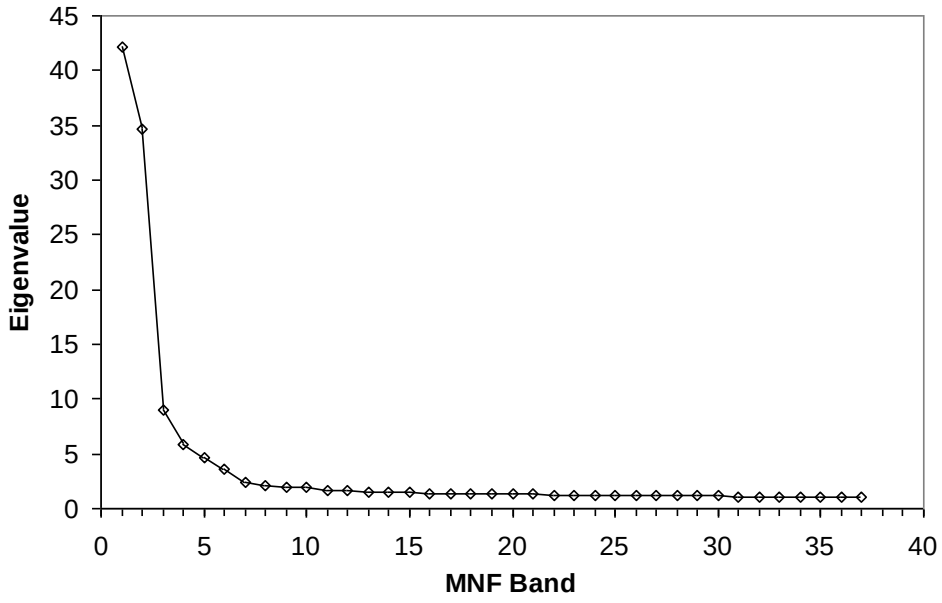

Figure 3.5 Eigenvalue plot for the 37 Minimum Noise Fraction (MNF) bands. The first eight MNF bands contained the majority of information and were retained for the SMA analysis.

3.2.3.2 Endmember Selection

An important step in successful SMA fraction estimation is the identification of all land cover classes present in the area of study (Jensen, 2005). In this study, there are three land cover types present: the non-native plant species *Phragmites*, Native Marsh Vegetation, and Water. These land cover classes are referred to as endmembers in SMA. Endmembers are defined as the relatively pure materials in the study area and all pixels in the study area are assumed to be a mixture of these endmembers. If the spectral signature of a pure pixel of each endmember is known, then by using SMA methods it is possible to determine the abundance fraction of endmembers in each pixel (Exelis Visual Information Solutions, 2012).

There are three methods in which the spectral signatures of endmembers are selected. The spectral signatures may be obtained from a spectral library that contains laboratory or field tested spectra of materials. Libraries exist for materials such as minerals and vegetation, e.g. USGS Mineral and Vegetation Spectral Library (Clark et al. 1993), man-made materials, e.g. John Hopkins University Spectral Library (Exelis Visual Information Solutions, 2012), etc. Endmember selection through this method is more

successful for mineral mapping as minerals tend to have a limited number of possible spectra which don't change with geographical location or time of year. Spectral libraries for vegetation tend to be relatively less complete as they may contain limited species or limited spectral variation which is needed to address changes in plant reflectance at specific times of the year.

Direct spectral reflectance of endmembers can be acquired by ASD measurements in the field or in the controlled environment of a laboratory. Accurate SMA fraction estimation using this method is highly dependent on acquiring spectral signatures of endmembers under similar conditions as when the hyperspectral imagery was captured. This reduces the chance of differences in spectral reflectance occurring due to changes in endmembers with time as is the case with vegetation.

The third way to obtain representative endmembers is by identifying pure endmember pixels in the hyperspectral imagery. This method tends to produce better SMA fraction results than field measurements because the image endmember contains the same errors resulting from calibration or atmospheric correction as the rest of the pixels in the study area (Exelis Visual Information Solutions, 2012). Since these errors are uniform across the image, fraction estimates are less likely to be influenced.

In this study, image derived endmembers were selected based on their Pixel Purity Index (PPI) values and the n-dimensional visualization of high value PPI pixels in MNF spectral space. Endmembers based on ASD measurements of pure species stands made in the field were included to demonstrate the importance of obtaining endmember spectral signatures close to the hyperspectral image acquisition date. Endmembers from publicly available spectral libraries for marsh species in this study were not available. The next sections describe the methods used to determine the endmembers for SMA.

3.2.3.3 Pixel Purity Index Endmember Selection

The goal of PPI mapping is to find the most spectrally pure pixels in the hyperspectral image. These pixels are most likely to represent the image endmembers since they represent pure land cover types. The PPI method determines the most spectrally pure

pixels by projecting an n-dimensional scatterplot onto a random unit vector. The pixels at both ends of the projected vector are recorded if they are within the user specified threshold of the most extreme pixels. The user defined threshold is set at 2 to 3 times the noise level in the data. Since MNF bands are used, the noise level is 1, so a threshold or 2 or 3 is specified. If a larger threshold is used, more extreme pixels are recorded at each iteration but there is a greater chance that they are spectrally less pure (Exelis Visual Information Solutions, 2012). This process is repeated for a user defined number of iterations and the total number of times each pixel is found to be extreme is noted. The output is a PPI map where the PPI value refers to the number of times each pixel was found to be "extreme". Therefore, pixels with high PPI values are spectrally unique and the most likely to represent the endmembers.

A Pixel Purity Index was calculated to determine the most spectrally pure pixels in the image. The PPI value image was opened in ArcGIS and the values were sorted from highest PPI value to lowest. The highest PPI value was selected and the pixel ID noted. This pixel was located in the CHRIS image and a spectral profile of this pixel was displayed and compared to ASD measurements taken in the field to identify the land cover it represented. When the pixels with the highest PPI values were found for each of the three land cover types, this set of spectral signatures became the first group of endmembers. The second highest PPI values for each land cover were then determined and used for the second group of endmembers. This was repeated a third time to yield three sets of image derived endmembers. The endmember group and PPI values for the specific endmembers are shown in Table 3.3.

Table 3.3 Endmembers chosen using Pixel Purity Index values.

	Land Cover		
Endmember Group	*Phragmites* PPI Value	Native Marsh Vegetation PPI Value	Water PPI Value
1	1655	1080	1622
2	1366	1080	1587
3	1362	1071	1524

3.2.3.4 N-Dimensional Visualization Endmember Selection

Endmembers were also selected through visualizing the PPI results in an n-dimensional visualizer and selecting the most pure pixels. The n-dimensional visualizer is an n-dimensional scatter plot where n corresponds to the number of MNF bands used to display the data (Exelis Visual Information Solutions, 2012). The position of a pixel in the n-dimensional spectral space is determined by the pixel reflectance value in each MNF band, and is therefore representative of the pixel's spectral signature. Pixels with pure spectral signatures tend to occupy the corners of the n-dimensional data cloud while less pure or mixed pixels occupy the space in between (Exelis Visual Information Solutions, 2012). By displaying the data using different combinations of MNF bands and rotating the data cloud, it is possible to locate the corners and therefore the endmember pixels.

Using this approach, pixels located in a corner of the data cloud were selected and the mean signature was compared to the ASD measurements and identified as one of the land cover types. If the cluster of pixels was representative of one of the endmembers, the mean spectral signature of these pixels was used as the endmember signature. The process was repeated until endmember pixels were located for all three land cover classes. Endmember group 4 refers to the image derived endmembers selected through n-dimensional visualization.

3.2.3.5 ASD Field Measurement Endmember Selection

Spectral measurements were taken with the ASD HH UV/NIR handheld spectrometer in mid-August and early October. Endmember signatures were computed by averaging the spectral measurements taken of each land cover. Both sets of endmembers were input to the SMA model for fraction estimation. Endmember set 5 and 6 refer to the August and October ASD measurements respectively.

3.2.4 Spectral Mixture Analysis

Spectral mixture analysis is a method which determines the relative abundance of endmembers in a pixel based on the pixel reflectance and endmember spectral signatures. SMA models are divided into two groups based on the type of mixing assumed to be occurring in the field of view. The linear mixing model is based on the assumption of linear mixing where photons interact with a single land cover type before reaching the sensor (Adams et al. 1993). The signature of the mixed pixel can be modelled as a linear sum of each endmember weighted by the fraction of each endmember within the pixel (Roberts et al. 1998). Alternatively, the nonlinear model assumes that mixing is more complex since photons interact with multiple land cover types before reaching the sensor (Adams et al. 1993). Many studies of wetland vegetation are based on the linear mixture assumption (e.g. Rosso et al., 2005, He et al., 2010). In this study linear mixing is assumed.

Linear spectral unmixing, makes four assumptions (Settle and Drake, 1993). 1) The occurrence of multiple scattering between different surface components is not significant. If this assumption is not met, the mixing is complex and results in nonlinear mixing. 2) The spectral signatures of each surface component are sufficiently different from one another to allow their separation. 3) The total land cover within each pixel is unity. 4) All of the endmembers present in the study area are known.

When photons have interacted with only a single land cover, the reflectance for that pixel is a linear sum of the reflectance received from each endmember. Each endmember will contribute the reflectance that is characteristic of that land cover and the energy will be proportional to the area covered (Adams et al. 1993). If the pixel land covers include vegetation, the fraction is equal to the proportion of canopy cover (Parker Williams and Hunt, 2002).

The Horwitz (1971) linear mixture model is used in this study and is described below as in Drake et al. (1999). n denotes the number of bands in the hyperspectral image, and c the number of land cover types, or endmembers, present. For any pixel, x_i represents the observed spectral signal in the ith hyperspectral band and f_j denotes the fraction of that

pixel covered by the *j*th land cover type. The spectral signature of any pixel is represented by the vector $x = \{x_1, x_2, ..., x_n\}^T$. The land cover fractions are represented by the vector $f = \{f_1, f_2, ..., f_c\}^T$. The superscript T in both cases denotes 'transpose'. The linear spectral mixture model is defined by equation (1):

$$x = \mathbf{M}f + e \quad (1)$$

where **M** is an (n x c) matrix whose columns are the endmember spectral signatures. Unmodelled portions of the spectrum are expressed by the residuals vector $e = \{e_1, e_2, ..., e_n\}^T$. f can be estimated by a modified least squares approach if **M** and **N** are known. N is the variance-covariance matrix of the noise term e. The least squares estimate for f is selected by minimizing the quadratic function in equation (2):

$$(x - \mathbf{M}f)^T \mathbf{N}^{-1} (x - \mathbf{M}f) \quad (2)$$

where f can be subject to two constraints:

$$f_1 + f_2 + ... f_c = 1 \quad (3)$$

and

$$0 \leq f_j \leq 1 \quad j = \{1, ..., c\} \quad (4)$$

Equation (3) constrains the sum of the individual endmember fractions to 1 and equation (4) constrains the individual endmember fractions to values between 0 and 1. A linear spectral model using both constraints is referred to as a fully constrained mixing model. In this study, a partially constrained linear unmixing model obeying equation (3) was performed using ENVI version 4.8 (Exelis Visual Information Solutions, Boulder, Colorado). However, this allows for the endmember fractions to be negative or greater than 1 which are both physically impossible. If pixels have a value below 0.0 or 1.0, this could be an indication that the endmember signatures are not representative, or that an endmember may be missing from the analysis (Exelis Visual Information Solutions, Boulder, Colorado). Therefore, to determine how many pixels could be modelled with physically possible fraction values for all land covers, the second constraint was applied

to the model fraction results. The results from applying this second constraint were used to compare the individual SMA models.

3.2.5 Spectral Mixture Analysis Accuracy Assessments

The six class classification from Worldview-2 was used as the ground truth for this study. Figure 3.6 outlines how the ground truth fractions were extracted from the classified Worldview-2 image for each CHRIS PROBA pixel. The Worldview-2 classification was reclassified into binary classifications where a value of 1 represented the land cover class of interest, and 0 represented all other classes. Binary classifications were performed for Native Marsh Vegetation, *Phragmites*, and Water. A grid of polygons representing the CHRIS pixels was created using a custom script in ENVI IDL. This grid was overlain on the Worldview-2 binary classifications and the zonal statistics for each 17m by 17m pixel was calculated in ArcGIS. The sum within each pixel was calculated using the zonal statistics tool and sum operator. The sum was divided by 1156 to yield the fraction of each land cover. Each CHRIS PROBA pixel represents 1156 individual 0.5m x 0.5m Worldview-2 pixels. Each individual Worldview-2 pixel represents approximately 0.0865% fraction cover for the CHRIS PROBA pixel. This process was repeated for all pixels within the study area.

The fractions calculated from the CHRIS PROBA imagery using SMA were compared to the ground truth fractions from the Worldview-2 classification in multiple ways. The number of pixels modelled refers to the number of pixels which meet the physical constraints placed on fractions with a pixel. Pixels with fraction values and sum of fraction values between -0.01 and 1.01 are considered to be feasible, allowing for slight fraction over- or underestimation. Model RMSE is a measure of the difference between the pixel reflectance and the fractional mixtures of the endmembers in the model (Rosso et al. 2005). An RMSE value is output for each pixel and the average of these RMSE values yields a measure of overall model fit. The difference between predicted and ground truth fractions was computed and averaged for each class. If ground truth and SMA fractions are accurate, the average difference should be close to 0. *Phragmites* ground truth fractions were plotted against SMA fractions and a linear regression performed. With the linear regression, a slope value close to 1, a y-intercept close to 0,

and R^2 value near to 1, all indicate SMA fractions that closely match ground truth fractions. The difference between predicted and ground truth fractions was computed and the frequency displayed as a histogram. The frequency was broken down into fraction cover increments of 0.05. Histograms that have a small spread and are centred around 0 indicate accurate SMA land cover fractions. Evaluating the SMA fractions with these methods will determine which endmember selection method is best for *Phragmites* fraction estimation in the marsh environment.

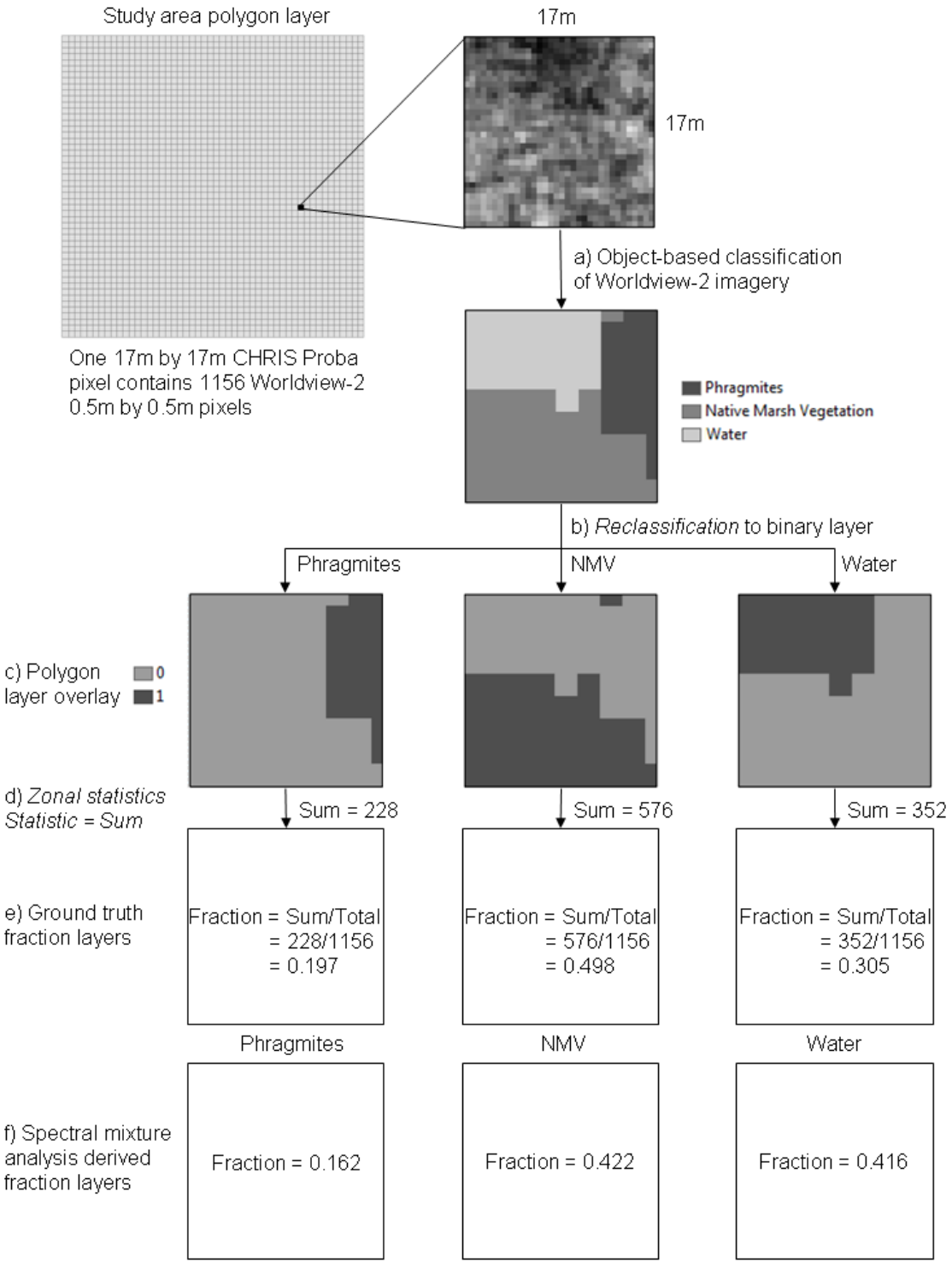

Figure 3.6 The method used to extract land cover ground truth fractions from the classified Worldview-2 image.

3.2.6 *Phragmites* Invasion Mapping

In this study, two thresholds are defined which can be applied to SMA fraction data to determine the status of *Phragmites* invasion within a pixel. One threshold is set at ⅓ of a pixel area. Since the sum of the three fractions must equal to 1, if *Phragmites* is less than ⅓, one of the other two fractions must be the dominant fraction. Therefore, if *Phragmites* fraction is below ⅓ then *Phragmites* has not reached dominance in the pixel. The second threshold is set at ½ of a pixel area. This represents the fraction value at which the pixel can be guaranteed to be dominated by *Phragmites*. As a result of defining these two thresholds, a third group of pixels is automatically defined. These pixels have *Phragmites* fraction values greater than ⅓ but less than ½. Depending on the fraction values of the other two classes, these pixels represent areas that may or may not be *Phragmites* dominated. The thresholds were applied to ground truth and SMA fraction layers to determine how well the SMA method can detect different stages of *Phragmites* invasion within individual pixels.

3.2.7 Dominant Fraction Classification

A classification was performed based on the dominant fraction within each pixel, as another method to assess the fractions estimated by the SMA method. The dominant fraction is defined as the land cover class with the highest percentage cover within each pixel. For example, in Figure 3.7 the fractions of *Phragmites*, Native Marsh Vegetation, and Water derived from ground truth and SMA are 0.197, 0.498, 0.305, and 0.162, 0.422, 0.416, respectively. In both cases, the dominant land cover is Native Marsh Vegetation so this pixel is classified as being Native Marsh Vegetation dominated in both layers. The Worldview-2 classification was classified in this manner and acted as the ground truth for the comparison of the SMA tests. These dominant classification results were compared in a confusion matrix and the user's accuracy (commission error), producer's accuracy (omission error), overall accuracy, and the Kappa statistic were used as accuracy measures. If SMA fractions are accurate, the classification based on the dominant class within each pixel will provide useful information about dominant land cover distribution in the marsh.

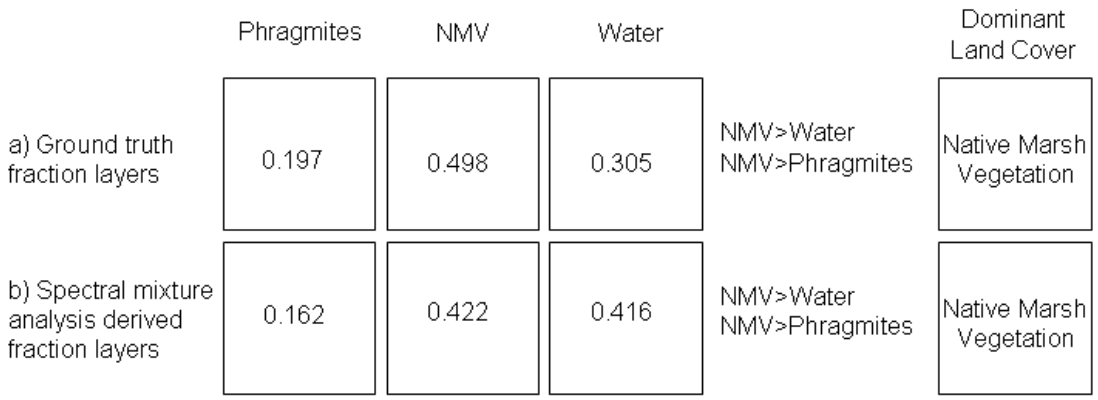

Figure 3.7 The method used to assign the dominant class to each pixel. An example is given showing the method for a single CHRIS PROBA pixel. a) The ground truth fractions for a single pixel are compared. Since the fraction of Native Marsh Vegetation (NMV) is greater than the fraction of *Phragmites* and Water, NMV is assigned as the dominant fraction. b) The procedure in a) is repeated for the fractions estimated from SMA.

3.3 Results and Discussion

3.3.1 ASD Measurements and Image Derived Spectral Signatures

The spectral curves of *Phragmites*, Native Marsh Vegetation, and Water from field measurements and from image pixels representing each endmember are shown in Figure 3.8. To better compare the field collected land cover spectral curves, ASD measurements were averaged over the corresponding CHRIS spectral bandwidths. *Phragmites* and Native Marsh Vegetation both show healthy, unstressed vegetation curves in August (Figure 3.8 (a) and (b) respectively). There is strong absorption in the blue and red portions of the spectrum where the primary chlorophyll absorption bands occur, indicating plant photosynthesis. The spectral curves also display high near-infrared reflectance typical of healthy green vegetation. They also show a steep red-edge which occurs due to strong absorption of red wavelengths and strong reflectance of energy in the near-infrared. However, in September and October, both Phragmites and Native Marsh Vegetation are showing signs of plant stress and/or seasonal senescence. Signs include a decrease in absorption in the blue and red regions corresponding to the chlorophyll bands and a decrease in the near-infrared reflectance indicating decreased photosynthesis, and a shift of the red-edge towards the shorter blue wavelengths. The

ASD spectral curves of water (c) remain consistent between sampling dates indicating that the spectral properties of Water did not change, which also shows that sampling was done consistently from one date to another. The image derived endmember for Water shows slightly increased reflectance in the green and near-infrared part of the spectrum compared to ASD measurements. This may be due to the limited number of pure water pixels in the study area. Most patches of water contained a small amount of emergent or floating aquatic vegetation which accounts for the slight increase in reflectance in the green and near-infrared.

Spectral measurements for *Phragmites* and Native Marsh Vegetation in August are similar through the visible range to the red-edge (440-740nm) but differ in the near-infrared (740-1040nm), with *Phragmites* having higher near-infrared reflectance. Greater differences between the two vegetation classes are seen in the September image derived endmember spectra. *Phragmites* has slightly increased reflectance in the blue and red portions of the spectrum and decreased reflectance in the near-infrared relative to the ASD measurement taken in August. Over this time period, *Phragmites* has begun to show early signs of seasonal senescence. The Native Marsh Vegetation curve has changed very rapidly between August and September. Large increases in reflectance in the blue and red regions of the spectrum combined with a large decrease in reflectance through the near-infrared suggests that Native Marsh Vegetation has gone through significant change likely indicating rapid senescence. The spectral differences are small and may indicate that *Phragmites* and Native Marsh Vegetation will soon reach similar stages of senescence.

The month by month change in the spectral curves provides valuable information as to when *Phragmites* and Native Marsh Vegetation are spectrally distinct. In August, both *Phragmites* and Native Marsh Vegetation are healthy and green and have only slight differences in the reflectance in the near-infrared. In October, both land covers show similar spectral curves which show signs of severe plant stress likely related to seasonal senescence. Since the spectral plots for the plant species in August and October are very similar, SMA methods may not produce accurate sub-pixel abundance estimates. Alternatively, the spectral curves exhibited in September provide important information

for the discrimination of *Phragmites* and Native Marsh Vegetation. Differences occur in the visible and near-infrared portions which result in very different spectral curves for the species at this time. Therefore, an image acquired in September may be the best input for sub-pixel abundance estimations for *Phragmites* derived from SMA methods. Neither ASD measured endmembers for August or October matched the spectral characteristics of the three land covers in September and are hypothesized to predict land cover fractions with poor accuracy.

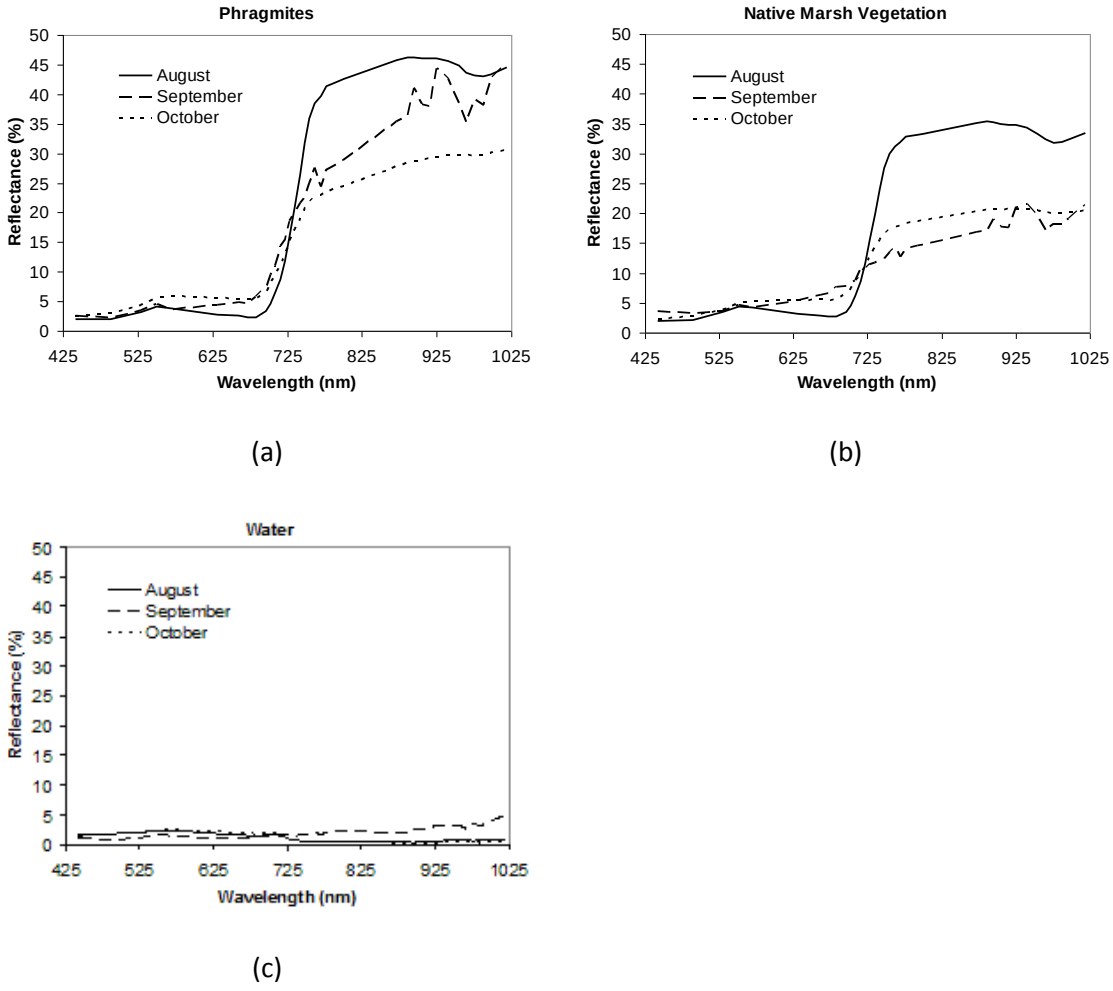

Figure 3.8 Reflectance spectra of the three land covers from field ASD spectroradiometer measurements and pure CHRIS PROBA image pixels.

3.3.2 Spectral Mixture Analysis Results

3.3.2.1 Model Performance

Results obtained from tests using endmembers from high Pixel Purity Index values will from now on be referred to as 'PPI models'. 'N-DV model' refers to the test using endmembers selected using the N-Dimensional Visualizer. A-ASD and O-ASD will refer to the endmembers selected from August and October ASD field measurements, respectively. The results of the spectral mixture analysis (SMA) are shown in Table 3.4. Pixels modelled refers to the number of pixels whose fraction values for all classes are between the values of -0.01 and 1.01, and whose sum of the three land cover fractions is also between -0.01 and 1.01. In this analysis, values one percent below 0 and above 1 were considered reasonable errors of fraction cover and pixel sums. Average Root Mean Square Error (RMSE) refers to the error associated with the model. After modelling, each pixel has an RMSE value which is an indicator of model fit. The RMSE values were averaged for all pixels within that model to give us overall average model RMSE. The absolute difference between predicted and ground truth was calculated for each land cover and averaged.

The N-DV model resulted in the lowest average difference between ground truth and predicted fractions for all classes (Table 3.4). This may be because the N-DV endmembers were the mean of multiple pixels, which accounts for variation within each class and thus an endmember that was more representative of the majority of the pixels. In contrast, using a single pixel as the land cover endmember in PPI models, does not account for any variation within each class. Of the three PPI models, Test1 resulted in the lowest average difference between ground truth and predicted fractions for all classes. PPI models resulted in the greatest number of pixels that were within the physical constraints placed on the model, being able to model roughly 81-84 percent of all pixels. Although the N-DV model endmembers had the lowest average difference, only 74% of the pixels yielded physically possible fraction estimates. Therefore, models with single endmembers based on PPI values resulted in comparable differences in fraction estimates to the N-DV model while being able to model more pixels. Although model RMSE is supposed to give an estimate of the error associated with the model, there was no relation

between how many pixels were physically modeled or the average difference between ground truth and predicted fractions for PPI or N-DV models. Higher average model RMSE was not associated with higher average fraction differences or lower number of pixels modelled except in the case of ASD models.

ASD models performed poorly compared to image derived endmember models. This was expected as ASD measured endmembers were not representative of the land cover types at the time of hyperspectral image acquisition. Better fractions estimates and a higher number of pixels modelled would have been expected had the ASD measurements been taken close to hyperspectral image acquisition. Due to the spectral differences between ASD and image endmembers and the subsequent poor SMA model performance, ASD models will not be considered in further analysis.

Table 3.4 Spectral Mixture Analysis model performance.

Test	Endmember Selection Method	Pixels Modelled (Total = 2500)		Average Pixel RMSE	Average Difference between Ground Truth and Predicted Fractions		
		Number	Percentage		*Phragmites*	NMV	Water
1	PPI Value	2044	81.76	0.006633	0.1659	0.2561	0.1741
2	PPI Value	2103	84.12	0.006021	0.1825	0.2634	0.1793
3	PPI Value	2068	82.72	0.005046	0.1776	0.2631	0.1808
4	N-DV	1854	74.16	0.005111	0.1592	0.2451	0.1538
5	ASD-A	1297	51.88	0.022008	0.2329	0.3603	0.3278
6	ASD-O	1231	49.24	0.011614	0.4262	0.5790	0.2375

3.3.2.2 Ground Truth Versus Spectral Mixture Analysis Plots

If SMA produces highly accurate fraction estimates of the three land covers, the SMA derived fractions match the ground truth fractions perfectly, and there should be a linear relationship with a slope of 1 and the y-intercept passing through 0 when predicted fractions are plotted against ground truth fractions. Figure 3.9 shows the predicted fraction (SMA fraction from CHRIS PROBA imagery) plotted against ground truth

fraction (from Worldview-2 classification) for *Phragmites* for the six tests. The gray line in the plots represents the 1 to 1 relationship expected when predicted fractions match their corresponding ground truth fractions. Points above the 1 to 1 line indicate the fraction was overestimated by SMA while below the 1 to 1 line indicates the fraction was underestimated by SMA.

Image derived endmember models outperformed both ASD models. ASD-O has a slope close to 1 and high $R^2 = 0.7003$, but this model predicts *Phragmites* fraction poorly as many pixels have fractions greater than 1. The regression line passes through the y-intercept at 0.427 meaning that fraction values are, on average, overestimated by >40% fraction cover. Differences between PPI models and the N-DV model are small and all models predict *Phragmites* fractions equally well.

Overall, model predictions of *Phragmites* cover are quite poor. When *Phragmites* ground truth fraction is high, SMA fraction are consistently underestimated. For low ground truth *Phragmites* fractions, SMA fractions tend to be overestimated. As a result of these two trends, slope values are low ranging from 0.5111 to 0.5651, and y-intercepts are positive passing through approximately 0.10 and 0.15 fraction cover. The plots also show large differences in individual predicted fractions and ground truth for mixed pixels. In general, fractions of mixed pixels have a large scatter on either side of the 1 to 1 line. These results suggest that CHRIS PROBA imagery and SMA may not be able to predict *Phragmites* cover for individual pixels with high accuracy.

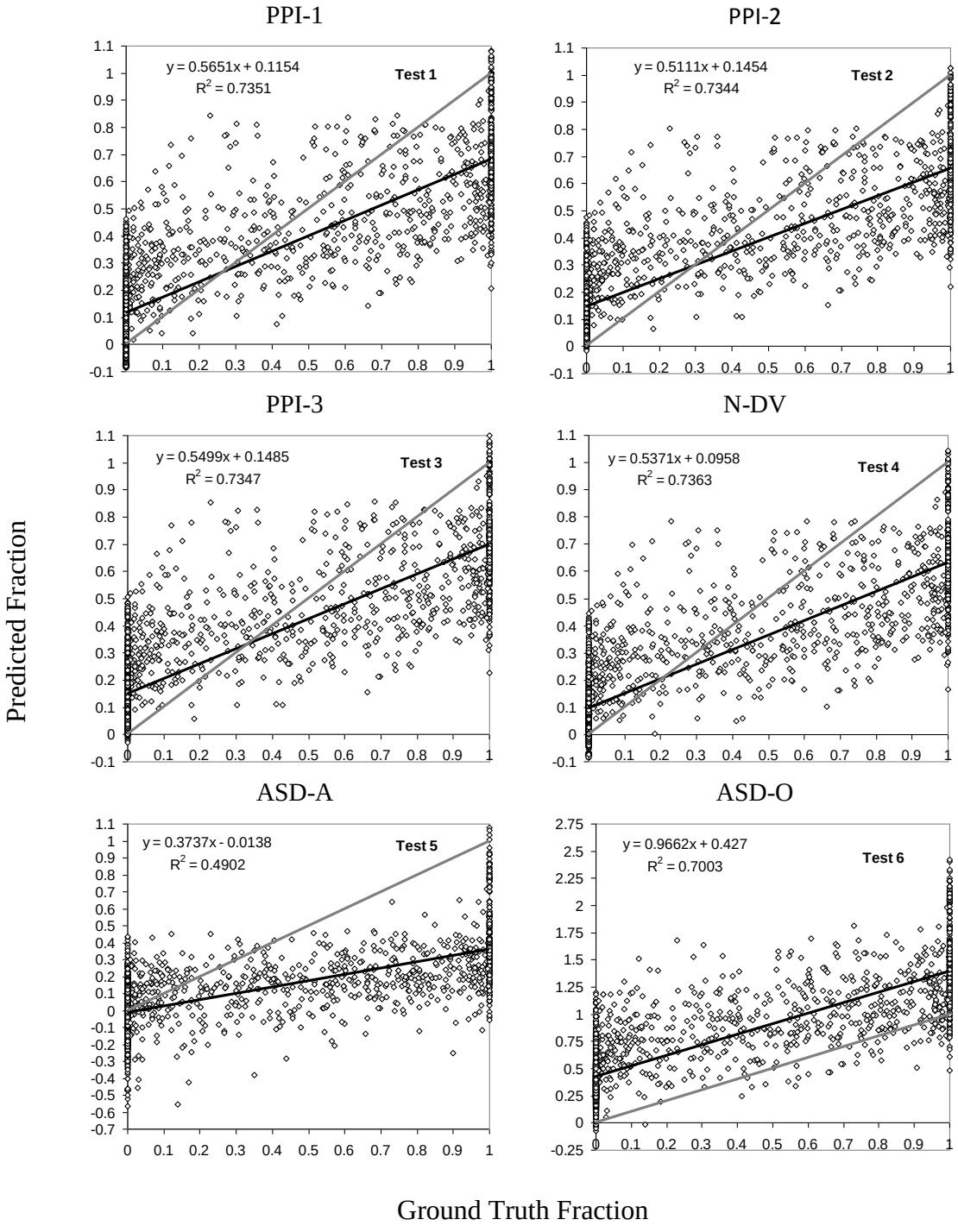

Figure 3.9 Regression plots of the six SMA models for the *Phragmites* class. The gray line represents the 1 to 1 line or a perfect match between predicted and ground truth fractions. The black line is the regression line of the *Phragmites* predicted and ground truth fractions.

3.3.2.3 *Phragmites* Fraction Difference Histogram

The difference between SMA and ground truth fractions can be summarized by the histograms in Figure 3.10. These histograms show the number of times SMA and ground truth fractions differed using 5% fraction increments. SMA fractions were subtracted from ground truth fractions meaning positive values indicate the fraction was overestimated by SMA while negative values indicate the fraction was underestimated by SMA.

The overall shape of the histograms for *Phragmites* fractions are very similar for the PPI models and the N-DV model. For PPI models, the main peak of values is slightly positive meaning many of pixels had slightly overestimated *Phragmites* fraction. The main peak for N-DV model was centred closest to 0. However, we would expect to see all pixels centred closely to 0 if the SMA fractions were close to the ground truth fractions. Instead, the histogram values range from -0.75 to +0.75 and a bimodal distribution is evident. Since the histograms are not tightly clustered around 0, a more detailed breakdown of the fraction differences is needed to determine exactly how SMA pixel fractions relate to ground truth.

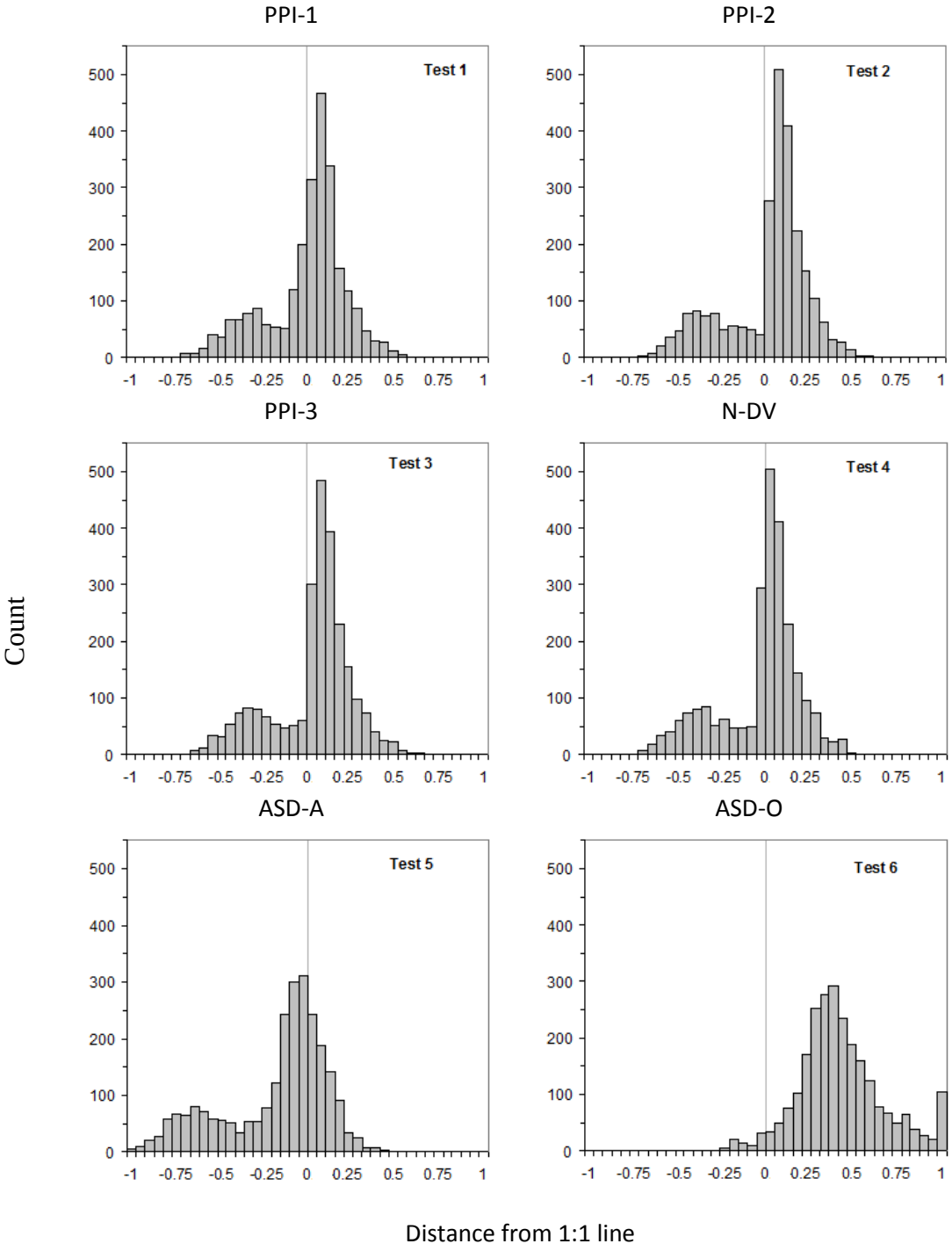

Figure 3.10 Fraction error histograms of the six SMA models for the *Phragmites* class. Positive values indicate the fraction was overestimated by SMA. Negative values indicate the fraction was underestimated by SMA.

The detailed breakdown of the histogram for Test1 (PPI-1) is shown in Figure 3.11. In histograms (b)-(d), the pixels are separated into different categories based on the amount of *Phragmites* occurring in the ground truth pixel and compared with the overall fraction error histogram (a).

The majority of slightly overestimated pixels are the result of SMA fractions predicting very low fractions of *Phragmites* for ground truth pixels with a *Phragmites* fraction of 0 (Figure 3.11 (b)). When no *Phragmites* was present, SMA fractions were 97.2% accurate in assigning a fraction value that could not make *Phragmites* the dominant land cover class (less than ⅓) (Table 3.5). Therefore, the SMA model is accurate at predicting low *Phragmites* fraction when ground truth fraction of *Phragmites* is 0.

The minor peak that is observed in the Test1 (PPI-1) histogram centred close to -0.30 corresponds to pixels where *Phragmites* ground truth fractions are 1 (Figure 3.11(c)). The SMA model consistently underestimates the fraction of *Phragmites* in these monodominant pixels. Although these fractions are underestimated, *Phragmites* as the dominant land cover (highest fraction within the pixel) is correctly predicted by SMA fractions in 92.0% of *Phragmites* monodominant pixels (Table 3.5).

In Figure 3.11 (d) we can see that SMA fractions for mixed pixels do not follow a pattern and are evenly spread out through -0.5 and +0.5 fraction difference. However, for mixed pixels in which *Phragmites* was dominant (highest fraction within the pixel) 69.6% of SMA predicted fractions also had *Phragmites* as dominant (Table 3.5). For mixed pixels in which *Phragmites* could not be dominant (cover <⅓), 60.0% were correctly identified as having a fraction that was not dominant (Table 3.5).

Although the Test1 histogram was not useful for determining how SMA fractions compared with ground truth fractions, breaking the distribution down into ground truth *Phragmites* categories yielded useful comparisons. These results suggest that SMA fractions cannot reproduce highly accurate ground truth fractions for every pixel. SMA fractions derived from CHRIS PROBA imagery seem to be indicators of *Phragmites* dominance within individual pixels. SMA fractions were highly accurate when *Phragmites* was not present in the pixel. They were also highly accurate for classifying a

pixel as being *Phragmites* dominant when the species was dominant in a pixel. In the case of mixed pixels, SMA fractions had fair accuracy predicting where *Phragmites* was and was not the dominant fraction in the pixel. SMA fractions resulted in 89.1% overall accuracy for the four scenarios covered (Table 3.5).

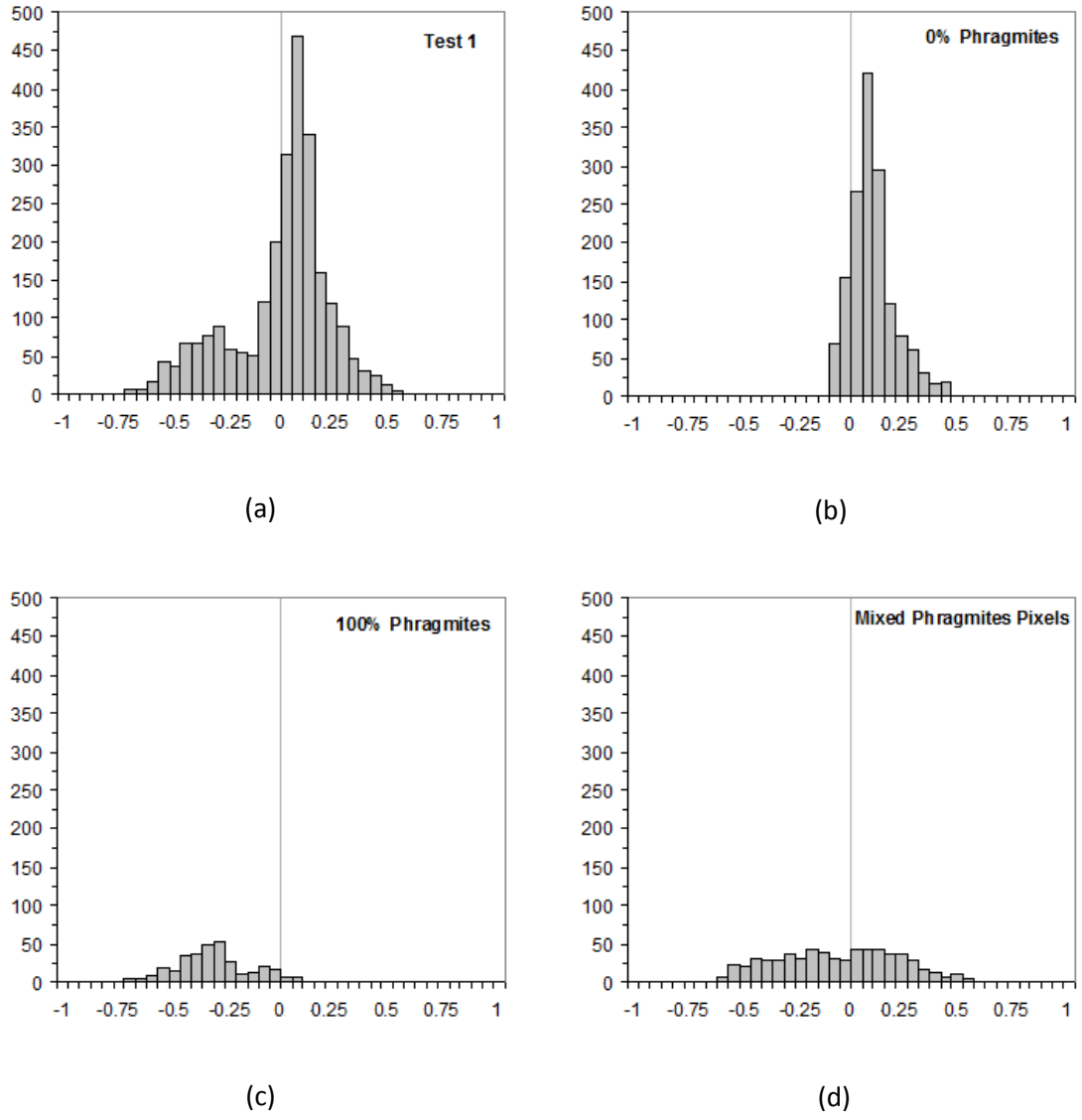

Figure 3.11 Fraction error histograms for Test1 (PPI-1) for the *Phragmites* class, broken down by Phragmites ground truth cover of 0%, mixed and 100%.

Table 3.5 Accuracy of the SMA fractions when Phragmites ground truth fraction is broken down into categories of 0, mixed and 1 fraction cover.

Phragmites Ground Truth Fraction	SMA Condition	Correct	Total	Accuracy (%)
0	< ⅓	1489	1532	97.2
Mixed and < ⅓	< ⅓	143	238	60.0
Mixed Dominant	Dominant	231	332	69.6
1	Dominant	301	327	92.0
Overall for four scenarios		2164	2439	89.1

3.3.2.4 Land Cover Abundance Layers

3.3.2.4.1 Grayscale Distribution and Abundance

The ground truth and SMA fraction maps for the three land covers for Test1 (PPI-1) are displayed in Figure 3.12. All three SMA fraction maps show similar overall pattern to their corresponding ground truth fraction maps. The main difference between ground truth and SMA maps is the dark contrast of ground truth maps compared to SMA maps. Ground truth maps tend to have very pure areas where the land cover type is or is not present whereas SMA maps tend to show a more continuous surface. Of the three land covers, the *Phragmites* SMA match the best with ground truth maps. Similarly, areas where *Phragmites* is absent in ground truth tend to show low *Phragmites* fractions in SMA maps. For Native Marsh Vegetation, the SMA fractions tend to be slightly underestimated compared to the ground truth map. The reason for this difference can be seen in the Water SMA fraction map. Water tends to be over predicted throughout pixels dominated by Native Marsh Vegetation leading to under prediction for Native Marsh Vegetation.

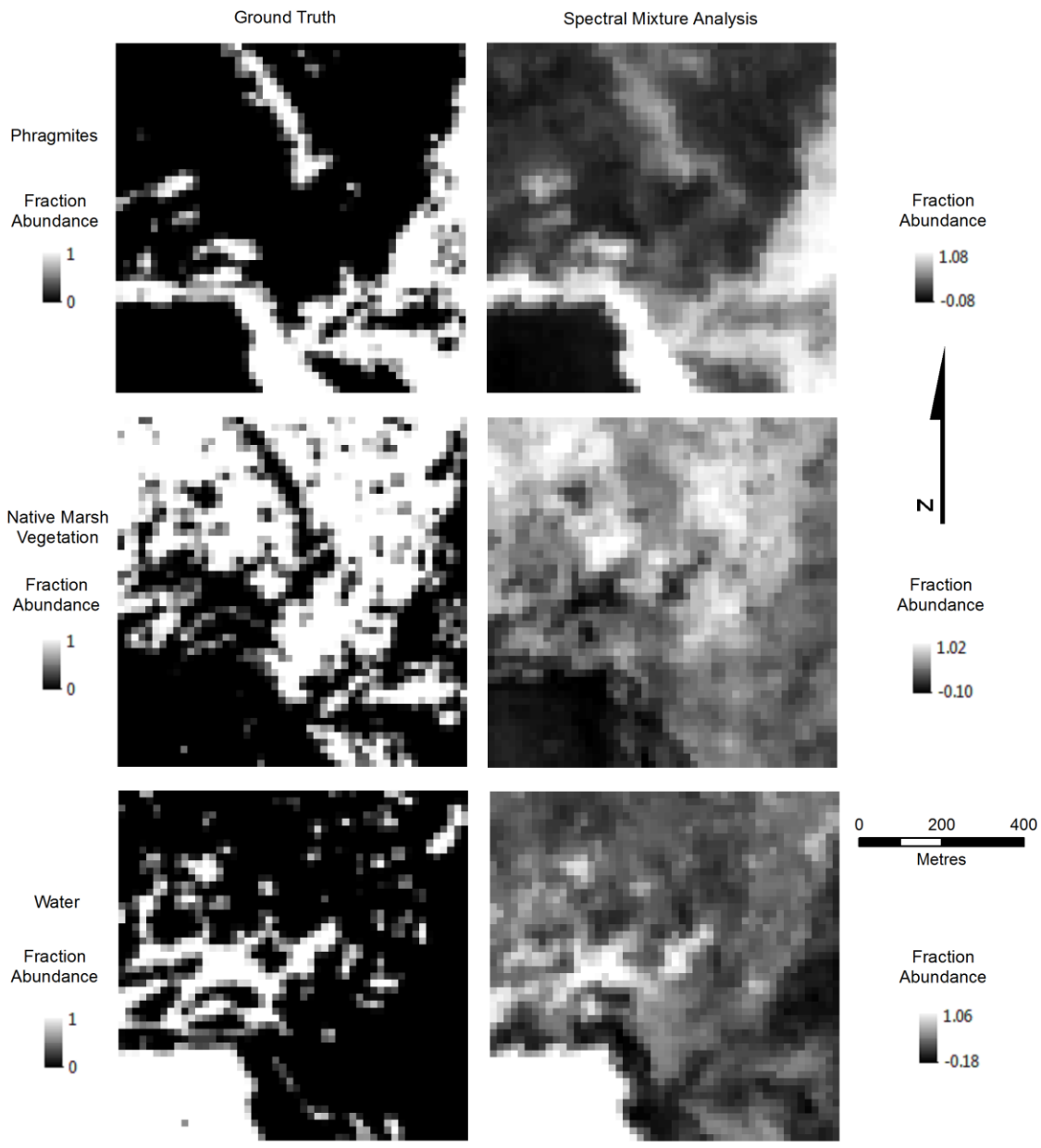

Figure 3.12 The ground truth and SMA predicted fraction maps for Test1 (PPI-1) for the three land cover types. Black pixels represent low fraction abundance whereas white pixels represent high fraction abundance.

3.3.2.4.2 Colour Composite Distribution and Abundance

In Figure 3.13, the three individual land cover fraction layers were combined as a Red, Green, and Blue colour image, representing *Phragmites*, Native Marsh Vegetation, and Water classes, respectively. Comparison of the ground truth and SMA colour composites show that the overall distribution of the three land covers can be reproduced by SMA fractions. The SMA map gives us confidence that the land cover present at different locations in the map would be found in the field. A colour composite map could point to investigate areas where the map colour is red, yellow or purple. Red pixels indicate areas that are dominated by *Phragmites*. Yellow pixels contain a mixture of *Phragmites* and Native Marsh Vegetation and these areas likely represent future *Phragmites* expansion. When pixels are purple, *Phragmites* is mixing with Water. These areas are likely to represent expanding fronts of *Phragmites* or places where water is too deep for a solid stand. Some differences between the maps are noticeable and may indicate areas that have changed between October 2010 and September 2011. One changed area is the southern portion of the marsh. In the ground truth image, this area contains bright green pixels indicating pure Native Marsh Vegetation. However, in the SMA colour composite, these bright green areas have turned to purple and gray. This may indicate that *Phragmites* is increasing at the expense of Native Marsh Vegetation. This is not a surprising change as these areas of Native Marsh Vegetation are surrounded by pixels with high *Phragmites*. The high similarity between ground truth and SMA colour composite maps make this a valuable product of the method. A colour composite interpretation key is given in Table 3.6.

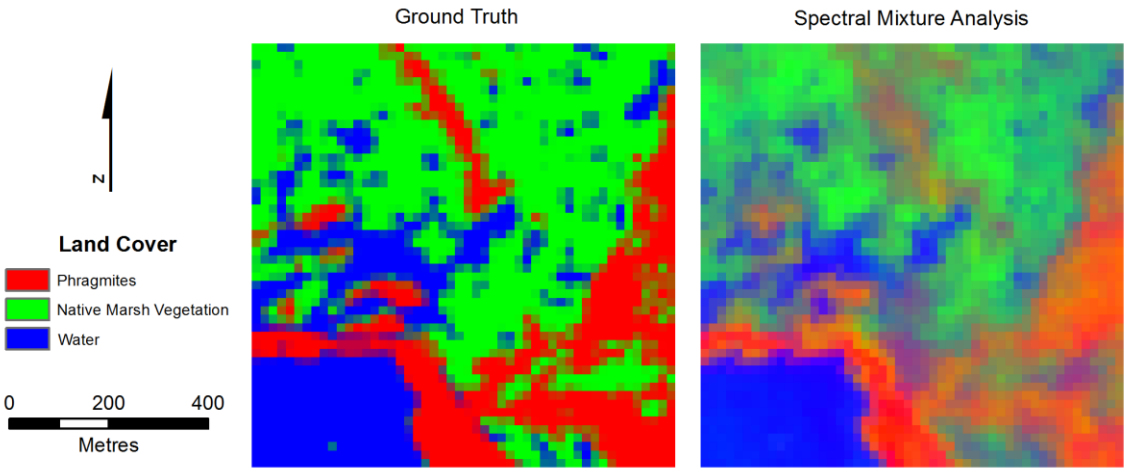

Figure 3.13 Colour composite maps for the ground truth and Test 1 SMA fraction layers. The Phragmites, Native Marsh Vegetation, and Water fraction images are displayed as red, green, and blue image layers, respectively.

Table 3.6 Colour composite interpretation key.

Colour Combination	Land Cover Combination	Map Colour
Red + Blue	*Phragmites* + Water	Purple
Green + Blue	Native Marsh Vegetation + Water	Cyan
Green + Red	Native Marsh Vegetation + *Phragmites*	Yellow
Red + Green + Blue	Even Mixture of *Phragmites*, Native Marsh Vegetation, and Water	Gray

3.3.2.4.3 Classified Worldview-2 as a Ground Truth Source

In the SMA land cover map, more mixing is predicted between Water and Native Marsh Vegetation than in the ground truth map. This appears as fewer bright green areas than in the ground truth fraction map. However, mixing between *Phragmites* and water is not observed as frequently. This highlights one problem with ground truth maps produced from high resolution imagery and object-based classification. The main reason for this discrepancy is differences in the vegetation canopy between Native Marsh Vegetation and *Phragmites* (Figure 3.14). In the study, Native Marsh Vegetation is dominated by *Typha* spp. The canopy of *Typha* is very open due to relatively low plant density and vertical leaf orientation that allows light to penetrate through the canopy to the surface.

Meyerson et al. (2000) found that in stands of *Typha*, the amount of light was 100% at 1.5m and 5 – 10% at the ground surface. On the other hand, the canopy of *Phragmites* is very dense due to high density of stalks and a horizontal leaf orientation. For *Phragmites* stands, Meyerson et al. (2000) found the amount of light was 10% at 1.5m 10% and 0% at the ground surface. Therefore there is a possibility of light reflection from water beneath the *Typha* canopy but this is not true in dense *Phragmites* stands. These canopy differences have different effects on the classification of Worldview-2 imagery with the object-based classification and CHRIS PROBA imagery with SMA method.

In Worldview-2 imagery, the reflectance of an individual 0.5m by 0.5m pixel may be representative of a very pure *Typha* pixel consisting of 90% *Typha* and 10% Water. In the immediate area surrounding this pixel are other pixels that are also very pure and have a similar spectral reflectance as each other. Using the object-based classification method, these four individual pixels are grouped together to form an object based on the low variation between their spectral values. During object classification, this *Typha* object is classified as Native Marsh Vegetation. This results in a 100% Native Marsh Vegetation canopy cover percentage for the four pixel object when in reality represents 90% Native Marsh Vegetation and 10% Water. If a 17m CHRIS pixel covers an area of these 90% Native Marsh Vegetation and 10% Water Worldview-2 pixels, the signature of this pixel will be a mixture of 90% Native Marsh Vegetation and 10% Water. When broken down into its component fractions by the SMA method, the fraction of Native Marsh Vegetation and Water will be 90% and 10% respectively. However, when this SMA pixel is compared to the ground truth fraction from object-based classification of Worldview-2 imagery, the Native Marsh Vegetation fraction will be underestimated by 10% while the Water will over estimated by 10%. This scenario is less likely to occur for *Phragmites*. The Worldview-2 pixels will contain pure *Phragmites* stands and result in correct object canopy cover. If the CHRIS PROBA pixel covers an area of these 100% pure *Phragmites* Worldview-2 pixels, the signature of this pixel will be 100% *Phragmites*. When compared to the ground truth, SMA fractions should be close for *Phragmites*.

Therefore, it is unlikely that Worldview-2 classification using object-based classification can represent 100% ground truth. It can be expected that SMA fractions will differ from ground truth for the Native Marsh Vegetation and Water classes due to the mixing of Water and *Typha* at the Worldview-2 pixel level. Based on the results from Chapter 2, it is unlikely that pixel-based methods will resolve this issue as classification accuracy was found to be lower for the pixel-based method. The most accurate ground truth for SMA fraction comparison is to estimate fractions in the field. For most studies, the ground truth accuracy provided by classification of high resolution imagery is sufficient. This method overcomes the issue of estimating the fraction coverage of *Phragmites* in a marsh environment which is very difficult.

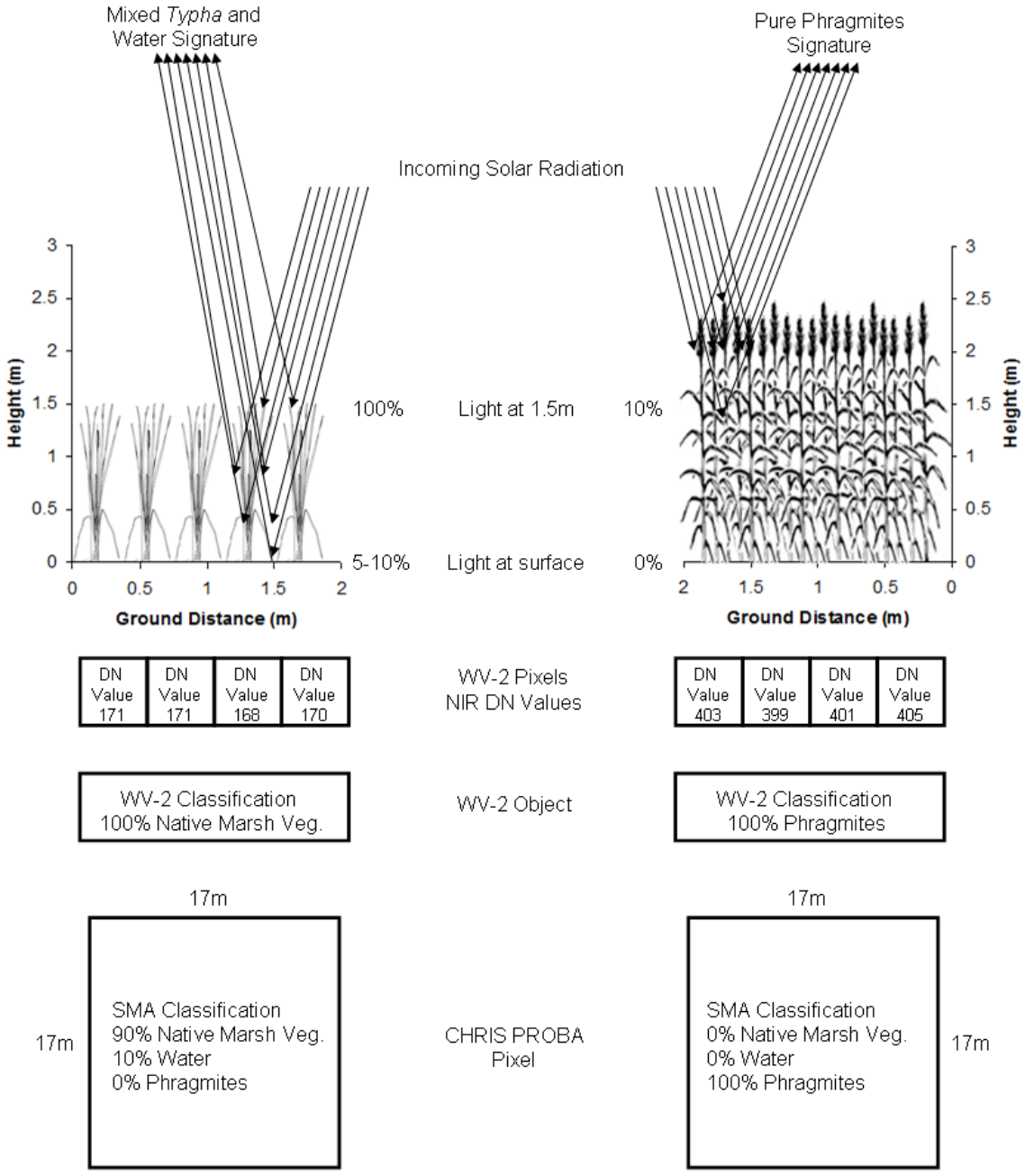

Figure 3.14 Canopy structure differences between *Typha* and *Phragmites*. The difference in plant density and canopy structure of *Typha* and *Phragmites* has an effect on Worldview-2 pixels for object-based classification and ground truth fraction estimation.

3.3.2.5 *Phragmites* Invasion Mapping

Two thresholds were defined to determine the status of *Phragmites* invasion within the individual pixels. This resulted in a three class *Phragmites* invasion map. The first class represents pixels not dominated by *Phragmites* (*Phragmites* fraction less than ⅓). The second class identifies pixels in which *Phragmites* fraction was greater than ⅓ and less than ½. The third class represents pixels where *Phragmites* fraction was greater than ½. SMA was highly accurate for identifying non-dominant *Phragmites* and *Phragmites* dominated pixels (Table 3.7). The intermediate dominant *Phragmites* class had the lowest accuracy. However, even though the accuracy was low for this class, the locations of these pixels appear to have ecological meaning (Figure 3.15). Many of the intermediate pixels occurred at the edge of *Phragmites* stands.

The spectral angle mapper (SAM) classifier was used to determine if similar results could be produced as the threshold classification. The SAM method classifies each pixel based on the angle between the reference spectrum and the hyperspectral image pixel measurement vector in n-dimensions. The pixel is assigned reference spectrum class that yields the smallest angle (Jensen, 2005). The final *Phragmites* and Other binary classification using the SAM classifier is shown in Figure 3.16. The SAM classifier with *Phragmites* and Other classes, produced a slightly lower accuracy than the SMA method with three classes representing *Phragmites* dominance (Table 3.8). Comparing the SMA and SAM maps clearly shows the advantages of using the SMA method. With SMA, we get the locations of the three *Phragmites* invasion classes which tell us about the status of *Phragmites* invasion. This is more useful than the SAM map which only tells us if the pixel is *Phragmites* dominated or not. In addition, the detailed three class *Phragmites* invasion map had a higher accuracy than the SAM map.

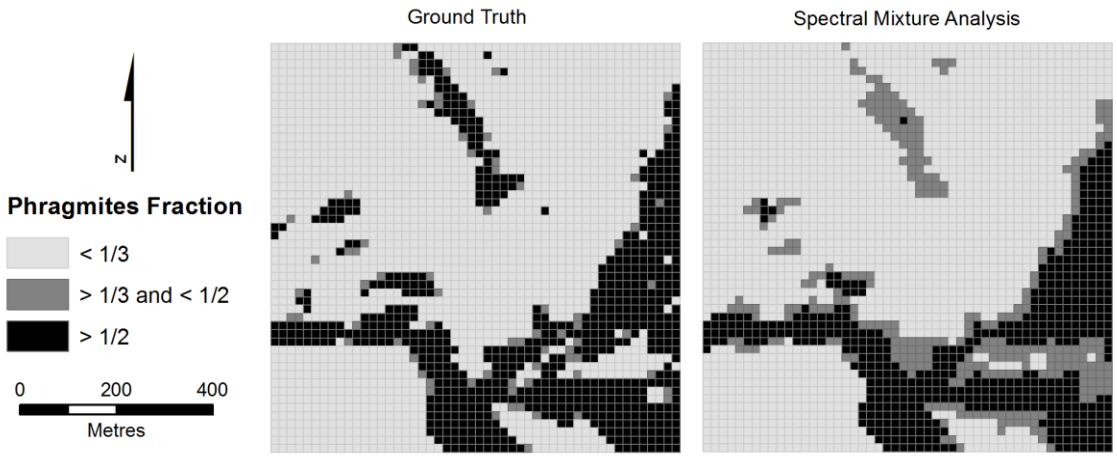

Figure 3.1524 *Phragmites* three class invasion map based on spectral mixture analysis (SMA) fractions and thresholds.

Table 3.7 Accuracy of the Phragmites invasion map from thresholding spectral mixture analysis (SMA) Phragmites fractions.

			Phragmites Fraction					
	Overall		<⅓		>⅓ and <½		>½	
Test	Accuracy	Kappa	UA	PA	UA	PA	UA	PA
Threshold	85.2	0.677	0.959	0.926	0.111	0.440	0.931	0.701

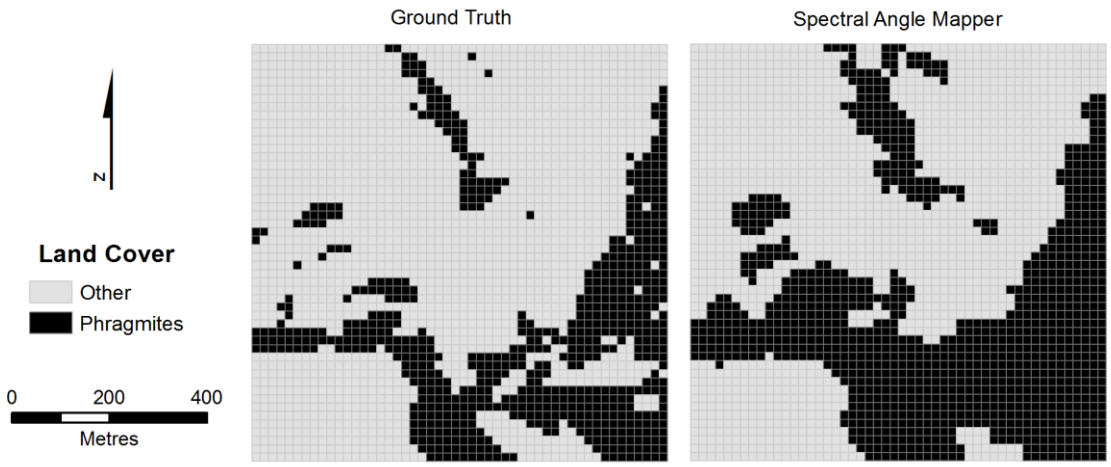

Figure 3.16 Spectral angle mapper (SAM) classification of *Phragmites* and Other land cover class map.

Table 3.8 Results of the spectral angle mapper (SAM) classification compared against the dominant fraction based on ground truth fractions from Worldview-2.

Test	Overall		*Phragmites*		Other	
	Accuracy	Kappa	UA	PA	UA	PA
SAM	84.2	0.655	0.976	0.630	0.795	0.989

3.3.2.6 Dominant Fraction Classification

Ground truth and spectral mixture analysis (SMA) fractions were classified based on the dominant fraction occurring within each pixel. A spectral angle mapper (SAM) classification was also performed as a comparison to the dominant classification of fractions. The SAM classifier is a hard form of classification meaning only one class is assigned to each pixel which is the same for the dominant fraction classification. Test1 endmembers were used as the reference spectrum for SAM classification since they produced the highest dominant fraction accuracies. The dominant fraction classification accuracy results are presented in Table 3.9. The dominant fraction classification maps for ground truth, Test1, and SAM are shown in Figure 3.16.

The best overall accuracy of 82.8% was achieved for Test1. *Phragmites* was over predicted where large pure stands occurred but was under predicted in Native Marsh Vegetation dominated areas. N-DV model had slightly lower overall and land cover accuracies compared to Test1 for all land cover classes. This was expected as the N-DV model did not perform as well as Test1 PPI model for other accuracy measures.

The SAM dominant land cover map produced an overall accuracy of 72.9%. Both image derived endmember SMA models resulted in dominant fraction maps that were more accurate than the SAM derived map. Accuracies were higher for image derived endmember models for all land cover classes. The SAM classifier tended to over predict *Phragmites* coverage and under predict small Water areas. Therefore, the dominant fraction classification yields better results than the SAM classifier even though both were based on the same endmember spectrums.

Table 3.9 Classification results based on the dominant fraction in each pixel.

	Overall		*Phragmites*		NMV		Water	
Test	Accuracy	Kappa	UA	PA	UA	PA	UA	PA
PPI-1	82.8	0.723	0.825	0.821	0.830	0.861	0.829	0.767
N-DV-4	80.7	0.678	0.854	0.692	0.763	0.917	0.895	0.702
SAM	72.9	0.563	0.630	0.976	0.764	0.777	1.000	0.354

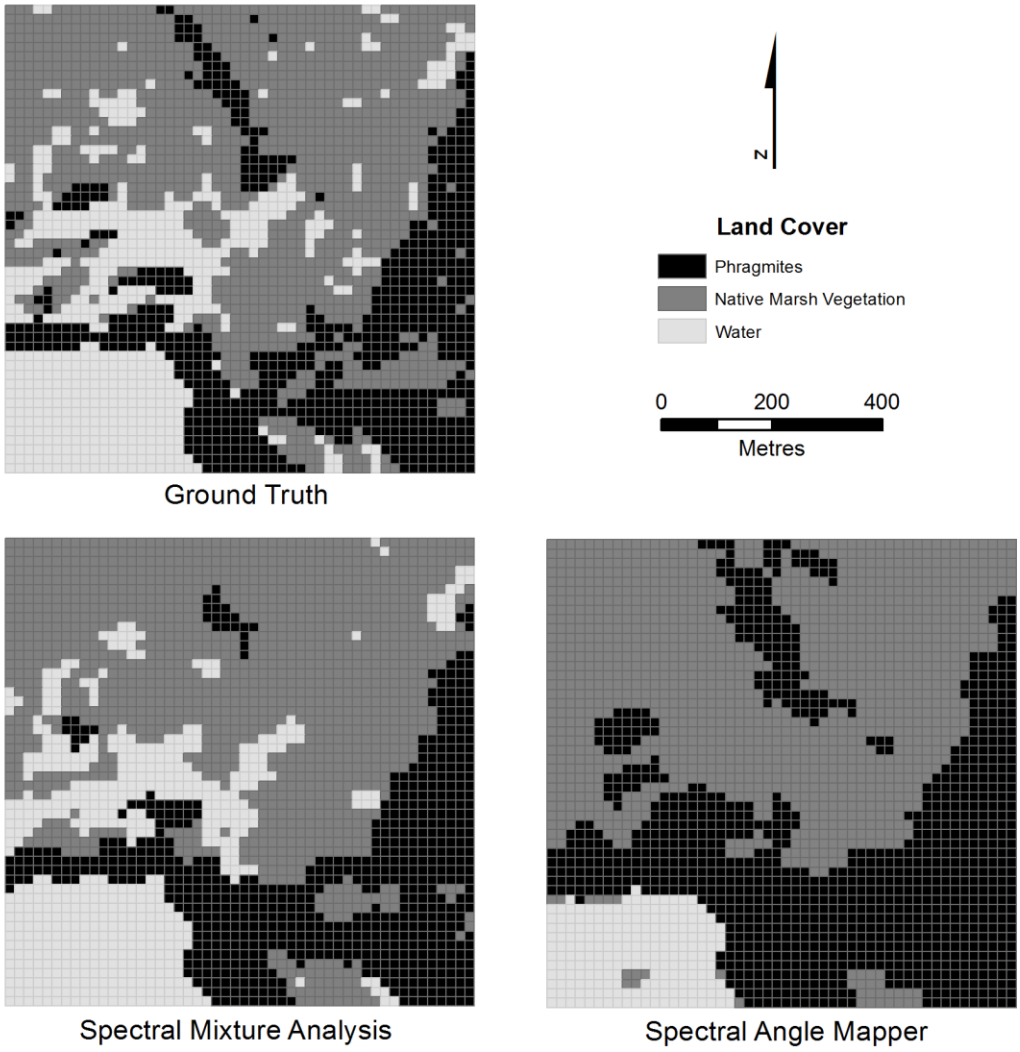

Figure 3.17 Classification maps based on the dominant land cover fraction in each pixel for a) ground truth from Worldview-2, b) spectral mixture analysis and c) spectral angle mapper from CHRIS PROBA.

3.4 Conclusions

Monitoring of the spectral response of invasive *Phragmites* and Native Marsh Vegetation species from August to October revealed that *Phragmites* might be best separated from Native Marsh Vegetation in September. At this time, the differences in the spectral reflectance of the two land covers seem to be the greatest of the three dates sampled. As spectral differences vary according to plant phenology, the geographical location within the Great Lakes may have an effect on the time when *Phragmites* and Native Marsh Vegetation are spectrally distinct.

Spectral mixture analysis (SMA) modelling of the three land covers using Analytical Spectral Device (ASD) derived endmembers did not produce accurate fraction results. This was a result of the time difference between hyperspectral image acquisition and ASD field measurements. To produce more accurate land cover fractions, the ASD endmembers should be acquired within a short time of image acquisition to closely match the spectral signature of land covers in the image.

Image derived endmembers produced more accurate pixel fractions for the three land covers than ASD endmembers. Large differences in fraction estimates were not found between SMA models using endmembers chosen by high Pixel Purity Index (PPI) values or interactive selection of individual pixels in the n-dimensional visualizer. This shows that intra-specific variation in land cover spectral reflectance is high and pixel fractions are not well estimated by using a single endmember spectrum for each land cover. Future *Phragmites* pixel fraction extraction studies employing SMA methods should test Multiple Endmember Spectral Mixture Analysis (MESMA) methods to account for the intra-specific spectral differences. MESMA allows multiple endmember signatures to be defined for each land cover class and for combinations of these endmembers to be optimized for each pixel to model fractions more accurately.

Evaluation of the SMA models with various accuracy measures revealed that land cover endmembers selected from pixels with the highest PPI value (Test1) performed slightly better than all other SMA models. Test1 produced physically possible fraction values for a high number of pixels and low average differences between predicted and ground truth fractions for all three land cover classes. High PPI endmembers representing the target land covers can be selected from the imagery if one of two things is known. If the spectral reflectance of the target land covers at the time of imagery acquisition is known, the spectral signature of the high PPI pixels can be labelled based on the comparison of these two signatures. Alternatively, if the identity of the land cover class at the location of the high PPI pixel is known, the PPI pixel is labelled as this class. This makes the selection of endmembers for SMA modelling simpler than trying to isolate and identify clusters of pixels in n-dimensional space.

Breaking down the *Phragmites* SMA fraction values based on the amount of *Phragmites* in the ground truth pixels revealed the nature of the errors in the fraction estimates. *Phragmites* fraction was over predicted in pixels with no *Phragmites*, which led to many pixels having small positive fraction errors. pixels with 100% *Phragmites* cover was consistently under estimated in pixels with 100% cover. Pixels containing a mixture of land covers including *Phragmites* had equal spread in fraction estimate errors. Although fraction estimates for *Phragmites* were not highly similar to ground truth, these differences did not have a large impact if the fractions were grouped into broader fraction categories. Ground truth pixels with 0% *Phragmites* fraction had 97.2% of their SMA fractions less than ⅓ meaning that *Phragmites* was non-dominant. Similarly, ground truth pixels with 100% *Phragmites* fraction had 92.0% of their SMA fractions greater than ½ meaning that *Phragmites* remained the dominant land cover class. Ground truth fractions containing mixed proportions of land classes including *Phragmites* resulted in fair accuracy. *Phragmites* SMA fractions matched the ground truth when grouped in broader relevant classes with 89.1% overall accuracy. Although the SMA model could not produce highly accurate *Phragmites* fraction estimates, fractions were still related to *Phragmites* abundance at a broader scale.

When individual fraction layers were displayed as grayscale maps, overall land cover patterns matched the ground truth very well. However, high ground truth fractions of Native Marsh Vegetation were less apparent in the SMA predicted grayscale map. Water fraction tended to be over predicted. This was particularly evident in the colour composite map where *Phragmites*, Native Marsh Vegetation, and Water were displayed as the Red, Green, and Blue bands, respectively. This result highlights a problem with using the object-based classification as a substitute for ground truth fraction estimates. Despite the 0.5m resolution, Native Marsh Vegetation and Water are more likely to mix in a Worldview-2 pixel than *Phragmites* and Water due to canopy structure differences between the dominant Native Marsh Vegetation species *Typha* and *Phragmites*. *Typha* has a less dense canopy relative to *Phragmites* and therefore is more likely to have its spectral signature affected by reflectance of water from the surface. Since this mixing occurs at the level of the Worldview-2 pixel, Native Marsh Vegetation is over predicted while Water is under predicted in the ground truth. He et al. (2010) found that water

lowered the accuracy of SMA fractions derived from Landsat TM data compared against ground truth derived from QuickBird-2 high resolution imagery. However, there was no mention of SMA fraction error resulting from errors in fractions based on the ground truth classification. This study shows that ground truth can be biased in favour of vegetation fraction leading to SMA fraction underestimation when vegetation is less dense. Despite this bias, this ground truth method is still accurate and useful compared to difficult field based fraction estimation in the marsh environment.

The *Phragmites* SMA fraction was separated into three classes based on the status of *Phragmites* invasion. Pixels could be *Phragmites*-non-dominant, -potentially dominant, and –dominant. These classes were based on *Phragmites* SMA fractions of <⅓, >⅓ and <½, and >½, respectively. A map with two classes, *Phragmites* and Other, where pixel class indicated dominant fraction was made using the SAM method. The three class SMA *Phragmites* invasion map had a higher accuracy than the SAM map. Therefore, SMA maps are more valuable since they have higher accuracy and provide more information about the state of *Phragmites* invasion within each pixel.

The SMA fraction layers were classified based on the highest fraction occurring within the pixel resulting in a single *Phragmites*, Native Marsh Vegetation, and Water map. The land cover class assigned to the pixel meant that that class was the dominant class. The SAM classifier was used to create a similar *Phragmites*, Native Marsh Vegetation, and Water map. The land cover class assigned to each pixel in the SAM map meant the signature of that pixel most closely matched the corresponding endmember used for SMA. The SAM method therefore produces a map with the same classes using the same input information as the SMA method. However, the SMA method produced an overall accuracy of 82.8%, close to 10% higher than the SAM map. Most importantly, the SMA method produced higher accuracies for the *Phragmites* class compared to the SAM method. Therefore, when the spectral signatures of the endmembers are known, using the SMA method to yield pixel fractions and then classifying the pixels based on the dominant fraction within each pixel results in higher accuracy than using the SAM method.

SMA fractions provide a wealth of information. Individual grayscale fraction layers give an accurate distribution of the three land cover types in the marsh. Combining the three land cover fraction layers in an RGB colour composite map yields valuable information about the location of *Phragmites* and the type of mixing occurring between classes in the study area. Classifying the *Phragmites* fraction layer based on thresholds produces a highly accurate map that shows the location and severity of *Phragmites* invasion within the study area. Finally, highly accurate information about the location of dominant vegetation in the marsh can be derived by classifying the SMA fraction layers based on the highest fraction within the pixel. All of this information can be used for assessing the state of the *Phragmites* invasion in the Great Lakes coastal marsh.

3.5 References

Adam, E., Mutanga, O., & Rugege, D. (2010). Multispectral and hyperspectral remote sensing for identification and mapping of wetland vegetation: a review. *Wetlands Ecology and Management, 18*(3), 281-296. DOI: 10.1007/s11273-009-9169-z.

Adams, J.B., Smith, M.O. and Gillepsie, A.R. (1993). Imaging spectroscopy: Interpretation based on spectral mixture analysis. In C. M. Pieters & P. Englert (Eds.), *Remote geochemical analysis: Elemental and mineralogical composition* (145-166). New York, NY: Cambridge University Press.

Artigas, F. J., & Yang, J. S. (2005). Hyperspectral remote sensing of marsh species and plant vigour gradient in the New Jersey Meadowlands. *International Journal of Remote Sensing, 26*(23), 5209-5220.

Arzandeh, S., & Wang, J. (2003). Monitoring the change of *Phragmites* distribution using satellite data. *Canadian Journal of Remote Sensing, 29*(1), 24-35.

ASD Technical Guide, 3rd Edition. (1999). Analytical Spectral Devices, Inc. (ASD) Technical Guide

Bedini, E., Van Der Meer, F., & Van Ruitenbeek, F. (2009). Use of HyMap imaging spectrometer data to map mineralogy in the Rodalquilar caldera, southeast Spain. *International Journal of Remote Sensing, 30*(2), 327-348.

Brockmann Consult. (2012). Help [VISAT V4.10.3]. Hamburg: Brockmann Consult.

Bookhout, T. A., Bednarik, K. E., & Kroll, R. W. (1989). The Great Lakes marshes. *Smith, LM, Pederson, RL, Kaminski, RM, Habitat Management for Migrating and Wintering Waterfowl in North America*, 131-156.

Catling, P. M., & Mitrow, G. (2012). The Recent Spread and Potential Distribution of *Phragmites australis* subsp. *australis* in Canada. *The Canadian Field-Naturalist, 125*(2), 95-104.

Chambers, R. M., Meyerson, L. A., & Saltonstall, K. (1999). Expansion of *Phragmites australis* into tidal wetlands of North America. *Aquatic Botany*, *64*(3), 261-273.

Clark, R.N., Swayze, G.A., Gallagher, A.J., King, T.V.V., and Calvin, W.M. (1993). The U. S. Geological Survey, Digital Spectral Library: Version 1: 0.2 to 3.0 microns, U.S. *Geological Survey Open File Report 93-592*, 1340 p.

DigitalGlobe. (2011). The DigitalGlobe Satellite Constellation. Available from <http://www.digitalglobe.com/downloads/corporate/Constellation_BR-CONST.pdf> [accessed (December 10, 2011)].

Drake, N. A., Mackin, S., & Settle, J. J. (1999). Mapping vegetation, soils, and geology in semiarid shrublands using spectral matching and mixture modeling of SWIR AVIRIS imagery. *Remote Sensing of Environment*, *68*(1), 12-25.

Edsall, T. A., Manny, B. A., & Raphael, C. N. (1988). *The St. Clair River and Lake St. Clair, Michigan: An ecological profile* (No. BR-85 (7.3)). National Fisheries Research Center-Great Lakes, Ann Arbor, MI (USA); Eastern Michigan Univ., Ypsilanti (USA). Dept. of Geography and Geology.

Environment Canada. (2003). *The Ontario great lakes coastal wetland atlas: A summary of information (1983-1997)* (Catalogue Number CW66-221/1997E). Peterborough, ON: Ontario Ministry of Education.

eoPortal Directory. (2012a). EO-1. Available from <https://directory.eoportal.org/web/eoportal/satellite-missions/e/eo-1> [accessed (November 28, 2012)]

eoPortal Directory. (2012b). PROBA-1. Available from <https://directory.eoportal.org/web/eoportal/ satellite-missions/p/proba-1> [accessed (November 28, 2012)]

Exelis Visual Information Solutions. (2012). ENVI Help. Boulder, Colorado: Exelis Visual Information Solutions.

Farnsworth, E. J., & Meyerson, L. A. (1999). Species composition and inter-annual dynamics of a freshwater tidal plant community following removal of the invasive grass, *Phragmites australis*. *Biological Invasions*, *1*(2), 115-127.

Ghioca-Robrecht, D. M., Johnston, C. A., & Tulbure, M. G. (2008). Assessing the use of multiseason Quickbird imagery for mapping invasive species in a Lake Erie coastal marsh. *Wetlands*, *28*(4), 1028-1039. DOI: http://dx.doi.org/10.1672/08-34.1.

Gilmore, M. S., Wilson, E. H., Barrett, N., Civco, D. L., Prisloe, S., Hurd, J. D., & Chadwick, C. (2008). Integrating multi-temporal spectral and structural information to map wetland vegetation in a lower Connecticut River tidal marsh. *Remote Sensing of Environment*, *112*(11), 4048-4060.

Green, A. A., Berman, M., Switzer, P., & Craig, M. D. (1988). A transformation for ordering multispectral data in terms of image quality with implications for noise removal. *Geoscience and Remote Sensing, IEEE Transactions on*, *26*(1), 65-74.

Guanter, L., Richter, R., & Moreno, J. (2006). Spectral calibration of hyperspectral imagery using atmospheric absorption features. *Applied Optics*, *45*(10), 2360-2370.

He, M., Zhao, B., Ouyang, Z., Yan, Y., & Li, B. (2010). Linear spectral mixture analysis of Landsat TM data for monitoring invasive exotic plants in estuarine wetlands. *International Journal of Remote Sensing*, *31*(16), 4319-4333.

Herdendorf, C. E. (1992). Lake Erie coastal wetlands: an overview. *Journal of Great Lakes Research*, *18*(4), 533-551.

Horwitz, H. M., Nalepka, R. F., Hyde, P. D., and Morganstern, J. P. (1971). Estimating the proportion of objects within a single resolution element of a multispectral scanner. University of Michgan, Ann Arbor, Michigan. NASA Contract NAS-9-9784.

Jensen, J. R. (2005). *Introductory digital image processing: A remote sensing perspective* (3rd ed.) (pp. 306, 338, 432, 444, & 456). Upper Saddle River, N.J.: Pearson Prentice Hall.

League, M. T., Colbert, E. P., Seliskar, D. M., & Gallagher, J. L. (2006). Rhizome growth dynamics of native and exotic haplotypes of *Phragmites australis* (common reed). *Estuaries and Coasts*, *29*(2), 269-276.

Lee K. H., & Lunetta, R.S. (1996). Wetland detection methods. In: Wetland and Environmental Application of GIS. Lyon, J.G., McCarthy, J. (eds). Lewis Publishers, New York, pp 249–284.

Mal, T. K., & Narine, L. (2004). The biology of Canadian weeds. 129. Phragmites australis (Cav.) Trin. ex Steud. *Canadian Journal of Plant Science*, *84*(1), 365-396.

Marks, M., Lapin, B., & Randall, J. (1994). *Phragmites australis* (*P. communis*): threats, management and monitoring. *Natural Areas Journal*, *14*(4), 285-294.

Meyerson, L. A., Vogt, K.A., and Chambers, R. M. (2000). Linking the success of *Phragmites australis* to the decoupling of ecosystem nutrient cycles. In M. Weinstein and D. Kreeger (eds.), Concepts and Controversies of Tidal Marsh Ecology. Dordrecht: Kluwer. pp. 817-834.

Meyerson, L.A., Saltonstall, K., and Chambers, R.M. (2009). *Phragmites australis* in Eastern North America: A Historical and Ecological Perspective. In Human impacts on salt marshes: a global perspective. Silliman, B.R., Grosholz, E.D., and Bertness, M.D. (eds). University of California Press, Berkeley, pp. 57-82.

Ontario Ministry of Natural Resources. (2011). Invasive Phragmites – Best Management Practices, Ontario Ministry of Natural Resources, Peterborough, Ontario. 15 pp.

Ozesmi, S. L., & Bauer, M. E. (2002). Satellite remote sensing of wetlands.*Wetlands Ecology and Management*, *10*(5), 381-402.

Parker Williams, A., & Hunt, E. R. (2002). Estimation of leafy spurge cover from hyperspectral imagery using mixture tuned matched filtering. *Remote Sensing of Environment*, *82*(2), 446-456.

Pengra, B. W., Johnston, C. A., & Loveland, T. R. (2007). Mapping an invasive plant, *Phragmites australis*, in coastal wetlands using the EO-1 Hyperion hyperspectral sensor. *Remote Sensing of Environment*, *108*(1), 74-81.

Roberts, D. A., Gardner, M., Church, R., Ustin, S., Scheer, G., & Green, R. O. (1998). Mapping chaparral in the Santa Monica Mountains using multiple endmember spectral mixture models. *Remote Sensing of Environment*, *65*(3), 267-279.

Roberts, D. A., Smith, M. O., & Adams, J. B. (1993). Green vegetation, nonphotosynthetic vegetation, and soils in AVIRIS data. *Remote Sensing of Environment*, *44*(2), 255-269.

Rosso, P. H., Ustin, S. L., & Hastings, A. (2005). Mapping marshland vegetation of San Francisco Bay, California, using hyperspectral data. *International Journal of Remote Sensing*, *26*(23), 5169-5191.

Saltonstall, K. (2002). Cryptic invasion by a non-native genotype of the common reed, *Phragmites australis*, into North America. *Proceedings of the National Academy of Sciences*, *99*(4), 2445-2449.

Saltonstall, K., Peterson, P. M., & Soreng, R. J. (2004). Recognition of *Phragmites australis* Subsp. *americanus* (Poaceae: Arunidnoideae) in North America: Evidence from Morphological and Genetic Analyses.

Settle, J. J., & Drake, N. A. (1993). Linear mixing and the estimation of ground cover proportions. *International Journal of Remote Sensing*, *14*(6), 1159-1177.

Surrey Satellite Technology Ltd. (2008). CHRIS Operations: CHRIS data format, Surrey Satellite Technology Limited, Surrey, UK, 37 p.

Tulbure, M. G., & Johnston, C. A. (2010). Environmental conditions promoting non-native *Phragmites australis* expansion in Great Lakes Coastal Wetlands. *Wetlands*, *30*(3), 577-587.

Tulbure, M. G., Johnston, C. A., & Auger, D. L. (2007). Rapid Invasion of a Great Lakes Coastal Wetland by Non-native *Phragmites australis* and *Typha*. *Journal of Great Lakes Research*, *33*, 269-279.

Wilcox, K. L., Petrie, S. A., Maynard, L. A., & Meyer, S. W. (2003). Historical distribution and abundance of *Phragmites australis* at Long Point, Lake Erie, Ontario. *Journal of Great Lakes Research*, *29*(4), 664-680.

Woodliffe, P. A. (1989). Inventory, Assessment, and Ranking of Natural Areas of Walpole Island.

Chapter 4

4 Conclusion

4.1 Summary

The sustainable management of wetlands relies on monitoring the distribution and quantity of the vegetation over time (Adam et al., 2010). This is especially important when an aggressive non-native species such as *Phragmites australis* becomes established and threatens to severely degrade the quality of the freshwater wetlands and coastal estuary environments in North America. Frequent monitoring permits the establishment of an invasion baseline, monitoring of the invasive plant propagation, and the possibility to implement an effective plan to deal with the invasion. Remote sensing provides a tool for the production of this important information which is more cost, labour, and time efficient relative to field based monitoring (Ozesmi & Bauer, 2002).

Mapping wetland vegetation at the species level with remote sensing methods is difficult as the high degree of similarity in spectral reflectance between species greatly reduces their separability (Adam et al., 2010). Very high-resolution multispectral satellite imagery lacks the spectral information needed to separate vegetation at the species level. Some success mapping at the species level can be achieved when additional information such as multiple images or height information from LiDAR are included in the analysis. However, additional information means extra expenses or may not be readily available.

Imagery from a single date is more likely to be accessible to a management team for the monitoring of wetland vegetation. Hyperspectral sensors, acquiring many narrow and contiguous spectral bands, allow for a high-resolution reflectance spectrum of each pixel to be measured (Jensen, 2005). Airborne hyperspectral sensors flown on planes provide an ideal combination of high-spatial and high spectral resolution imagery which allows for detailed vegetation mapping. However, the cost and infrequent acquisition of imagery is a barrier to their use for repeated mapping over large areas. Hyperspectral sensors on satellite platforms combine the frequent acquisition of imagery with the high-resolution reflectance spectrum of each pixel, but at lower spatial resolution than satellite

multispectral or airborne hyperspectral imagery. The spatial resolution becomes a problem if the average size of the marsh vegetation patches is smaller than the image pixel as this leads to multiple land covers within a single pixel (Artigas & Yang, 2005).

Chapter 2 presented an object-based classification method for the extraction of *Phragmites* cover from a single date Worldview-2 high-spatial resolution satellite image. The Worldview-2 sensor collects imagery in four additional spectral bands than traditional high-spatial resolution satellite sensors (e.g. QuickBird-2, IKONOS-2). Separate classifications were performed on four and eight band sets of imagery, and their accuracy for separating the land cover classes was evaluated.

Chapter 3 described the use of a single date hyperspectral satellite image from the CHRIS PROBA sensor to map the sub-pixel abundance of *Phragmites*, native marsh vegetation, and water using a linear spectral mixture analysis method. Individual layers were produced showing the spatial distribution and abundance of the three land cover types in the marsh. A *Phragmites* invasion map showed pixels that were *Phragmites* dominated, potentially dominated, and non-dominated. Fraction layers of the three classes were classified based on the dominant fraction occurring within each pixel showing the spatial distribution of the dominant land cover in the marsh.

4.2 Conclusions

The research presented in this thesis has answered the research questions posed in the introduction:

1. The *Phragmites* cover in the Great Lakes coastal marsh at Walpole Island was classified with a high overall accuracy of 94.0% from a single high-resolution Worldview-2 satellite image using the object-based method.

2. Object-based classification methods were developed for four and eight band imagery sets to investigate differences in classification accuracy with the addition of the four spectral bands. The four extra spectral bands were found to increase the overall classification accuracy from 92.7% to 94.0%. The improvement in accuracy resulted from the decreased confusion between the Tree and *Phragmites* classes.

3. Linear spectral mixture analysis of CHRIS PROBA hyperspectral imagery produced fraction maps predicting the distribution and fraction of land cover types which matched the ground truth pattern with good accuracy.

4. The classified Worldview-2 image from Chapter 2 was used as ground truth to evaluate the fractional abundances of the *Phragmites*, native marsh vegetation and water classes. Mixing between native marsh vegetation and water at the level of the Worldview-2 pixel is believed to bias the ground truth fractions of these two classes. Native marsh vegetation and water ground truth fractions are overestimated and underestimated, respectively.

5. The *Phragmites* fraction layer was reclassified to provide information about the state of *Phragmites* invasion in the marsh. The *Phragmites* invasion map had a high overall accuracy of 85.2% when compared to ground truth.

6. The individual fraction layers were combined to provide a distribution map of the dominant land cover types in the marsh. When compared to ground truth, this map had a high overall accuracy of 82.8% for the *Phragmites*, native marsh vegetation, and water classes.

4.3 Contributions of this Research

The main contribution of the study in Chapter 2 is it is the first known use of Worldview-2 high-resolution eight band imagery and the object-based method for mapping a Great Lakes coastal wetland with the emphasis on extracting *Phragmites* cover. This satellite combines high-spatial resolution with increased spectral resolution compared with traditional high-resolution sensors. The results of the research show that a single date of imagery acquired late in the growing season, when spectral differences between *Phragmites* and other vegetation are greatest, is sufficient for mapping *Phragmites* with high accuracy. Worldview-2 imagery acquired late in the growing season, could be used by wetland managers for creating a baseline for *Phragmites* invasion, mapping its annual invasion. This could assist in developing a plan to deal with the invasion. Utilizing a single image from Worldview-2 reduces the cost associated with a vegetation monitoring program while providing similar accuracies to those methods using additional information such as multi-season imagery and/or height information from LiDAR.

Chapter 3 adds to the research on using hyperspectral satellite imagery for mapping *Phragmites* in the Great Lakes region. The research presented is the first known use of CHRIS PROBA hyperspectral satellite imagery to map the sub-pixel abundance of *Phragmites* in a Great Lakes coastal wetland. Pengra et al. (2007) used 30m Hyperion hyperspectral satellite imagery and the Spectral Correlation Mapper algorithm to map *Phragmites* on Green Bay, Lake Michigan, and it is the only other known study to use satellite hyperspectral imagery for *Phragmites* mapping in the Great Lakes. This research shows that accurate detailed information about the state of *Phragmites* invasion can be extracted from CHRIS PROBA using sub-pixel abundances. CHRIS PROBA land cover fractions can be combined to create a dominant land cover map for the marsh. These fraction layers could be updated every year to monitor the spread of the invasive species, and determine how the dominant vegetation distribution is changing.

4.4 Possible Future Research

4.4.1 High Resolution Imagery

Future research using a single date Worldview-2 image could focus on generating additional information from the image to use for more accurate classification of *Phragmites*. For example, the texture of image objects could be calculated and used as additional information to separate *Phragmites* objects from other land cover class objects. eCognition provides texture measures based on Haralick gray-level co-occurrence matrices (GLCM) to be calculated for each object (Haralick et al., 1973; Haralick, 1979). Texture layers have been used to increase of accuracy of *Phragmites* classifications using radar data (Arzandeh & Wang, 2002) and high-resolution multispectral imagery (Laba et al. 2010). The additional four spectral bands of Worldview-2 imagery could allow for specific band indices to be developed to aid in discriminating *Phragmites* from other vegetation. Gilmore et al. (2008) found that simple band indices calculated from QuickBird-2 bands, allowed for the classification of *Phragmites* from other species.

4.4.2 Multiple Endmember Spectral Mixture Analysis

The spectral mixture analysis method used in Chapter 3 is a very basic spectral unmixing model since it only allows for a single reference spectrum to be defined per land cover class. Other spectral unmixing models such as multiple endmember spectral mixture analysis (MESMA), has been used to produce better results than SMA (e.g. Somers et al., 2011) and may produce better fraction estimates for the three land covers. Unlike basic SMA, MESMA allows for multiple endmembers to be defined for each land cover class. For example, additional endmembers could be defined for the *Phragmites* class which represent pure *Phragmites* stands in slightly different plant stages. The spectrums will be slightly different from each other, allowing for the spectral variability within the *Phragmites* class to be better accounted for. Multiple endmembers are defined for each class. The endmembers are grouped into different combinations and a basic SMA model is run for each combination. After these endmember combinations have been tested in the SMA models, the pixels are evaluated one at a time using the resulting fractions,

RMSE and residual values (Roberts et al., 1998) to select the best SMA model fit for each pixel.

4.5 References

Adam, E., Mutanga, O., & Rugege, D. (2010). Multispectral and hyperspectral remote sensing for identification and mapping of wetland vegetation: a review. *Wetlands Ecology and Management, 18*(3), 281-296.

Artigas, F. J., & Yang, J. S. (2005). Hyperspectral remote sensing of marsh species and plant vigour gradient in the New Jersey Meadowlands. *International Journal of Remote Sensing, 26*(23), 5209-5220.

Arzandeh, S., & Wang, J. (2002). Texture evaluation of RADARSAT imagery for wetland mapping. *Canadian Journal of Remote Sensing, 28*(5), 653-666.

Gilmore, M. S., Wilson, E. H., Barrett, N., Civco, D. L., Prisloe, S., Hurd, J. D., & Chadwick, C. (2008). Integrating multi-temporal spectral and structural information to map wetland vegetation in a lower Connecticut River tidal marsh. *Remote Sensing of Environment, 112*(11), 4048-4060.

Haralick, R. M., Shanmugam, K., & Dinstein, I. H. (1973). Textural features for image classification. *Systems, Man and Cybernetics, IEEE Transactions on,* (6), 610-621.

Haralick, R. M. (1979). Statistical and structural approaches to texture. *Proceedings of the IEEE, 67*(5), 786-804.

Jensen, J. R. (2005) *Introductory digital image processing: A remote sensing perspective* (3rd ed.) (pp. 431). Upper Saddle River, N.J.: Pearson Prentice Hall.

Laba, M., Blair, B., Downs, R., Monger, B., Philpot, W., Smith, S., Sullivan, P. & Baveye, P.C. (2010). Use of textural measurements to map invasive wetland plants in the Hudson River National Estuarine Research Reserve with IKONOS satellite imagery. *Remote Sensing of Environment, 114*(4), 876-886.

Ozesmi, S. L., & Bauer, M. E. (2002). Satellite remote sensing of wetlands. *Wetlands Ecology and Management, 10*(5), 381-402.

Pengra, B. W., Johnston, C. A., & Loveland, T. R. (2007). Mapping an invasive plant, *Phragmites australis*, in coastal wetlands using the EO-1 Hyperion hyperspectral sensor. *Remote Sensing of Environment, 108*(1), 74-81.

Roberts, D. A., Gardner, M., Church, R., Ustin, S., Scheer, G., & Green, R. O. (1998). Mapping chaparral in the Santa Monica Mountains using multiple endmember spectral mixture models. *Remote Sensing of Environment, 65*(3), 267-279.

Somers, B., Asner, G. P., Tits, L., & Coppin, P. (2011). Endmember variability in spectral mixture analysis: A review. *Remote Sensing of Environment, 115*(7), 1603-1616.

Appendices

A.1 Smoothing Filter-based Intensity Modulation

Image fusion is a commonly used method to increase the information in an image. The Worldview-2 satellite acquires eight multispectral bands of 2m resolution and one panchromatic band with 0.5m resolution. Therefore, the multispectral bands can be enhanced with the greater spatial information provided by the panchromatic band. In this study, the Smoothing Filter-based Intensity Modulation (SFIM) image fusion technique described by Liu (2000) was used to create a new dataset with both high spatial and spectral information. The multispectral bands were resampled to the same resolution as the panchromatic band to ensure precise pixel alignment. An averaging filter equal to or greater than the ratio between the high spectral resolution band and the high spatial resolution band is then applied to the high spatial resolution band. The multispectral band resolution was 2m and the panchromatic band resolution was 0.5m so a 5x5 averaging filter was applied. The fusion technique is described by the equation:

$$DN(\lambda_{sim}) = DN(\lambda_{low})DN(\gamma_{high})/DN(\gamma_{mean}) \quad (1)$$

where $DN(\lambda_{sim})$ is the value of the SFIM pansharpened higher resolution pixel in a multispectral channel corresponding to $DN(\lambda_{low})$. $DN(\gamma_{high})$ is the value of the corresponding pixel in the high resolution panchromatic channel, and $DN(\gamma_{mean})$ is the value of the corresponding pixel in the low-pass filtered panchromatic band. This equation was applied to each of the eight Worldview-2 multispectral bands. The result is eight multispectral bands with 0.5m resolution. These pansharpened bands and the original panchromatic band were used as input layers for classification.

A.1 References

Liu, J. G. (2000). Smoothing filter-based intensity modulation: a spectral preserve image fusion technique for improving spatial details. *International Journal of Remote Sensing*, *21*(18), 3461-3472. DOI: 10.1080/01431160110088772.

A.2 Land Cover Types of Walpole Island First Nation

Figure A2.1 *Phragmites australis* (Cavenilles) Trinius ex. Steudel subsp. *australis*, Common Reed, growing on a marsh dike.

Figure A2.2 *Phragmites australis* (Cavenilles) Trinius ex. Steudel subsp. *australis,* Common Reed, growing in the coastal marsh.

Figure A2.3 *Phragmites australis* (Cavenilles) Trinius ex. Steudel subsp. *australis,* Common Reed, in the flowering/fruiting stage.

Figure A2.4 *Phragmites australis* (Cavenilles) Trinius ex. Steudel subsp. *australis,* Common Reed, is the dominant species in many parts of the marsh.

Figure A2.5 Native Marsh Vegetation.

Figure A2.6 Native Marsh Vegetation – *Typha* spp., Cattails.

Figure A2.7 Native Marsh Vegetation – *Pontederia cordata*, Pickerelweed.

Figure A2.8 Native Marsh Vegetation - *Scirpus* spp., Bulrush.

Figure A2.9 Native Marsh Vegetation – *Nymphaea odorata*, Fragrant White Water Lily.

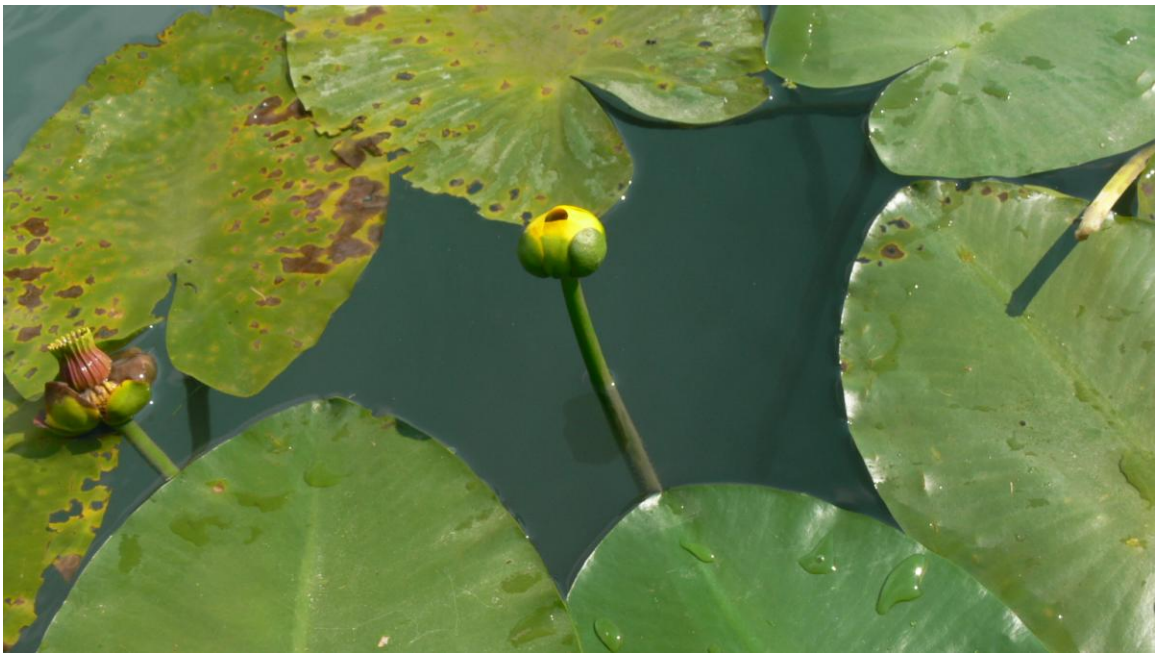

Figure A2.10 Native Marsh Vegetation - *Nuphar variegatum*, Yellow Pond Lily.

Figure A2.11 Native Marsh Vegetation – *Zizania palustris*, Wild Rice.

Figure A2.12 Forest and Tallgrass Prairie are found inland away from the marsh.

Figure A2.13 Tallgrass Prairie.

Figure A2.14 Agriculture, Tallgrass Prairie, and Forest land cover types.

Figure A2.15 Corn is a major crop type grown in WIFN.

Figure A2.16 Soybeans are a main crop type grown in WIFN.

Figure A2.17 Asphalt roads are common in the urban areas of WIFN.

Figure A2.18 Gravel roads allow access to the agricultural areas of WIFN.

Figure A2.19 Roads on the marsh dikes are made of compacted soil.

Figure A2.20 Manicured grass is found in urban areas of WIFN.

Figure A2.21 Drainage ditch between agricultural fields.

Figure A2.22 The St. Clair River is a major shipping channel that allows cargo vessels to travel between the upper and lower Great Lakes.

Figure A2.23 The coastal marshes of WIFN extend into Lake St. Clair.

Figure A2.24 The islands of WIFN are separated by the Bassett, Chematogan, Johnston (shown here), and the Snye channels.

Figure A2.25 The "heart" of WIFN, Goose Lake.

Figure A2.26 Snooks Lake, Squirrel Island, WIFN.

Curriculum Vitae

Name: Nicholas Lantz

Post-secondary Education and Degrees:

University of Western Ontario
London, Ontario, Canada
2005 – 2010
B.Sc. Double Major with Honors
Major in Conservation Biology
Major in Geographic Information Science

University of Western Ontario
London, Ontario, Canada
2010 – 2012
M.Sc. Geography (Remote Sensing)

Honours and Awards:

Natural Sciences and Engineering Research Council of Canada
Undergraduate Student Research Award
2010

Western Graduate Research Scholarship
2010 – 2012

Ontario Ministry of Training, Colleges and Universities
Ontario Graduate Scholarship
2010 – 2011

Natural Sciences and Engineering Research Council of Canada
Alexander Graham Bell Canada Scholarship
2011 – 2012

Related Work Experience:

Teaching Assistant
University of Western Ontario, Department of Geography
2010 – 2011

Research Assistant
University of Western Ontario, Department of Geography
2012

Conferences:

Lantz, N., and Wang, J. (2012). "Classification of Multispectral Imagery for Mapping an Invasive Wetland Plant", presented at the 33rd Canadian Symposium on Remote Sensing, June 11 – 14, 2012.